8-2010

DESIGN OF ADVANCED ION-EXCHANGE MEMBRANES AND THEIR PERFORMANCE ASSESSMENT FOR DOWNSTREAM CHROMATOGRAPHIC BIOSEPARATIONS

Bharatkumar Bhut
Clemson University, bbhut@g.clemson.edu

DESIGN OF ADVANCED ION-EXCHANGE MEMBRANES AND THEIR
PERFORMANCE ASSESSMENT FOR DOWNSTREAM
CHROMATOGRAPHIC BIOSEPARATIONS

_____

A Dissertation
Presented to
the Graduate School of
Clemson University

_____

In Partial Fulfillment
of the Requirements for the Degree
Doctor of Philosophy
Chemical Engineering

_____

by
Bharat V. Bhut
August 2010

_____

Accepted by:
Dr. Scott M. Husson, Committee Chair
Dr. Kenneth A. Christensen
Dr. Charles H. Gooding
Dr. Douglas E. Hirt
Dr. S. Ranil Wickramasinghe

ABSTRACT

This doctoral research focuses on the design, development and characterization of advanced ion-exchange membranes and their performance evaluation as process chromatography media for downstream bioseparations. Chromatography is a widely used unit operation in the biopharmaceutical industry for the downstream purification of protein therapeutics. The rapid developments in biotechnology and the pharmaceutical potential of biomolecules have increased the worldwide demand for protein therapeutics dramatically. Considering that 50−90% of the total cost of bioprocesses is due to the downstream recovery and purification, high-productivity and high-resolution separation techniques that will enable cost-effective production are essential to the biopharmaceutical industry. In recent years, membrane chromatography has been promoted as a promising alternative to more conventional packed-bed resin chromatography. Although the potential for membrane chromatography is great, the historically lower binding capacity of membranes compared to resin media has limited its broad implementation. Therefore, primary objectives of this dissertation were to prepare advanced weak and strong anion-exchange membranes with ultrahigh and completely reversible protein binding capacities and to demonstrate the high-throughput and high resolution that these membranes enable in the separation of a target protein from a complex media (cell lysate).

The research presented here pertains to the use of atom transfer radical polymerization (ATRP) to prepare surface-modified weak and strong anion-exchange

membranes for chromatographic bioseparations. Surface-initiated atom transfer radical polymerization (ATRP) was used to graft poly(2-dimethylaminoethyl methacrylate), (poly(DMAEMA)), and poly([2-(methacryloyloxy)ethyl]trimethylammonium chloride), (poly(MAETMAC)), nanolayers from the internal pore surfaces of commercial regenerated microporous membranes. Characterization of physicochemical and performance properties of newly designed, surface-modified membranes was performed using various analytical techniques.

The central theme of my research was to investigate how polymer architecture influences the separation performance properties of surface-modified ion-exchange membranes. In one study, the grafting density and average molecular weight of polymer chains grown from the membrane pore surfaces were varied independently and optimized to prepare weak anion-exchange membranes with ultra-high and completely reversible dynamic binding capacity. The effects of polymer grafting density, average molar mass of polymer and linear flow velocity on the dynamic binding capacity were studied. This study yielded weak anion-exchange membranes with very high volumetric protein binding capacities (static binding capacity~140 mg BSA/mL and dynamic capacity ~130 mg/mL) at high linear flow velocities (>350 cm/h) and relatively low transmembrane pressure drop (<3 bar). In a second study, a systematic evaluation was performed on the role of polymer molecular architecture on the separation performance of strong anion-exchange membranes. Anion-exchange membranes with different polymer chain densities were prepared using surface-initiated ATRP. The effect of polymer chain density, and, thus the, degree of polymer grafting, on the mass transfer resistances and

accessibility of large biopolymers (IgG and DNA) was studied. From this detailed study, I have prepared a unique protocol to design strong Q-type anion-exchange membranes with unusually high volumetric protein binding capacities (dynamic binding capacity ~140 mg IgG/mL and ~27 mg DNA/mL) at high linear flow velocities (>190 cm/h) and relatively low transmembrane pressure drop (<3.5 bar). Overall, findings from my PhD studies strengthen the argument that membrane chromatography can be a higher capacity and higher throughput process than resin chromatography.

Finally, I evaluated the protein separation performance of my newly designed anion-exchange membrane adsorber and compared it to a commercial membrane adsorber and resin column. One aspect of this study was to compare the protein separation performance of membrane chromatography with resin column chromatography. Anion-exchange chromatography was used under salt-gradient and pH-gradient elution to separate anthrax protective antigen protein from periplasmic *Escherichia coli* lysate. Overall, this part of the work demonstrates that membrane chromatography is a high-capacity, high-throughput, high-resolution separation technique, and that resolution in membrane chromatography can be higher than resin column chromatography under preparative conditions and at much higher (15 times higher than widely used resin column) volumetric throughput.

DEDICATION

I dedicate this dissertation to my beloved wife, Hetal Bhut, and my parents, Mrs.

Hansa and Mr. Vallabh Bhut.

ACKNOWLEDGEMENTS

I have no words to thank my beloved wife Hetal for her unconditional support to my professional career decisions and being my inspiration and strength. Finally, I thank my parents for their encouragement and believing in my decisions.

TABLE OF CONTENTS

LIST OF TABLES

LIST OF FIGURES

List of Figures (Continued)

List of Figures (Continued)

List of Figures (Continued)

Figure   Page

List of Figures (Continued)

Figure   Page

List of Figures (Continued)

Figure   Page

List of Figures (Continued)

INTRODUCTION

1.1 Downstream separation and purification of therapeutic biomolecules

Biopharmaceutical products (e.g., peptides, proteins, DNAs, oligonucleotides, viruses) come from many sources such as human and animal tissue and body fluids, plant material, microbial fermentation, cell culture and raw broths from bioreactors [Subramanian et al., 2007]. Irrespective of the original source, bioprocess materials must undergo several separation and purification steps to recover the final biopharmaceutical material with desired form and specifications. The train of bioprocess unit operations can be bifurcated into the upstream and downstream processes. A set of unit operations beyond the "bioreaction step" is called downstream processing. In general, the downstream processes can be divided further into harvest (cell removal/clarification) and purification [Shukla et al., 2007].

Harvest of therapeutic protein products from bioprocess streams is achieved using a combination of several unit operations. The primary focus of the harvest is to collect the desired product into the solution, remove suspended material and cell debris and reduce the process volume for further purifications. During harvest, the intracellular products are released into the solution using cell concentration followed by cell disruption methods. After cell disruption, the clarification of process fluid often is performed using centrifugation and microfiltration followed by sterile depth filtration [Van Reis et al., 2007].

The purification can be sub-divided into three stages: product capture, intermediate purification, and polishing. In the product capture stage, the objectives are to isolate, concentrate and stabilize the target product from the bioreactor effluent material. During the intermediate purification stage, the objective is to remove most of the intracellular impurities such as other host cell proteins and DNA, RNA, endotoxins and viruses. In the polishing stage, the objective is to achieve high purity by removing any remaining trace impurities or closely related substances (e.g., isomers, degradation products, dimers and deamidated forms) [Zhou et al., 2008]. Chromatography is essential and is a widely used unit operation for all three stages of purification; indeed, it is often at the core of any biopharmaceutical purification process. The ability of chromatography to achieve the required purities of therapeutic biomolecules is incomparable to any other unit operation [Ahuja et al., 2000, Subramanian et al., 2007]. The mode of chromatography operation can be classified based on the functional groups of the stationary phase used to prepare the adsorptive bed. The primary classification is divided into the two categories: affinity and non-affinity chromatography. Affinity chromatography uses an immobilized ligand that interacts specifically at a well-defined site (specific domain) on the desired biomolecules (e.g., protein A affinity chromatography). Non-affinity chromatography is based on the interactions of ligand(s) with various amino acid residues distributed over the biomolecule surface (e.g., ion-exchange, hydrophobic interaction and hydroxyapatite chromatography). Shukla et al. [2007] provide a detailed classification of process chromatography.

The most widely discovered therapeutic biomolecule products are recombinant

proteins, monoclonal antibodies and nucleic acid–based drugs [Subramanian et al., 2007].

Monoclonal antibodies (mAb) were identified as therapeutic products in the early 1990s.

Since then, mAbs have become the largest segment of therapeutic protein drug molecules

in the biopharmaceutical industry. The downstream processing train for a therapeutic

biomolecule depends on its type, origin, desired quality specification and demand.

Following is an example of a generic purification process for antibody purification [Zhou

et al., 2006, 2008]. A large-scale antibody purification process often involves a minimum

of two chromatography steps: first, recombinant Protein A affinity chromatography as the

primary capture step and, second, anion-exchange chromatography in flow-through mode

of the operation as a polishing step for impurity removal. In many cases, a third

chromatography step, cation-exchange chromatography in capture mode, is used just after

the protein A affinity chromatography to insure additional clearance of host cell proteins

(HCPs) and product-related impurities (e.g., deamidated or acidic species and dimmer)

that Protein A affinity cannot. Anion-exchange chromatography in flow-through

separation mode has proven to be the most powerful technique to remove a variety of

impurities such as HCPs, DNA, RNA, viruses and endotoxin [Gottschalk et al., 2004;

Van Reis et al., 2007; Zhou et al., 2006, 2008].

Protein A chromatography is highly specific, has the ability to handle feed stream

directly from cell culture harvest and offers very high purity in a single step purification.

It is a traditional choice for antibody purification. However, Protein A chromatography

columns are very expensive, provide relatively lower binding capacity and come with

inherent limitations associated with Protein A leaching [Follman et al., 2004; Gottschalk et al., 2005]. Therefore, in recent years, cation-exchange chromatography for capture step purification has been under investigation to replace Protein A chromatography. A few such case studies published based on detailed process economics comparison highly favor the use of ion-exchange chromatography as an alternative to Protein A chromatography [Arunakumari et al., 2007; Follman et al., 2004; Ghosh et al. 2008].

Ion-exchange chromatography is the most widely used and a universal unit operation in the biopharmaceutical industry for the downstream processing of protein therapeutics at capture, intermediate and polishing step purifications [Bhut et al., 2010; Curling et al., 2007; He et al., 2008; Subramanian et al., 2007]. Ion-exchange chromatography separates biomolecules based on the differences in their net surface charge. The primary advantages of ion-exchange chromatography include its simple and arguably the most understood separation principle, high adsorption capacity, high separation resolution and ease of operation. Ion-exchange media are used as stationary phases to prepare the ion-exchange chromatography adsorptive bed. Ion exchangers contain charged functional (ion-exchange) groups attached to a self-supporting solid base matrix. The functional groups can be charged positively (anion exchangers) or negatively (cation exchangers) and interact with oppositely charged amino acid residues of biomolecules primarily via Coulombic interactions. Further division can be made into weak and strong ion exchangers based on the operational pH range. The pH operating window for weak ion exchangers is smaller compared to strong ion exchangers. For strong anion or cation exchangers, the functional groups are always present in ionized form in aqueous media

4

(e.g., quaternary amino groups are charged positively and sulfonic acid groups are charged negatively).

1.2 Developments in process chromatography media

A wide variety of process chromatography media or matrices with numerous interaction modes are available in the market today. The performance of a chromatography product depends on the physical and chemical properties of the adsorptive material, more commonly known as the stationary phase. The stationary phase is composed of primarily a self-supporting base matrix and interacting ligands coupled to the matrix surface. Historically, the inventions in chromatographic stationary phase media relate to the discovery of interacting ligands and matrix materials. Following Tswett's invention of chromatography in 1903 [Tswett et al., 1906], several researchers in the 1950s developed protein chromatography on new resin matrices. Chromatography was applied first to the separation of low-molecular-weight biochemical substances by Cohen [Cohn et al., 1946]. However, the complex requirements of protein separation such as high porosity, hydrophilic matrix surface and larger particle size led to the invention of several resin matrices.

Among several noteworthy inventions, cellulose-based ion exchanger [Peterson et al., 1954], cross-linked dextrans [Porath et al., 1959], polyacrylamide [Hjerten et al., 1961] and agarose [Hjerten et al., 1964] are viewed as the most revolutionary. Since these early works, inventions have been more focused on ligand discovery and matrix improvements. The discovery of the affinity interaction mechanism between Protein A

and immunoglobulins and the development of the Protein A chromatography purification method in the 1960s at Uppsala University, Sweden, brought a revolution in purification of monoclonal antibodies [Hjelm and Kronvall et al., 1972]— one of the most successful classes of therapeutic biomolecules. In order to keep pace with the increasing demands of the biotechnology industry for increased product throughput, manufacturers of chromatographic resins have developed myriad resins since 1960s [Curling et al., 2007]. In recent years, the advancements and developments of chromatography media are focused primarily on overcoming diffusion mechanism-based mass transfer limitations.

The rapid developments in biotechnology and the pharmaceutical potential of biomolecules have increased the demand of biopharmaceutical drugs exponentially. From 1980 to 1994, 29 new biologic entities were approved with an average time of 61 months from investigational new drug to licensure [Curling et al., 2007]. The Biotechnology Industrial Organization cites that 254 bio-tech based drugs were approved from 1982 to 2005 [Curling et al., 2007]. The therapeutic biomolecule market is driven primarily by recombinant protein and monoclonal antibody based drug products [Pavlou et al., 2004, 2005]. After the discovery of human recombinant protein by Eli Lilly in 1982, the recombinant DNA (rDNA) protein therapeutics sector has been at the center of the biopharmaceutical industry. The recombinant protein therapeutics market grew from $21,470 million in 2001 to $32,065 million in 2003. Specifically, 10 leading products saw their sales increase from $12,923 million in 2001 to $18,362 million in 2003, capturing 57% of the total market size. Five US (Amgen, Biogen IDEC, J & J, Eli Lilly and Schering Plough) and two European (Novo Nordisk and Roche) companies captured

75% market share. The recent report from Pavlou et al. [2005] suggested that the recombinant protein therapeutics market value would continue to grow from $34,807 million in 2004 to $53,150 million in 2010.

Following the success of recombinant proteins, therapeutic monoclonal antibodies (mAbs) represent the second wave of innovation created by the biotechnology industry during the past 20 years [Reichert et al., 2004; Walsh et al., 2006]. Between 2001 and 2002, the value of the global therapeutic mAb market grew by 37% to US $5.4 billion. Chimeric mAbs were the undisputed leaders, with 43% growth and US $3.8 billion in sales, followed by humanized mAbs with more than US $1.4 billion in sales and growth of 29%. Sellappan et al. [2007] reported that the sales of bio-based therapeutic products reached $90 billion in 2008. As of 2006, there were roughly 2,500 biotech-based drugs in the discovery phase, another 900 in preclinical trials, and more than 1,600 in clinical trials [Walsh et al., 2006].

Advent of the biotechnology era brought enormous expansion of chromatography applications as a primary tool of downstream processing of biologics. Revenues earned by chromatography products in the U.S. were estimated at $596.3 million in 2006, and the market is expected to continue growing through 2013 with estimated revenue to reach $1.018 billion at compound annual growth rate of 7.9% [Sellappan et al., 2007].

The cost of therapeutic proteins is significantly higher than traditional small molecule drugs. The small-molecule therapeutics manufactured using traditional chemical synthesis routes typically cost less than $5 g^{-1}. However, the cost of therapeutic proteins produced in cell-culture media ranges from $100 to $1000 g^{-1} depending upon

the drug type [Subramanian et al., 2007]. Higher dosages of several biotherapeutic drugs are not viable commercially due to the sky rocketing costs. Therefore, the advancements in the manufacturing processes of these therapeutic drugs are highly important to reduce the cost. In order to make the therapeutic bio-based drugs affordable, a reduction in manufacturing cost is required by a factor of 10−100, and this cost reduction is only possible by the optimization of upstream and downstream processes. Currently, for cell-derived products, the downstream processing costs represent 50−80% of the total production cost [Ghosh et al., 2003; Langer et al., 2007; Lightfoot et al., 2004; Low et al., 2007; Subramanian et al., 2007; Wurm et al., 2004]. Therefore, focus on improving the process economics of downstream separations by employing high-productivity and high-resolution separation techniques are essential to the biopharmaceutical industry.

The cost of upstream processing is inversely proportional to the product titer; therefore, the primary focus of the optimization in upstream processing is to increase the product titer in order to meet increasing demand for product. Due to advent of molecular biotechnology and engineered cell lines, the upstream processes have made unprecedented progress in the last decade. Therapeutic proteins with titer >5 g/L have become feasible in recent years [Langer et al., 2007; Wurm et al., 2004]. However, this success shifts the production burden to the downstream processing because the cost of downstream processing increases in proportion with the mass of product in the feed stream, not product titer. The study reported by Subramanian et al. [2007] suggests that increasing product titer to >5 g/L may increase the percentage of downstream processing cost up to 90%. There is, thus, enormous economic pressure to identify and employ a

high-throughput and high-resolution recovery and purification method that will enable the cost-effective production of the projected masses of protein therapeutics needed in the near term [Bhut et al., 2008, 2009, 2010].

1.3 Membrane chromatography: An alternative to resin column chromatography

Historically, resin-based chromatography has been a work horse for the biopharmaceutical industry. While effective and reliable, this unit operation has several limitations [Charcosset et al., 1998; Ghosh et al., 2002; Roper et al., 1995; Thommes et al., 1995; Zeng et al., 1999; Zhou et al., 2006]. The packed-bed resin column chromatography is a pressurized unit operation and the pressure drop across the column increases with operation due to media deformation or compression and pore blocking by accumulation of colloidal debris from the feed stream. In porous resins, the majority of binding sites (>90%) are located inside the pores of the resin [Belter et al., 1988]. Transport of biomolecules inside the small size pores of resin beads occurs primarily via an intraparticle diffusion mechanism. Diffusion is a relatively slower mode of transport; therefore, large residence times are required for effective utilization of resin binding sites, and the overall process time increases significantly. Taken together, resin column chromatography is a low throughput and relatively high pressure drop unit operation. Further, intraparticle diffusion-controlled transport through the resin pores leads to a residence time-dependent binding capacity. Thus, increasing flow velocity in an attempt to increase throughput is futile because the binding capacity of resins decreases with increasing flow velocity, particularly for larger biologics. The scale-up of a packed-bed

chromatography column requires adjustment of column aspect ratio to optimize binding capacity versus desired volumetric throughput. The separation resolution of a resin column increases with decreasing average particle size. However, decreasing the particle size of the resin leads to an increase in back pressure such that flow rates need to be decreased, again resulting in lower volumetric throughput. Short-circuiting due to flow channeling is a critical problem in resin column chromatography that results in the improper utilization of the adsorptive bed. These limitations combined with tremendous pressure from global competition and government regulations are forcing the biopharmaceutical industry to look for an alternative to resin column chromatography.
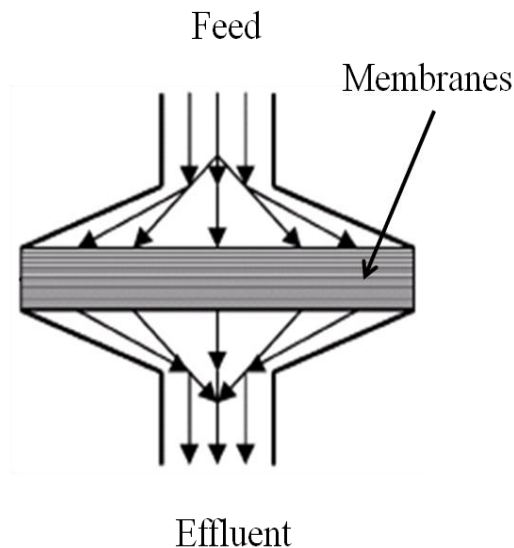
Scheme 1.1 Schematic representation of fluid flow in a membrane adsorber.

In recent years membrane chromatography has been promoted as a promising alternative to the conventional resin chromatography [Ghosh et al., 2002]. Membrane chromatography devices are composed of one or more micro-to-macroporous adsorptive

membranes in series packed into a membrane module (Scheme 1.1). Membrane chromatography devices often are termed 'membrane adsorbers' because of their primary separation mechanism. Microporous or macroporous membranes are derivatized using various surface chemistries to incorporate adsorptive moieties. Membrane chromatography modules are similar to standard filtration modules and exist in traditional flat or spiral-wound sheet and hollow fiber configurations [Roper et al., 1995]. The idea of membrane chromatography was introduced several years ago as a technology especially suited for large-scale processes — an unmet need of biotech and biopharmaceutical industries [Thommes et al., 1995; Zhou et al., 2006]. Since then many important academic publications have demonstrated the feasibility of the concept, describing the purification of various proteins using membrane chromatography.

Scheme 1.2 shows the basic mechanism of bind-and-elute mode membrane chromatography. In the first step, the membrane bed is equilibrated with low ionic strength application buffer. Next, the protein sample with specific concentration and constant flow rate is injected to membrane bed under adsorptive process conditions (e.g., loading net negatively charged protein to a positively charged anion-exchange membrane bed). Under such conditions, injected protein molecules bind to the chromatography media. As the adsorptive bed capacity is approached, un-adsorbed protein molecules begin to breakthrough and that generates a breakthrough curve. The bound proteins are fractionated using either ionic strength gradient or pH gradient. In my research, both methods were used to fractionate target proteins. The details about these experiments will be discussed in the Chapter 4.
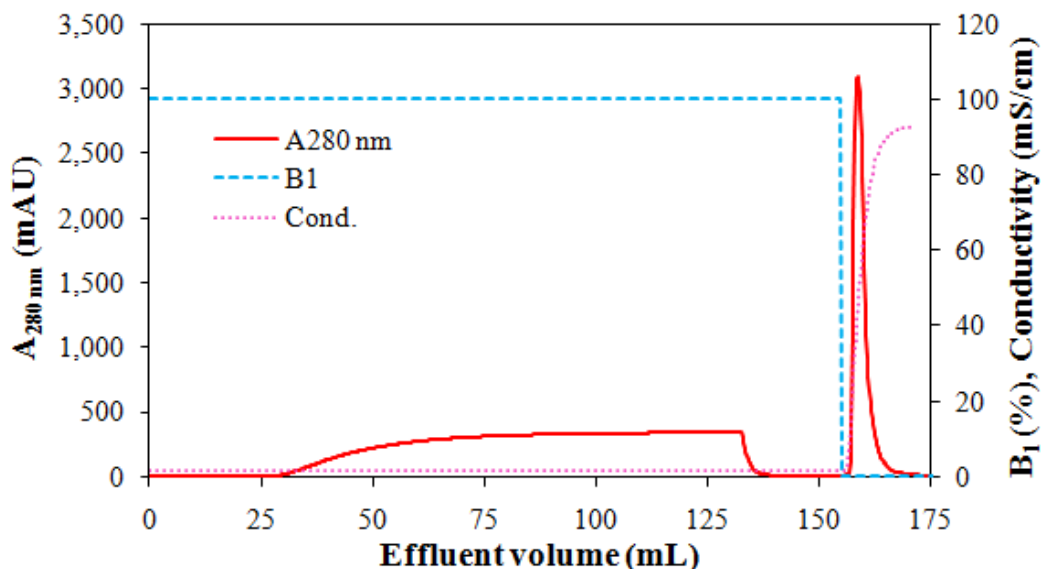
Scheme 1.2 Schemetic representation of bind-and-elute mode membrane chromatography (application buffer B_1: low ionic strength buffer; elution buffer E_1: high ionic stregth buffer). Solid line represents the absorbance. Dotted line represents conductivity. Dashed line represents the % of application buffer B_1.

Membrane chromatography offers several advantages over resin column chromatography. In macroporous membranes, biomolecule transport occurs primarily via convection; therefore, membrane chromatography is a high volumetric throughput unit operation. The dynamic protein binding capacity of macroporous membranes is independent of the linear flow velocity over a wide range; therefore, high volumetric flow rates can be used without loss of capacity. Membrane adsorbers with flow rate-independent dynamic capacities offer nearly linear scalability and flexibility of design parameters for large-scale operations. Membranes can handle highly concentrated feed streams, which reduces the cost of consumables [Lim et al., 2007]. Since the average pore size of macroporous membranes is much larger than resin beads, large size biopolymers

(IgG, DNA, virus) can access binding sites easily, and, hence, the dynamic binding capacities of membrane adsorbers for large biomolecules can be much higher than that of traditional beads [Singh et al., 2008]. For membranes with micron-sized pores, the mass loading capacity of these high molecular weight impurities increases with increasing size of the impurity [Etzel et al., 2006]. This trend directly contrasts that for resin particles, whereby large enough impurities do not access internal pores of the resin particles. As a result, these impurities bind only on the outer surface of the resin particles, resulting in low volumetric protein binding capacities [Endres et al., 2003]. In surface-functionalized membranes, adsorptive sites are in direct contact with the bulk flowing product stream; therefore, very high separation speed is achieved without compromising the separation resolution. Furthermore, the disposable and prepacked membrane chromatography modules offer a reduction in capital requirement, better process flexibility, and elimination of cleaning validation, packing and storage costs [Lim et al., 2007].

The advantages of membrane chromatography are being realized for polishing step purifications in the bioprocess separation train to remove trace level biological macromolecules such as DNA, RNA and virus particles. Specifically, anion-exchange membrane chromatography is gaining significant share at polishing step purification in flow-through mode of operation. The primary optimization parameter for efficient polishing step operation is the separation speed [Phillips et al., 2005]. Therefore, membranes with low-to-moderate binding capacity and high volumetric flow rate operability are ideal for polishing step purification. Indeed, membrane chromatography has been applied successfully at both the lab scale [Haber et al., 2004; Knudsen et al.,

13

2001; Yu et al., 2008] and large-scale [Deshmukh et al., 2000; Phillips et at., 2005; Zhou et al., 2006] to remove trace impurities (DNA, virus, host cell proteins).

Although the potential for membrane chromatography is great, the broader implementation of membrane chromatography in downstream capture step purification has been slow because membrane adsorbers have lower per volume protein binding capacities than resin columns. The lower binding capacity of a membrane adsorber is attributed to lower surface area per unit bed volume. This obstacle has been pointed out frequently as a bottleneck for the broader implementation of membrane chromatography [Ghosh et al., 2002; Klein et al., 2000; Van Reis et al., 2007; Zhou et al., 2008]. In consideration of membrane chromatography as a potential alternative technology to resin column chromatography for the purification of proteins from a bioreactor harvest, its advantages cited earlier often are overshadowed by the lower dynamic binding capacities. Among several efforts to improve the economic viability of membrane chromatography, increasing the volumetric adsorption capacity of membranes is the most essential effort. Therefore, a primary goal of this dissertation was to develop advanced weak and strong anion-exchange membranes with ultra-high and completely reversible protein binding capacities for membrane chromatography devices.

1.4 Preparation of adsorptive membranes using surface modification

Adsorptive chromatography membranes are composed of a microporous or macroporous, self-supporting membrane matrix and functional ligands attached to the internal pore surface of the matrix. The preparation process of an adsorptive membrane

can be divided into the preparation of the base membrane matrix and surface modification of the membrane matrix to incorporate the protein binding ligand [Roper et al., 1995; Zeng et al., 1999]. In my PhD research project, the concept was to surface modify commercial macroporous membranes used as the base membrane matrix. Therefore, the discussion will be focused on surface modification methods to incorporate adsorptive moieties onto the internal pore surface of a base membrane.

Selection of membrane support and method to incorporate the interactive ligand onto the membrane matrix are the most essential aspects in the design and development of an efficient adsorptive membrane for chromatographic separations [Roper et al., 1995; Zeng et al., 1999]. Following are the properties of an ideal membrane substrate for membrane chromatography: Membrane should be macroporous to allow high volumetric flow rate at relatively low transmembrane pressure. It should have a hydrophilic and neutral surface to prevent undesired interactions and thereby minimize nonspecific binding. It must contain a high density of functional groups to activate a wide variety of surface chemistries. Finally, it should have adequate mechanical strength and chemical resistivity, particularly to chemicals used in the surface modification and those used in membrane cleaning. Macroporous regenerated cellulose membranes with average pore diameter of 1 μm fulfills the criteria outlined here, and, therefore, they were selected as the base membrane substrate in my PhD research work. Flat sheet and hollow fiber are the most commonly used geometric configurations for membrane chromatography operations. In the case of flat-sheet membranes, a stack of several membranes or spiral wound designs are most common for use at the laboratory and large-scale operations. I

have used flat-sheet membranes stacked together to prepare adsorptive beds for membrane chromatography applications.

Many microporous or macroporous membranes are relatively inert and hydrophilic (cellulose) or hydrophobic (poly(vinylidene difluoride) (PVDF), polyethylene (PE), and polypropylene (PP)). These common examples must be modified to function as adsorptive chromatography membranes. A few commercial membranes (polysulfone (PS), poly(ether sulfone) (PES), polyamide (PA)) are hydrophilic and have ion-exchange surface functionality as the end groups of the polymer chains used to prepare the membrane; therefore, in theory, they can be used directly as adsorptive membranes. However, realistically, these end group functionalities are not sufficient to act as protein binding ligands because they are at low density and usually work as single point binding sites. Furthermore, macroporous membranes have 100-fold lower surface area than conventional process chromatography resins on a per volume basis [Bhut et al., 2010; Barrande et al., 2009; Dephillips et al., 2000; Wang et al., 2009]. Therefore, these membranes have to be modified to acquire a high density of functional groups, and, thus, high protein adsorption capacity.

Historically, two major methods have been employed to achieve this objective: coating and graft polymerization. The coating method is the most widely used and the simplest method to modify membrane matrices using functional polymers at industrial scale applications [Dileo et al., 2007; Hou et al., 2006; Kozlov et al., 2009; Wu et al., 2008]. Traditional coating techniques are dip coating, spray coating, meniscus coating and the like. In the coating method, the porous membrane substrate is wetted by polymer

16

or copolymer solution. The polymer coating is fixed on the membrane substrate by curing at high temperature or using a phase inversion method. There are several disadvantages of this traditional technology. The control over polymer coating film thickness is labor intensive and often requires the optimization of a large set of process parameters to achieve the desired thickness. Furthermore, it is difficult to control the pore size and pore-size distribution inside the polymer-coated membrane. Phase inversion is a complex phenomenan that often results in small size pores. As with resins, small pore sizes lead to high mass transfer resistances and limited accessibility of the biomolecules into the membrane pores [Dileo et al., 2007; Hou et al., 2006; Kozlov et al., 2009; Wu et al., 2008].

Incorporating adsorptive functionality onto the pore surface of the base membranes via polymer grafting is an active area of research for investigators seeking to prepare membrane adsorbers [Bhut et al., 2008, 2009; Hagiwara et al., 2005; He et al., 2008; Jain et al., 2007; Singh et al., 2005, 2008; Wang et al., 2009]. Grafted polymer chains extend into the protein solution that fills the membrane pores, providing a 3-dimensional 'scaffold' for protein molecules to adsorb and that leads to relatively high protein binding capacities. A variety of micro- to macroporous membranes has been modified with different strategies on the laboratory scale to produce membranes for bioseparations. In my PhD research work, surface-initiated graft polymerization was used to grow polymer chains from the base membrane surface by monomer addition. Following is the list of commonly used graft polymerization methods to modify the surface of porous membranes.

Radiation-induced graft polymerization via e-beam or γ-ray irradiation is used to prepare surface-modified membranes. Among several noteworthy approaches, Hagiwara et al. [2005] used radiation-induced graft polymerization to graft glycidyl methacrylate on porous polyethylene hollow-fiber membranes and performed subsequent chemical modifications to incorporate anion-exchange groups into these membranes for bioseparations. Kobayashi et al. [1993] prepared anion-exchange membranes by radiation-induced grafting of diethylaminoethyl methacrylate (DEAEMA) and vinyl pyridine (VP) onto the porous polyethylene hollow-fiber membrane. This method has several critical limitations. It creates surface functionality by excitation with high energy irradiation, which has low selectivity and can lead to scission of chemical bonds and ultimately degradation of the membranes.

Grafting of polymer onto the surface via plasma treatment is another widely used method to modify the surface of membranes. The central idea of this technique is to use a low pressure gas containing electrons, photons, ions and other charged species that create surface functionality without much alteration of bulk properties of the base membranes [Ulbricht et al., 1995, 2005; Wavhal et al., 2003]. The surface functionality generated by this method can be hydroxyl, amine, carboxyl or epoxy groups. These functional groups are relatively easy to use to graft polymer onto the surface of base membranes. Ulbricht et al. [2005] describes the excitation of polyacrylonitrile (PAN) ultrafiltration membranes with low temperature helium or helium/water plasma treatment and further graft polymerization to hydrophilize the surface of these membranes. One of the major drawbacks of plasma treatment is that it often results in the degradation of the base

polymeric substrate. The ablation etching of base membrane due to plasma treatment also results in the loss of polymeric base material and alteration of membrane morphology [Ulbricht et al., 2005].

Ultraviolet radiation-based photochemical grafting has been used frequently to prepare ion-exchange membranes. In most cases, a photoinitiator is used to create radicals necessary for initiating surface-graft polymerization. The photoinitiator can be excited selectively based on UV wavelength and that is the biggest advantage of this technique. A number of examples are outlined in the literature to graft polymer onto the membrane surface using this technique. Among many noteworthy approaches, Yusof et al., [2006] described photo-initiated, surface-selective graft polymerization to produce high-capacity (~80 mg lysozyme/mL) cation-exchange membranes for lysozyme purification. That same research group [He et al., 2008] recently produced strong anion-exchange membranes by UV photografting from hydrophilized PP membranes using a synergistic photoinitiator immobilization method that yielded high binding capacity for bovine serum albumin (BSA) (80 mg BSA/mL). The Belfort group at Rensselaer Polytechnic Institute and the Ulbricht group at University of Duisburg-Essen have done extensive work using this technique to modify membrane surfaces. While useful to produce a large number of binding sites, the control over the modification, as required to avoid pore blocking, is difficult using this method. As I highlight later in the dissertation, this lack of control is a significant drawback because the control over modification is also important to optimize the molecular architecture of grafted polymer chains [Bhut et al., 2008, 2009].

Atom Transfer Radical Polymerization (ATRP) is relatively a new method and has been used recently by our group and others for the surface modification of polymeric and inorganic membranes [Balachandra et al., 2003; Bhut et al., 2008, 2009; Friebe et al., 2007, 2009; Jain et al., 2007; Singh et al., 2005, 2008, 2008; Sun et al., 2006; Tomer et al., 2009]. ATRP is catalyst-activated, controlled polymerization technique that can be carried out at low temperature to prepare polymer chains with low polydispersity and precisely designed polymer architecture [Börner et al., 2002; Matyjaszewski et al., 2001]. ATRP allows relatively fine and independent control over grafting density and average molecular weight of polymer chains grafted from the surface of base membranes. Therefore, the ATRP process parameters could be used to increase the degree of polymer grafting, thus, the ion-exchange capacity, without blocking the membrane pores or drastic reduction in permeability. As a catalyst-activated process, ATRP can be done in-situ for pre-designed membrane chromatography modules without the concern of concurrent solution-phase polymerization [Bhut et al., 2008, Singh et al., 2005] and without the limitation of radiation-based methods that would require a transparent module housing.

Pertinent to the discussion of membrane adsorbers, Husson and co-workers have demonstrated the use of this technique to modify PVDF membranes, using polymerization time as independent variable to control pore size polydispersity and ion-exchange capacity [Singh et al., 2005]. They also described the use of surface-initiated ATRP to produce weak cation-exchange membranes functionalized by poly(acrylic acid) from the surface of the regenerated cellulose membranes [Singh et al., 2008]. Bruening and co-workers described the use of ATRP to incorporate immobilized metal ion affinity

functionalities within porous alumina membranes [Balachandra et al., 2003; Jain et al., 2007; Sun et al., 2006]. The primary focus of my PhD research was to design and develop unique surface-initiated ATRP protocols to coat base membrane substrates with ultrathin polymer film. Specifically, the objective was to graft polymers with tertiary and quaternary amine functionalities to prepare weak and strong anion-exchange membranes with benchmark performance properties for downstream chromatographic bioseparations.

1.5 Surface-initiated atom transfer radical polymerization

Grafting of polymer on the pore surface of a base membrane can be achieved using "grafting to' and "grafting from" methods. In grafting to approaches, as shown in Scheme 1.3(A), the polymer chains are grown in advance and then attached to the surface using physisorption or covalent coupling chemistry between the surface functionality of base membrane and reactive end groups of the preformed polymer chains [Edmondson et al., 2004; Toomey et al., 2004]. The primary advantage of this technique is that the polymer chains can be characterized fully and their molecular architecture can be controlled precisely prior to the grafting onto the surface. However, this method generally leads to a relatively lower grafting density of polymer chains. The macromolecular size of the polymer chains requires long times (e.g., weeks) to reach equilibrium. In additional to this kinetic drawback, the steric hindrance caused by already attached polymer chain resists the attachment of new polymer chains. This condition is thermodynamically unfavorable because the addition of more chains would require stretching of neighboring

21

attached polymer chains (i.e., decrease in entropy). This leads to a consequence that high

grafting density comes at the expense of lower polymer film thickness and vice versa.

In "grafting from" approaches, the polymer chains are grown from the surface of

base membrane by addition of monomer molecules from the solution using surface-

initiated polymerization, as depicted in Scheme 1.3(B). This approach leads to relatively

higher grafting density of polymer chains. Also, this method offers independent control

of polymer chain grafting density and polymer layer thickness because monomer

molecules are added as the polymerization reaction proceeds [Zhao et al., 2000].

Furthermore, the "grafting from" approach can be used to graft polymer with wide

variety of functionality since the attachment of chains to the surface is not limited by end

group functionality. In my PhD research, I have used the "grafting from" approach to

incorporate the adsorptive functionalities onto the pore surfaces of commercially

available regenerated cellulose membranes.
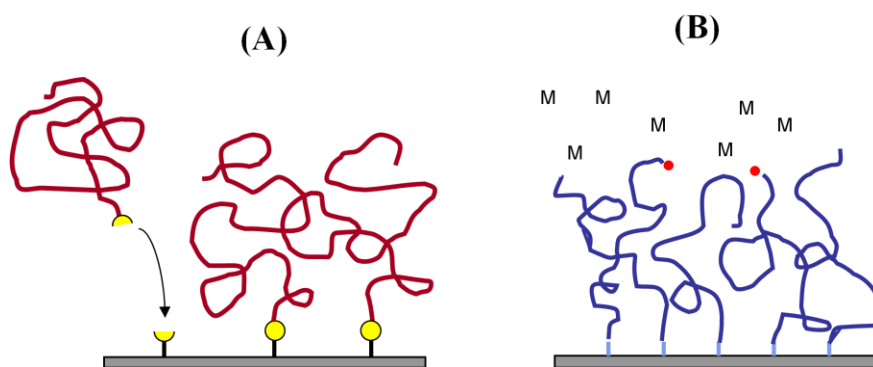
Scheme 1.3 Schematic representation of two different approaches to graft polymer chains on a membrane substrate. (A): Grafting to, (B): Grafting from. Permission to reproduce was provided by Dr. S. M. Husson.

Surface-initiated polymerization methods include conventional free radical [Prucker

et al., 1998; Schmidt et al., 2002], anionic [Jordan et al., 1999] and cationic [Jordan et al.,

22

1998] polymerizations. The reversible addition-fragmentation chain-transfer radical polymerization (RAFT) [Baum et al., 2002], nitroxide-mediated radical polymerization (NMRP) [Bartholome 2003; Matyjaszewski et al., 1999], photoiniferter-mediated photopolymerization (PMP) [Rahane et al., 2005, 2008] and atom transfer radical polymerization (ATRP) [Matyjaszewski et al., 1999; Zhao et al., 2000] are relatively newer and 'controlled' polymerization methods to graft polymer chains using surface-initiated polymerization. The research work outlined here is focused on the use of ATRP to graft polymer nanolayers from the pore surfaces of regenerated cellulose membranes. The Husson group uses surface-initiated ATRP extensively to graft polymer thin films from porous and non-porous substrates, including membrane substrates [Bhut et al., 2008, 2009; Singh et al., 2005, 2008, 2008, Tomer et al., 2009].
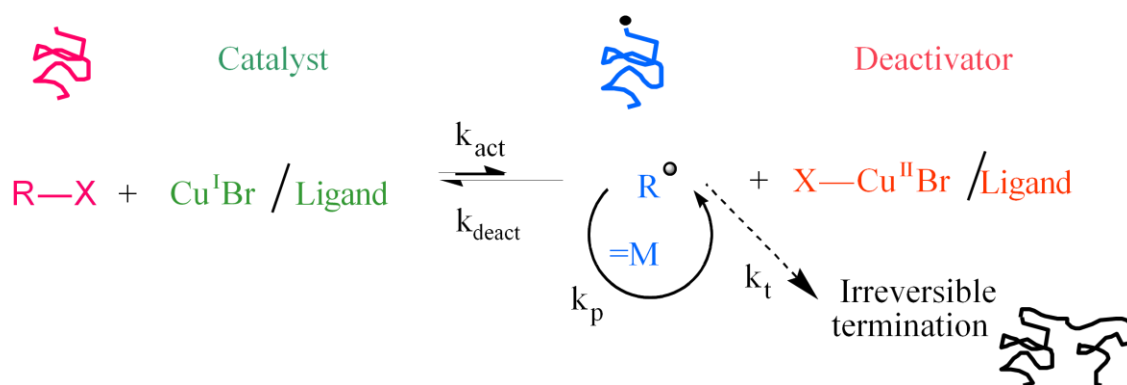
Scheme 1.4 General mechanism of atom transfer radical polymerization. Permission to reproduce was provided by Dr. S. M. Husson.

ATRP is a controlled radical polymerization technique. Scheme 1.4 represents the general mechanism of ATRP. A typical ATRP system consists of an initiator, a transition metal complex comprising a metal halide and a ligand, solvent(s) and monomer. During

the process, the transition metal complex, also called catalyst, undergoes one electron oxidation by abstraction of halogen atom X from the dormant species R-X. This process creates an active radical and transition metal complex in a higher order oxidation state. The process proceeds with an equilibrium rate constant K calculated as the quotient of activation (k_{act}) and deactivation (k_{deact}) constants. The dormant species (R-X) are initiator molecules at the beginning of the reaction (time t = 0) and dormant polymer chain at any time during the polymerization (time t = t). The active radical reacts with monomer from the solution and polymerization proceeds with the same mechanism as conventional radical polymerization. The radicals or active polymer chains may also react with another unsaturated species and can undergo irreversible bimolecular termination. The uniqueness of ATRP is that the equilibrium is shifted toward dormant species by maintaining very low equilibrium rate constant K ($k_{deact} \gg k_{eact}$). Therefore, a very low number of radicals or growing polymer chains are present at any instant during polymerization, and, because of that, the possibility of irreversible termination is minimized. A well-controlled ATRP protocol yields polymer with a low percentage of terminated polymer chains. During ATRP, the growing or active polymer chains are deactivated reversibly to the dormant species and again to the active chains. This feature allows the growth of polymer chains slowly and uniformly [Matyjaszewski et al., 2001].

Higher degrees of polymer grafting from the internal pore surface of the base membrane lead to reduced average pore size, and, thereby, membrane permeability. However, a high degree of polymer grafting is necessary to design membranes with high protein adsorption capacity. Thus, the trade-off between permeability and adsorption

24

capacity exists for surface-modified adsorptive membranes. Surface-initiated ATRP allows precise control over the degree of polymer grafting to design chromatography membranes with optimum performance properties. Surface-initiated ATRP was employed as the primary tool in my doctoral research to accomplish the goal of designing high-performance anion-exchange chromatography membranes.

1.6 Adsorptive membrane characterization

In general, membranes can be classified in two main groups: porous and nonporous. The term 'porous' is used for both ultrafiltration and micro- to macrofiltration membranes with pore diameters of roughly 10 nm and larger. In my doctoral research work, regenerated cellulose macrofiltration membranes were used as base membrane support matrix. The pore diameter of the membranes was between 0.1 to 2 μm with majority of pores in the range of 0.8 to 1.2 μm.

Membrane physicochemical characterization leads to the determination of structural, morphological and functional properties of base membrane supports and surface-modified membranes [Bhut et al., 2008; He at al., 2008; Roper et al., 1995; Wang at al., 2009]. Structure related properties include the average pore size and pore-size distribution. Morphological properties include the visualization of pore structure and surface topology. Characterization of functional properties may include chemical functionality and surface properties such as hydrophilicity or hydrophobicity. I have used Scanning Electron Microscopy (SEM), Atomic Force Microscopy (AFM) and Attenuated Total Reflection Fourier-Transform Infrared Spectroscopy (ATR-FTIR) techniques for

the characterization of physicochemical properties. ATR-FTIR was used to provide information on the change in surface functionality of polymer-grafted membranes. SEM was used to investigate the effect of surface modification on the membrane pore morphology. AFM was used to visualize the surface topology and to obtain surface roughness values of unmodified and polymer-modified cellulose membranes.

Permeability of adsorptive membranes is important parameter for their application as a chromatography media. Permeability of a membrane bed is measured by flowing a specific liquid through the membrane bed. For adsorptive chromatography membranes, buffer solutions are used to measure the permeability. Flux through the membrane bed can be described by Darcy's law, which states that the flux (J) through the membrane is proportional directly to the applied pressure (ΔP).

$$J = A \times \Delta P \tag{1.1}$$

A is the permeability constant, which depends on porosity, viscosity and pore geometry (pore size and pore-size distribution). Among several equations developed to characterize the flow through porous membrane bed, Hagen-Poiseuille and Kozeny-Carman equations are used most commonly [Mulder et al., 1996]. The aim of measuring flow through an adsorptive chromatography membrane is to obtain the relationship between applied pressure and flux [Bhut et al., 2008; He et al., 2008; Jain et al., 2007; Singh et al., 2008, 2008; Sun et al., 2006, Wang et al., 2009]. As mentioned earlier, most chromatography membranes are surface modified to increase the adsorption capacity. However, polymer grafting leads to a reduction in pore size, and, thereby, the flux through membranes. Flux is widely used to evaluate the effect of polymer coating on the average pore size of

membrane. Bhut et al. [2009] measured flux of surface-modified membranes to demonstrate that increasing degree of polymer grafting led to a decrease in the permeability of modified membranes. He et al. [2008] described the effect of salt contraction on the permeability of phosphate buffer solution through anion-exchange membranes. Wang et al. [2009] measured permeability to study the effect of salt concentration and degree of polymer grafting on the flux through polymer grafted membranes.

As described in the Section 1.3, adsorption capacity is the most important feature to assess the viability of membrane chromatography for large-scale applications. Adsorption capacity of any chromatography media is reported as static (equilibrium) and dynamic binding capacities. Static binding capacity is the maximum amount of protein bound to the chromatography media. Static binding capacity is measured by incubating chromatography media into the protein solution for enough time to saturate the binding sites [Bhut et al., 2010; Knudsen et al., 2001; Wang et al., 2009]. Dynamic binding capacity describes the amount of protein that binds to the chromatography media under flow-through process conditions. Dynamic binding capacity of adsorptive columns depends on the flow velocity, sample preparation (e.g., protein concentration and type, buffer composition, concentration and type) and properties of the mobile phase. Dynamic binding capacity is determined by loading a protein sample with specific concentration and constant flow rate under adsorptive process conditions (e.g., loading net negatively charged protein to a positively charged anion-exchange membrane bed). Under such conditions, injected protein molecules bind to the chromatography media. As the

adsorptive bed capacity is approached, un-adsorbed protein molecules begin to breakthrough and that generates a breakthrough curve [Etzel et al., 2006; Haber et al., 2004; Knudsen et al., 2001; Phillips et al., 2005; Zhou et al., 2006, 2008]. Binding capacity is reported frequently as the amount of protein bound to the adsorptive bed (mg) divided by the adsorptive bed volume (mL). The relationship between flow velocity and dynamic binding capacity is the most useful and often is measured as the first step to screen chromatography media for separation of specific biomolecules [Knudsen et al., 2001; Urthaler et al., 2005; Syrén et al., 2007]. In my research, I have used protein binding capacity measurements extensively to evaluate the effects of my surface-initiated graft polymerization protocol and chromatography process parameters on the binding capacities of newly designed surface-modified membranes.

1.7 Downstream bioseparation using membrane chromatography

The interactions of biomolecules with the stationary phase in membrane chromatography are identical to those in the packed-bed resins, when using the same functional group chemistry. The basic difference between the two stationary phase platforms is that membrane chromatography uses a self-supporting membrane as the base matrix, whereas traditional resin chromatography uses a resin bead as the base matrix. Oftentimes, the protein binding ligands are the same for membrane and resin column chromatography [Ahuja et al., 2000; Shukla et al., 2007]. Many successful applications of membrane chromatography using affinity (e.g., Protein A, protein G, metal ion ligand) [Yu et al., 2008], ion-exchange (e.g., anion, cation) [Bhut et al., 2010; Gottschalk et al.,

28

2004, 2005; Lim et al., 2007] and hydrophobic interactions are reported in the literature [Kuczewski et al., 2010]. My PhD research focused on ion-exchange membrane chromatography, thus, the following discussion will be limited to this type of membrane chromatography.

Membrane anion- and cation-exchange chromatography has been applied successfully at capture, intermediate and polishing stages. Among several noteworthy applications, the following are the most relevant to the research work carried out in my PhD studies. Membrane chromatography has been applied successfully at both the lab scale [Haber et al., 2004; Knudsen et al., 2001; Yu et al., 2008] and large-scale [Deshmukh et al., 2000; Phillips et at., 2005; Zhou et al., 2006] to remove trace impurities (DNA, virus, host cell proteins), also called polishing step purifications. Teeters et al. [2003, 2004] demonstrated that the dynamic binding capacity of plasmid DNA was higher for a membrane adsorber than a resin column. Knudsen et al. [2001] proved that the anion-exchange membrane chromatography is a reasonable alternative to resin column chromatography for the removal of trace level impurities. Haber et al. [2004] studied the effects of flow velocity and feed concentration on dynamic binding capacity of plasmid DNA. Anion-exchange membranes gave base-line separation of plasmid DNA isomers and higher dynamic binding capacity than a resin column with the same quaternary amine chemistry. Zhou et al. [2006, 2008] conducted a comprehensive cost analysis to demonstrate that membrane chromatography is a viable alternative to column chromatography as a polishing step to remove trace impurities from protein solution for process-scale antibody production.

Despite the success of membrane adsorbers in bioprocess polishing steps, broad implementation of membrane chromatography in bioprocess capture steps has been slow because commercial membrane adsorbers have lower per volume protein binding capacities than resin columns. However, the literature contains a number of examples of protein purification using membrane chromatography with commercial ion-exchange membranes. Suck et al. [2006] demonstrated the application of membrane chromatography for separation of two model proteins, human serum albumin (HSA) and immunoglobulin G (IgG). That same group used anion-exchange membrane chromatography to separate enzyme penicillin acylase from the crude *Escherichia coli* supernatant. Santarelli et al. [1998] reported the separation of IgM from the supernatant of a human hybridoma cell culture using membrane ion-exchange chromatography. The volumetric flow rate effects on separation resolution, recovery and capacity also were studied using model binary protein mixtures. Ghosh and coworkers [Yu et al., 2008] used cation-exchange and Protein A affinity-based membrane chromatography methods for the primary capture and preliminary purification of an anti-*Pseudomonas aerugenosa* O6ad human IgG1 monoclonal antibody from transgenic tobacco. Based on resolution and recovery comparisons, they demonstrated that using a combination of the cation-exchange and Protein A membrane chromatography, in that order, separation with both high purity and recovery was achieved at high volumetric throughput. In separate research [Yu et al., 2008] they also demonstrated that cation-exchange chromatography can be considered as a viable alternative to Protein A-based chromatography for the purification of mAbs.

However, comparisons of membrane and resin chromatography for separation of recombinant proteins from complex bio-mixtures (e.g., cell lysate, plant extract) are rare in the literature, particularly at the preparative scale. Deshmukh et al. [2000] compared the separation performance of a resin column and membrane adsorber for the fractionation of antisense oligonucleotides and found that the separation performance was similar for both stationary phases. The comparison was reported based on a single experiment. Kreuß et al. [2008] reported detailed comparison of a commercial membrane adsorber and resin columns and found that the membrane adsorber offers significantly higher separation speed, but the dynamic binding capacity and resolution were lower than resin columns for the fractionation of glycosylated and non-glycosylated caseinomacropeptide.

The separation properties of membrane adsorbers depend on the surface-modification protocol to prepare these membrane adsorbers. The idea of my PhD research was to increase volumetric protein binding capacities of membrane adsorbers and, at the same time, maintain and demonstrate the high-throughput and high separation resolution for separation of a target protein from a complex bio-mixture. Therefore, one of the objectives of my PhD research was to report a case study on the detailed comparison of our newly designed membrane adsorber with a commercial membrane adsorber and resin column to separate a therapeutic target protein from *E. coli* cell lysate under preparative scale conditions.

1.8 Outline of the dissertation

The research work performed in this dissertation is organized in four individual projects and they are defined as chapters. Chapter 2 describes the preparation of weak anion-exchange membranes using surface-initiated atom transfer radical polymerization for chromatographic bioseparations. The objective of this study was to design and execute a two-step surface modification protocol to graft polymer with weak anion-exchange functionality from the internal pore surfaces of commercial regenerated microporous membranes. Surface-initiated atom transfer radical polymerization was used to graft poly(2-dimethylaminoethyl methacrylate), (poly(DMAEMA)), nanolayers from the pore surfaces of cellulose membranes. Chapter 2 also describes the characterization of physicochemical and performance properties of newly designed, surface-modified membranes using various analytical techniques.

Chapter 3 describes the preparation of weak anion-exchange membranes with exceptionally high and completely reversible protein binding capacity. The goals of this research work were to increase the dynamic protein adsorption capacities significantly (compared to initial work in Chapter 2) and to characterize the protein chromatography performance properties of the newly designed membranes. Grafting density and average molecular weight of polymer chains grown from the membrane pore surfaces were used as independent process variables to prepare surface-modified weak anion-exchange membranes with ultra-high and completely reversible dynamic binding capacity. The effects of polymer grafting density, average molar mass of polymer, linear flow velocity and buffer ionic strength on dynamic binding capacity were studied.

In Chapter 4, the protein separation performance of our newly designed chromatography membranes was evaluated and it was correlated to the transport properties of the membrane adsorber. The objectives of this study were to evaluate and compare the protein separation performance of our newly designed weak anion-exchange membrane adsorber with a commercial membrane adsorber and to compare the protein separation performance of membrane chromatography with resin column chromatography. Anion-exchange chromatography (AEC) was used to separate anthrax protective antigen (PA) protein from periplasmic *E. coli* lysate. AEC was used under bind-and-elute mode of separation and two comprehensive sets of data were collected using salt gradient and pH-gradient elution. The separation performance was evaluated based on visual inspection of the chromatogram, sodium dodecyl sulfate-polyacrylamide gel electrophoresis (SDS-PAGE) analysis of effluent fractions, and purity and recovery data obtained using densitometric analysis of the SDS-PAGE gels. Effects of process variables, sample load volume and volumetric flow rate, on the separation resolution of the membrane adsorbers were studied.

Chapter 5 provides a systematic evaluation of the role of polymer molecular architecture on the separation performance of surface-modified, strong anion-exchange membranes. The objective of this research was to investigate the effect of high degree of polymer grafting on the mass transfer resistances and accessibility of large biomolecules (IgG, DNA) and virus particles during bind-and-elute chromatography. Surface-initiated atom transfer radical polymerization was used to graft poly([2-(methacryloyloxy)ethyl]trimethylammonium chloride), (poly(MAETMAC)), nanolayers

from the internal pore surface of commercial regenerated cellulose membranes. The effect of polymer chain density on the accessibility of IgG and DNA was studied by measuring dynamic binding capacities of surface-modified membranes. Specifically, the effect of linear flow velocity on dynamic binding capacity was studied to determine the predominant mode of the mass transport and accessibility limitations.

Chapter 6 summarizes the conclusions of my doctoral research work and gives recommendations for future study.

1.9 References

Ahuja, S., Handbook of bioseparations, Vol. 2 (Separation Science and Technology), Academic Press, San Diego, CA, 2000.

Arunakumari, A., Wang, J., Ferreira, G., Alternatives to protein A: Improved downstream process design for human monoclonal antibody production, BioPharm. Int. 20(2), (2007) 36–40.

Balachandra, A. M., Baker, G. L., Bruening, M. L., Preparation of composite membranes by atom transfer radical polymerization initiated from a porous support, J. Membr. Sci. 227 (2003) 1-14.

Barrande, M., Beurroies, I., Denoyel, R., Tatarova, I., Gramblička, M., Polakovič, M., Joehnck, M., Schulte, M., Characterisation of porous materials for bioseparation, J. Chromatogr. A 1216 (2009) 6906-6919.

Bartholome, C., Beyou, E., Bourgeat-Lami, E., Chaumont, P., Zydowicz, N., Nitroxide-mediated polymerizations from silica nanoparticle surfaces: "Graft from" polymerization of styrene using a triethoxysilyl-terminated alkoxyamine initiator, Macromol. 36 (2003) 7946-7952.

Baum, M., Brittain, W. J., Synthesis of polymer brushes on silicate substrates via reversible addition fragmentation chain transfer technique. Macromol. 35 (2002) 610-615.

Belter, P.A., Cussler, E.L., Hu, W.S., eds., Bioseparations: Downstream processing for biotechnology, Wiley, New York, 1988.

Bhut, B. V., Christensen, K. A., Husson, S. M., Membrane chromatography: Protein purification from *E. coli* lysate using newly designed and commercial anion-exchange stationary phases, J. Chromatogr. A (2010) doi:10.1016/j.chroma.2010.05.049.

Bhut, B. V., Husson, S. M., Dramatic performance improvement of weak anion-exchange membranes for chromatographic bioseparations, J. Membr. Sci. 337 (2009) 215-223.

Bhut, B. V., Wickramasinghe, S. R., Husson, S. M., Preparation of high-capacity, weak anion-exchange membranes for protein separations using surface-initiated atom transfer radical polymerization, J. Membr. Sci. 325 (2008) 176-183.

Börner, H. G., Duran, D., Matyjaszewski, K., Silva, M. D., Sheiko, S. S., Synthesis of molecular brushes with gradient in grafting density by atom transfer radical polymerization, Macromol. 35 (2002) 3387–3394.

Charcosset, C., Purification of proteins by membrane chromatography, J. Chem. Technol. Biotechnol. 71 (1998) 95-110.

Cohn, E. J., Strong, L. E., Hughes, W. L., Jr., Mulford, D. J., Ashworth, J. N., Melin, M., and Taylor, H. L., Preparation and properties of serum and plasma proteins. IV. A system for the separation into fractions of the protein and lipoprotein components of biological tissues and fluids. J. Am. Chem. Soc. 68 (1946) 459-475.

Curling, J., Gottschalk, U., Process chromatography: Five decades of innovation. BioPharm. Int. 20 (2007) 10-19.

DePhillips, P., Lenhoff, A. M., Pore size distributions of cation-exchange adsorbents determined by inverse size-exclusion chromatography, J. Chromatogr. A 883 (2000) 39-54.

Deshmukh, R. R., Warner, T. N., Hutchison, F., Murphy, M., Leitch II, W. E., Leon, P. D., Srivatsa, G. S., Cole, D. L., Sanghvi, Y. S., Large-scale purification of antisense oligonucleotides by high-performance membrane adsorber chromatography, J. Chromatogr. A 890 (2000) 179-192.

Dileo, A. J., McCue, J., Moya, W., Quinones-Garcia, Socie, N. P., Thom, V., Yuan, S., Porous adsorptive or chromatographic media, U.S. Patent, US 2007/0256970 A1, 2007.

Edmondson, S., Osborne, V. L., Huck, W. T. S., Polymer brushes via surface-initiated polymerization. Chem. Soc. Rev. 33 (2004) 14-22.

Endres, H. N., Johnson, J. A. C., Ross, C. A. , Welp, J. K., Etzel, M. E., Evaluation of anion-exchange membrane for the purification of plasmid DNA, Biotechnol. Appl. Biochem. 37 (2003) 259–266.

Etzel, M. E., Riordan, W., Membrane chromatography: analysis of breakthrough curves and viral clearance, in: Shukla, A. A., Etzel, M. E., Gadam, S., (Eds.), *Process scale bioseparations for the biopharmaceutical industry*, Taylor & Francis, Boca Raton, FL, 2006.

Follman, D. K., Fahrner, R. L., Factorial screening of antibody purification processes using three chromatography steps without protein A, J. Chromatogr. A 1024 (2004) 79–85.

Friebe, A., Ulbricht, M., Controlled pore functionalization of poly(ethylene terephthalate) track-etched membranes via surface-initiated atom transfer radical polymerization, Langmuir 23 (2007) 10316-10322.

Friebe, A., Ulbricht, M., Cylindrical pores responding to two different stimuli via surface-initiated atom transfer radical polymerization for synthesis of grafted diblock copolymers, Macromol. 42 (2009) 1838-1848.

Ghosh, R., Protein bioseparation using ultrafiltration: Theory applications and new developments, Imperial College Press, 2003.

Ghosh, R., Protein separation using membrane chromatography: opportunities and challenges, J. Chromatogr. A 952 (2002) 13–27.

Gosse M. E., Manocchia M., The first biopharmaceuticals approved in the United States: 1980–1994. Drug Information J. 30 (1996) 991–1001.

Gottschalk, U., Fischer-Fruehholz, S., Reif, O., Membrane adsorbers—A cutting edge process technology at the threshold. Bioprocess Int. 5 (2004) 56–65.

Gottschalk, U., Downstream processing of monoclonal antibodies: From high dilution to high purity, Biopharm. Int. 18 (2005) 42-58.

Haber, C., Skupsky, J., Lee, A., Lander, R., Membrane chromatography of DNA: conformation-induced capacity and selectivity, Biotech. Bioeng. 88 (2004) 26-34.

Hagiwara, K., Yonedu, S., Saito, K., Shiraishi, T., Sugo, T., Tojyo, T., Katayama, E., High performance purification of gelsolin from plasma using anion-exchange porous hollow-fiber membrane, J. Chromatogr. B 821 (2005) 153–158.

He, D., Ulbricht, M., Preparation and characterization of porous anion-exchange membrane adsorbers with high protein-binding capacity, J. Membr. Sci. 315 (2008) 155–163.

Hjelm, H., Hjelm, K., Sjoquist, J., Protein A from Staphylococcus aureus. Its isolation by affinity chromatography and its use as an immunosorbent for isolation of immunoglobulins. FEBS Lett. 28(1), (1972) 73–76.

Hjertén S. Agarose as an anticonvection agent in zone electrophoresis. Biochim Biophys Acta. 53 (3), (1961) 514–517.

Hjertén S. The preparation of agarose spheres for the chromatography of molecules and particles. Biochim Biophys Acta. 79 (1964) 393–398.

Hou, C. J., Konstantin, P., Yang, Y., Negatively charged membrane, US 7132049 B, 2006

Jain, P., Sun, L., Dai, J., Baker, G. L., Bruening, M. L., High-capacity purification of his-tagged proteins by affinity membranes containing functionalized polymer brushes, Biomacromol. 8 (2007) 3102–3107.

Jordan, R., Ulman, A., Kang, J. F., Rafailovich, M. H., Sokolov, J., Surface-initiated anionic polymerization of styrene by means of self-assembled monolayers. J. Am. Chem. Soc. 121 (1999) 1016-1022.

Jordan, R., Ulman, A., Surface-initiated living cationic polymerization of oxazolines. J. Am. Chem. Soc. 120 (1998) 243-247.

Klein, E., Affinity membranes: a 10-year review, J. Membr. Sci. 179 (2000) 1–27.

Knudsen, H. L., Fahrner, R. L., Xu, Y., Norling, L. A., Blank, G. S., Membrane ion-exchange chromatography for process-scale antibody purification, J. Chromatogr. A 907 (2001) 145-154.

Kreuß, M., Krause, I., Kulozik, U., Separation of a glycosylated and non-glycosylated fraction of caseinomacropeptide using different anion-exchange stationary phases, J. Chromatogr. A 1208 (2008) 126-132.

Kobayashi, K., Tsuneda, S., Saito, K., Yamagishi, H., Furusaki, S., Sugo, T.V., Preparation of microfiltration membranes containing anion-exchange groups, J. Membr. Sci. 76 (1993) 209–218.

Kozlov, M., Media for membrane ion-exchange chromatograph, U.S. Patent, US 2009/0130738 A1, 2009.

Kronvall, G., A surface component in group A, C, and G streptococci with non-immune reactivity for immunoglobulin. G, J. Immunol. 111 (1973) 1401–1406.

Kuczewski, M., Fraud, N., Faber, R., Zarbis-Papastoitsis, G., Development of a polishing step using a hydrophobic interaction membrane adsorber With a PER.C6$^{®}$-derived recombinant antibody, Biotechnol. Bioeng. 105 (2010) 296-305.

Langer, E.S., Downstream production challenges in 2007: Study indicates problems may not be resolved before 2011, Biopharm. Int. 5(6), (2007) 22-28.

Lightfoot, E. N., Moscariello, J. S., Bioseparations, Biotechnol. Bioeng. 87 (2004) 259–273.

Lim, J. A. C., Sinclair, A., Kim, D. S., Gottschalk, U., Economic benefits of single-use membrane chromatography in polishing - A cost of goods model, BioProcess Int. 5(2), (2007) 60–64.

Low, D., O'Leary, R., Pujar, N. S., Future of antibody purification, J. Chromatogr. B 848 (2007) 48–63.

Matyjaszewski, K., Miller, P. J., Skukla, N., Immaraporn, B., Gelman, A., Luokala, B. B., Siclovan, T. M., Kickelbick, G., Vallant, T., Hoffmann, H., Pakula, T., Polymer at interfaces: Using atom transfer radical polymerization in the controlled growth of homopolymers and block copolymers from silicon surfaces in the absence of untethered sacrificial initiator. Macromol. 32 (1999) 8716-8724.

Matyjaszewski, K., Xia, J., Atom transfer radical polymerization, Chem. Rev. 101 (2001) 2921–2990.

Mulder, M., Basic principles of membrane technology, (2nd Edition), Kluwer Academic, The Netherlands, 1996.

Pavlou, A. K., Reichert, J. M., Recombinant protein therapeutics—success rates, market trends and values to 2010, Nat. Biotechnol. 22 (2004) 1513–1519.

Pavlou, A. K., Belsey, M. J., The therapeutic antibody market to 2008, Eur. J. Pharm. Biopharm. 59 (2005) 389–396.

Peterson, E. A., Sober, H. A., Chromatography of proteins. I Cellulose ion-exchange adsorbents. J. Am Chem Soc. 76 (1954) 751–755.

Phillips, M., Cormier, J., Ferrence, J., Dowd, C., Kiss, R., Lutz, H., Carter, J., Performance of a membrane adsorber for trace impurity removal in biotechnology manufacturing, J. Chromatogr. A 1078 (2005) 74-82.

Porath, J., Flodin, P., Gel filtration: A method for desalting and group separation, Nature 183 (1959) 1657-1659.

Prucker, O., Rühe, J., Synthesis of poly(styrene) monolayers attached to high surface area silica gels through self-assembled monolayers of azo initiators. Macromol. 31 (1998) 592-601.

Rahane, S. B., Kilbey II, S. M., Metters, A. T., Kinetic modeling of surface-initiated photoiniferter-mediated photopolymerization in presence of tetraethylthiuram disulfide, Macromolecul. 41 (2008) 9612-9618.

Rahane, S. B., Kilbey II, S. M., Metters, A. T., Kinetics of surface-initiated photoiniferter mediated photopolymerization, Macromolecul. 38 (2005) 8202-8210.

Reichert, J. M., Pavlou, A. K., Monoclonal antibodies market, Nature Rev. 3 (2004) 383-384.

Van Reis, R., Zydney, A. L, Bioprocess membrane technology, J. Membr. Sci. 297 (2007) 16-50.

Roper, K. D., Lightfoot, E. N., Separation of biomolecules using adsorptive membranes, J. Chromatogr. A, 702 (1995) 3-26.

Santarelli, X., Domergue, F., Clofent-Sanchez, G., Dabadie, M., Grissely, R., Cassagne, C., Characterization and application of new macroporous membrane ion exchangers, J. Chromatogr. B 706 (1998) 13-22.

Schmidt, R., Zhao, T., Green, J. B., Dyer, D. J., Photoinitiated polymerization of styrene from self-assembled monolayers on gold. Langmuir 18 (2002) 1281-1287.

Sellappan, S., BioMarket trends: Liquid chromatography market proliferates, Gen. Eng. Biotechnol. News, 27 (2007) 19.

Shukla, A. A., Etzel, M. R., Gadam, S., Process scale bioseparations for the biopharmaceutical industry, CRC Press, Boca Raton, FL, 2007.

Singh, N., Chen, Z., Tomer, N., Wickramasinghe, S. R., Soice, N., Husson, S. M., Modification of regenerated cellulose ultrafiltration membranes by surface-initiated atom transfer radical polymerization, J. Membr. Sci. 311 (2008) 225–234.

Singh, N., Husson, S. M., Zdyrko, B., Luzinov, I., Surface modification of microporous PVDF membranes by ATRP, J. Membr. Sci. 262 (2005) 81–90.

Singh, N., Wang, J., Ulbricht, M., Wickramasinghe, S. R., Husson, S. M., Surface-initiated atom transfer radical polymerization: a new method for the preparation of polymeric membrane adsorbers, J. Membr. Sci. 309 (2008) 64–72.

Subramanian, G., Bioseparation and bioprocessing, 2nd ed., Wiley-VCH, Weinheim, 2007.

Suck, K., Walter, J., Menzel, F., Tappe, A., Kasper, C., Naumann, C., Zeidler, R., Scheper, T., Fast and efficient protein purification using membrane adsorber systems, J. Biotechnol. 121 (2006) 361-367.

Sun, L., Dai, J., Baker, G. L., Bruening, M. L., High-capacity, protein-binding membranes based on polymer brushes grown in porous substrates, Chem. Mater. 18 (2006) 4033–4039.

Syrén, P., Rozkov, A., Schmidt, S. R., Strömberg, P., Milligram scale parallel purification of plasmid DNA using anion-exchange membrane capsules and a multi-channel peristaltic pump, J. Chromatogr. B 856 (2007) 68–74.

Teeters, M. A., Conrardy, S. E., Thomas, B. L., Root, T. W., Lightfoot, E. N., Adsorptive membrane chromatography for purification of plasmid DNA, J. Chromatogr. A 989 (2003) 165-173.

Teeters, M. A., Root, T. W., Lightfoot, E. N., Adsorption and desorption behavior of plasmid DNA on ion-exchange membranes Effect of salt valence and compaction agents, J. Chromatogr. A 1036 (2004) 73–78.

Teeters, M. A., Root, T. W., Lightfoot, E. N., Performance and scale-up of adsorptive membrane chromatography, J. Chromatogr. A 944 (2002) 129–139.

Thommes, J., Kula, M. R., Membrane chromatography-An integrative concept in the downstream processing of proteins, Biotechnol. Prog., 11 (1995) 357-367.

Tomer, N., Mondal, S., Wandera, D., Wickramasinghe, S. R., Husson, S. M., Modification of nanofiltration membranes by surface-initiated atom transfer radical polymerization for produced water filtration, Sep. Sci. and Tech. 44 (2009) 3346–3368.

Toomey, R., Mays, J., Tirrell, M., In situ thickness determination of adsorbed layers of poly(2-vinylpyridine)-polystyrene diblock copolymers by ellipsometry. Macromol. 37 (2004) 905-911.

Tswett, M. S., Physical chemical studies on chlorophyll adsorptions, Berl. Deutsch. Botan. Ges. 24 (1906) 316-323.

Ulbricht, M., Belfot, G., Surface modification of ultrafiltration membranes by low-temperature plasma. 2. Graft polymerization onto polyacrylonirile and polysulfone, J. Membr. Sci. 111 (1995) 193-215.

Ulbricht, M., Yang, H., Porous polypropylene membranes with different carboxyl polymer brush layers for reversible protein binding via surface-initiated graft copolymerization, Chem. Mater. 17 (2005) 2622–2631.

Urthaler, J., Schlegl, R., Podgornik A., Strancar, A., Jungbauer, A., Necina, R., Application of monoliths for plasmid DNA purification Development and transfer to production, J. Chromatogr. A 1065 (2005) 93–106.

Walsh, G., Biopharmaceutical benchmarks 2006, Nat. Biotechnol. 24 (2006) 769–776.

Wang, J., Faber, R., Ulbricht, M., Influence of pore structure and architecture of photo-grafted functional layers on separation performance of cellulose-based macroporous membrane adsorbers, J. Chromatogr. A 1216 (2009) 6490–6501.

Wavhal, D. S., Fisher E. R., Membrane surface modification by plasma-induced polymerization of acrylamide for improved surface properties and reduced protein fouling. Langmuir 19 (2003) 79-85.

Wu, X., Hou, C. J., Dharia, J., Konstantin, P., Yang, Y., Positively charged membrane, US 7396465 B2, 2008.

Wurm, F. M., Production of recombinant protein therapeutics in cultivated mammalian cells, Nat. Biotech. 22 (2004) 1393–1398.

Yu, D., McLean, M. D., Hall, J. C., Ghosh, R., Purification of a human immunoglobulin G1 monoclonal antibody from transgenic tobacco using membrane chromatographic processes, J. Chromatogr. A 1187 (2008) 128–137.

Yu, D., McLean, M. D., Hall, J. C., Ghosh, R., Purification of monoclonal antibody from tobacco extract using membrane-based bioseparation techniques, J. Membr. Sci. 323 (2008) 159–166.

Yusof, A. H. M., Ulbricht, M., Effects of photo-initiation and monomer composition on performance of graft copolymer based membrane adsorbers, Desalination 200 (2006) 462–463.

Zeng, X., Ruckenstein, E., Membrane chromatography: preparation and applications to protein separation, Biotechnol. Prog. 15 (1999) 1003-1019

Zhao, B., Brittain, W. J., Polymer brushes: Surface-immobilized Macromol.. Prog. Polym. Sci. 25 (2000) 677-710.

Zhao, B., Brittain, W. J., Synthesis, characterization, and properties of tethered polystyrene-*b*-polyacrylate brushes on flat silicate substrates. Macromol. 33 (2000) 8813-8820.

Zhou J. X., Tressel, T., Basic concepts in Q membrane chromatography for large-scale antibody production, Biotechnol. Prog. 22 (2006) 341-349.

Zhou J. X., Tressel, T., Gottschalk, U., Solamo, F., Pastor, A., Dermawan, S., Hong, T., Reif, O., Mora, J., Hutchison, F., Murphy, M., New Q membrane scale-down model for process-scale antibody purification, J. Chromatogr. A 1134 (2006) 66.

Zhou J. X., Tressel, T., Yang, X., Seewoester, T., Implementation of advanced technologies in commercial monoclonal antibody production, Biotechnol. J. 3 (2008) 1185.

CHAPTER 2

PREPARATION OF HIGH-CAPACITY, WEAK ANION-EXCHANGE MEMBRANES

FOR PROTEIN SEPARATIONS USING SURFACE-INITIATED ATRP

2.1 Introduction

With the advent of biotechnology, worldwide demand for protein therapeutics is increasing rapidly. As of 2006, Walsh et al. [2006] estimated that there were roughly 2,500 biotech-based drugs in the discovery phase, another 900 in preclinical trials, and more than 1,600 in clinical trials. Based solely on estimated sales for recombinant proteins [Pavlou et al., 2004] and monoclonal antibodies (Mabs) [Pavlou et al., 2004], the total market for biopharmaceutical products is expected to reach or exceed $70 billion by 2010 [Walsh et al., 2006].

Considering that more than 60% of the total cost of downstream bioprocesses is due to the downstream recovery and purification [Ghosh et al., 2003; Lightfoot et al., 2004], high productivity and high resolution separation techniques are essential to the biopharmaceutical industry. Historically, resin-based chromatography has been a workhorse for the industry. While effective and reliable, this unit operation has low mass throughput [Knudsen et al., 2001], and the projected masses of biotherapeutic products that will need to be purified in the near future will put tremendous pressure on current downstream processing facilities, forcing manufacturers to consider process alternatives

45

to conventional resin-based chromatography for product recovery and purification [Low et al., 2007]. Among the higher throughput process technologies being reconsidered is membrane chromatography.

Specifically, chromatography using anion-exchange membranes in flow-through mode is attractive for the removal of high molecular weight process impurities such as host cell proteins, DNA, virus particles, et al. as part of a mAb purification train [Ghosh et al., 2003; Thömmes et al., 2007]. For membranes with micron-sized pores, the mass loading capacity of these high molecular weight impurities increases with increasing size of the impurity [Etzel et al., 2006]. This trend directly contrasts that for resin particles, whereby large enough impurities do not access internal pores of the resin particles. As a result, these impurities bind only on the outer surface of the resin particles, resulting in low volumetric ion-exchange capacities [Endres et al., 2003]. Furthermore, the capacities of resin beds vary with process flow rate; whereas, ion-exchange membranes maintain nearly constant capacity, largely independent of flow rate [Knudsen et al., 2001].

While the potential is great for utilizing anion-exchange membranes in flow-through mode for removal of high molecular weight process impurities, this purification step has less impact on process economics than the initial product capture step [Low et al., 2007], which typically is a bind-and-elute affinity chromatography step. Knudsen et al. [2001] highlight potential barriers that may be limiting the implementation of anion-exchange membranes in a bind-and-elute product capture step. Notably, membranes cost significantly more than resins on a per volume basis. Thus, if throughput were to remain constant, then manufacturers would need to increase significantly the number of cycles

46

that the ion exchange beds are used per batch of product in order to maintain constant cost or to realize a cost savings [Knudsen et al., 2001]. Yet, increased throughput is recognized as a critical need for the future, and membranes offer the potential for a significant improvement in throughput compared to resins. In this case, maintaining cost will require only modest increases in bed cycles [Knudsen et al., 2001]. Nevertheless, because of the need for additional validation studies and sanitation steps when multiple cycles are performed, minimizing the number of cycles will be critical for ion-exchange membranes to find increased use as the primary capture step. One avenue to achieve this end result is to increase the volumetric capacity of ion-exchange membranes beyond current values. It is thus a primary objective of this study to create high-capacity anion-exchange membranes by applying polymer grafting principles to incorporate anion-exchange functionality into commercial membrane supports.

Polymer grafting methods to incorporate ion-exchange functionalities into base membranes have been a focus for previous researchers [Kawai et al., 2003; Singh et al., 2005, 2008; Yusof et al., 2008]. For protein chromatographic operations, a wide range of micro- to macroporous membranes have been modified with different strategies. Relevant to work outlined here are methods used to grow polymer chains from the base membrane surface by monomer addition. Among many noteworthy approaches, Yusof and Ulbricht [2008] recently described photo-initiated, surface selective graft polymerization to produce cation-exchange membranes for lysozyme purification. Kawai et al. [2003] describes the use of radiation-induced graft polymerization to incorporate ion-exchange, hydrophobic and affinity functionalities on membrane surfaces for chromatographic

separations. The literature also contains examples of incorporation of poly(2-dimethylaminoethyl methacrylate) (poly(DMAEMA)) into cellulose, which is the system of this study. Redox-initiation [Hebeish et al., 1997] and preirradiation [Jun et al., 2001] have been used to graft poly(DMAEMA) onto cellulose fibers. Lee et al. [2004] used atom transfer radical polymerization (ATRP) and Roy et al. [2008] used reversible addition-fragmentation chain transfer polymerization to prepare antibacterial cellulose surfaces based on quaternized poly(DMAEMA).

The research presented here pertains to the use of ATRP to modify surfaces of commercial regenerated cellulose membranes to produce weak anion-exchange membranes for membrane chromatography applications. ATRP is a catalyst-activated, controlled polymerization technique that can be carried out under mild conditions (low temperature) to prepare polymer chains with low polydispersity and precisely designed polymer architecture [Singh et al., 2005, 2008; Yoshida et al., 2003]. Husson and co-workers have demonstrated the use of this technique to modify PVDF membranes, using polymerization time as independent variable to control pore-size polydispersity and ion-exchange capacity [Singh et al., 2005]. That group also described the use of surface-initiated ATRP to produce weak cation-exchange membranes functionalized by poly(acrylic acid). They achieved high volumetric ion-exchange capacity for lysozyme (static ~ 99 mg/mL, dynamic ~ 71 mg/mL) [Singh et al., 2008].

The goal of this research was to produce high capacity weak anion-exchange membranes for protein chromatography, for the reasons outlined above. Polymerization time was used as independent variable to achieve high capacity while maintaining

48

adequate permeability. Surface-initiated ATRP was used to graft poly(DMAEMA) anion-exchange nanolayers from membrane surfaces. AFM and SEM measurements were used to study the impact of surface modification on membrane morphology. Kinetic studies of surface-initiated ATRP on model flat substrates were performed to approximate layer thickness evolution during graft polymerization from membrane surfaces. Protein static binding capacity and permeability were measured to evaluate performance properties of surface modified membranes.

2.2 Experimental

2.2.1 Materials

Spontaneously wetting regenerated cellulose (RC) membranes (RC 60) with 75 µm thickness, 47 mm diameter, and 1 µm average pore diameter were purchased from Whatman, Inc. The following chemicals and solvents were purchased from Sigma-Aldrich, with purities given in wt.%: 2-(dimethylamino)ethyl methacrylate (DMAEMA, 98%), glycidyl methacrylate (GMA, 97%), copper(I) bromide (98%), copper(I) chloride (99.99%), copper(II) chloride (99.999%), 1,1,4,7,10,10-hexamethyltriethylenetetramine (HMTETA, 97%), triethylamine (TEA, ≥99%), 2-bromoisobutyryl bromide (2-BIB, 98%), ethyl 2-bromoisobutyrate (EBrIB, 98%), 1,1,4,7,7-pentamethyldiethylenetriamine (PMDETA, 99%), hydrogen peroxide solution (50 wt.% in H$_2$O), sulfuric acid (reagent grade, 95-98%), 2-bromo-2-methylpropionic acid (BPA, 98%), tetrahydrofuran (THF, anhydrous, ≥99.9%), 2-propanol (≥99.8%), ethanol (anhydrous, ≥99.5%), methanol (≥99.9%), water (ACS reagent grade, HPLC), toluene

(anhydrous, ≥99.8%), chloroform (anhydrous, ≥99%), methyl ethyl ketone (MEK, spectrophotometric grade, ≥99%) and neutral, activated aluminum oxide. Prior to polymerization, the DMAEMA and GMA were passed through a column of the neutral aluminum oxide to remove inhibitor compounds.

A stock solution of phosphate buffered saline (PBS) was prepared from bioreagent 1X powder concentrate received from Fisher Scientific and deionized water from a Milli-Q water purification system (Millipore, Inc). PBS buffer (10 mM, pH 7.4) was used for permeability and protein static binding capacity measurements. Albumin from bovine serum (further purified fraction V, ~99%, M_r ~ 66 kDa) was from Sigma. Single-sided, polished silicon substrates (1 cm × 3 cm) were purchased from Silicon Quest International and used for ellipsometry measurements.

2.2.2 Membrane surface modification

Scheme 2.1 illustrates the two-step modification procedure. Initiator molecules were anchored to the membrane pore surfaces in a first step. ATRP was used in the second step to graft poly(DMAEMA) chains from the initiator sites. In order to increase measurement precision for the small volumes used in each step, we prepared one large volume of solution for each set of 10 membranes that we modified and used syringes (Hamilton, Inc.) with range of 0−50 µL or 0−100 µL and a precision of ± 1 µL. In the sections that follow, we give the volumes used per membrane sample or silicon substrate, along with the final solution concentration of each component.

Scheme 2.1
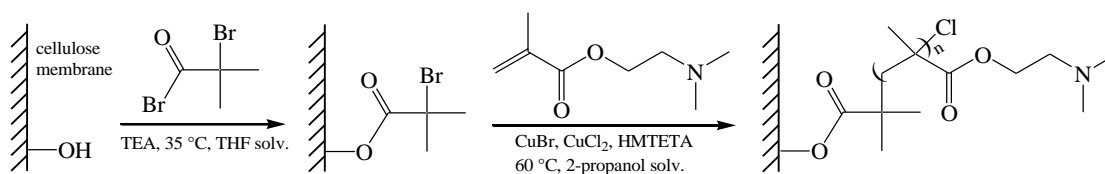
2.2.2.1 Initiator functionalization of regenerated cellulose membranes

Regenerated cellulose membranes were washed by immersion in 10 mL of tetrahydrofuran for 10-12 minutes before initiator functionalization. Initiator functionalization was carried out in solution at 35 °C. Membranes were removed from the THF and dried for 5 minutes before placing into the solution for initiation. A typical solution comprised the initiator precursor, 2-BIB (3 mM, 14.0 µL), a neutralizing agent, TEA (3 mM, 15.7 µL), and solvent anhydrous THF (37.5 mL).

During this modification step, the acid bromide group of the initiator reacts with the hydroxyl groups of the cellulose membrane to covalently anchor α-bromoester initiator groups on the membrane surface. The reaction produces hydrobromic acid (HBr) as a by-product. To avoid potential detrimental effects of HBr to the base membrane, TEA was used to neutralize this strong acid by-product. After 2 hours, the membrane was removed from the reaction mixture, washed thoroughly with THF and HPLC water, and stored in THF until the surface-initiated polymerization.

2.2.2.2 Surface-initiated ATRP of 2-(dimethylamino)ethyl methacrylate

Initiator-functionalized membranes were modified further by surface-initiated ATRP. A typical procedure follows. Monomer, DMAEMA (12.65 mL, 2 M) was added to the solvent, 2-propanol (22.85 mL), in a flask, and this mixture was de-oxygenated by three

cycles of freeze-pump-thaw. High-purity nitrogen was introduced into the flask

headspace after each evacuation stage. The flask was then removed from the Schlenk line

under nitrogen atmosphere and transferred to the glove box (MBraun UNIlab, $O_2 < 1$

ppm, $H_2O < 1$ ppm). 2-Propanol (2 mL) was de-oxygenated by three freeze-pump-thaw

cycles as described, and activator, copper(I) bromide (5.38 mg, 1.0 mM), deactivator,

copper(II) chloride (0.50 mg, 0.1 mM), and amine ligand, HMTETA (0.0224 mL, 2.2

mM) were added to it. Next, this mixture was placed into an ultrasonic bath for 15

minutes until it became homogeneous, indicating the formation of a fully soluble catalyst

complex. Catalyst and monomer solutions were mixed well inside the glove box to form

the polymerization reaction mixture. The temperature of the reaction mixture was raised

to 60 °C by placing the flask into a constant-temperature glass bead bath (ISOTEMP

145D, Fisher). To start polymerization, an initiator-functionalized membrane was

removed from THF, dried for 5 minutes, and placed into the reaction mixture. The entire

procedure was carried out inside the glove box to avoid oxidation of the copper catalyst.

Polymerization time was used as independent variable to control the mass of

poly(DMAEMA) grafted from the regenerated cellulose membrane.

2.2.3 Kinetic study of polymer growth from silicon substrates

2.2.3.1 ATRP of poly(glycidyl methacrylate) (PGMA)

PGMA was polymerized via ATRP in solution. Glycidyl methacrylate (GMA, 15 mL,

0.11 mol) was added to solvent toluene (25 mL) in a flask, and the mixture was de-

oxygenated by three cycles of freeze-pump-thaw, as described earlier. Activator,

copper(I) chloride (56 mg, 0.57 mmol), and amine ligand, PMDETA (0.238 mL, 1.14

mmol) were added to the GMA solution inside the glove box. The reaction mixture was stirred slowly to form a fully soluble catalyst complex. To start polymerization, initiator, ethyl 2-bromoisobutyrate (0.073 mL, 0.50 mmol) was introduced into the reaction mixture with a micro-volume syringe. Polymerization was done at 40 °C in a constant-temperature glass bead bath. After 30 minute, the flask was removed from the glove box, and the reaction mixture was diluted with 400 mL of chloroform and then passed through a neutral alumina column to remove catalyst. Solvent was removed by evaporation at 40 ºC, under vacuum (667−1067 Pa) until the solution became a thick slurry. The remaining PGMA solution was dried in a vacuum oven (667−1333 Pa) at 50 °C until a constant weight was observed.

2.2.3.2 Surface functionalization of silicon substrates

Silicon substrates were washed and cleaned with de-ionized water by placing them in an ultrasonic bath for 30 minutes. Cleaned silicon substrates were placed in a 1:4 (v/v) mixture of hydrogen peroxide (50 wt. % in H_2O) and sulfuric acid (95−98%) at 80 °C for 1 hr. [Caution: This mixture reacts violently with organic compounds. It should be used in small volumes with proper supervision and safety wear. Special precautions should be exercised in its disposal to avoid contact with organics.] Next, the silicon substrates were rinsed thoroughly with de-ionized water, and dried. A 0.2 wt.% PGMA solution was prepared in anhydrous MEK. PGMA was deposited onto the silicon substrates from this solution using a dip coater (Mayer Fientechnik D-3400). PGMA-coated silicon substrates were annealed at 110 °C for 30 minute under vacuum (400−667Pa). Annealing was done to react some of the epoxy groups of PGMA to silanol groups on the silicon surface. 2-

Bromo-2-methyl propionic acid (BPA) was reacted to the remaining epoxy groups of PGMA from the vapor phase at low pressure (400−667Pa) and 100 °C to form α-bromoester initiator groups on the silicon wafer surface. After BPA reaction, the silicon substrates were washed thoroughly with MEK and dried.

2.2.3.3 Surface-initiated ATRP of 2-(dimethylamino)ethyl methacrylate from silicon substrates

Poly(DMAEMA) was grown from initiator-functionalized silicon substrates by surface-initiated ATRP. Monomer, DMAEMA (6.75 mL, 2 M), was mixed with solvent, 2-propanol (13.25 mL), in a flask, and the mixture was de-oxygenated by three cycles of freeze-pump-thaw and transferred to the glove box. Activator, copper(I) bromide (2.87 mg, 1.0 mM), deactivator copper(II) chloride (0.89 mg or 1.79 mg, 0.2 mM or 0.4 mM), and the amine ligand, HMTETA (0.0131 or 0.0152 mL, 2.4 or 2.8 mM) were added to the monomer solution inside the glove box. Polymerization was carried out by placing an initiator-functionalized silicon substrate into this reaction mixture. Polymerization was done at 40 °C or 60 °C. Polymerization time, Cu(I)/Cu(II) molar ratio, and temperature were used as independent variables to control polymer growth rate from the flat silicon surfaces. Polymerization was terminated at regular intervals by removing silicon substrates from the solution and washing thoroughly with ethanol and HPLC water.

2.2.4 Physicochemical characterization

2.2.4.1 ATR-FTIR

Attenuated total reflectance Fourier-transform infrared spectroscopy (ATR-FTIR) was used to provide information on the surface chemistry of unmodified (base), initiator-

functionalized, and polymer-modified membranes (for 20 h polymerization time). Details of the instrument and operating parameters were given previously [Singh et al., 2005].

2.2.4.2 AFM

Atomic force microscopy (AFM) was used to visualize the surface topology and to obtain surface roughness values of unmodified, initiator-functionalized and polymer-modified cellulose membranes. Images were obtained by a BioScope AFM (Veeco) with Nanoscope IIIA controller. A 50 µm ×50 µm area was scanned using tapping mode at 1.0 Hz frequency and 256 scan rates. Root-mean-square (RMS) roughness values were calculated with NanoScope software (Version 5.12).

2.2.4.3 SEM

Scanning electron microscopy (SEM) (S-3400N, Hitachi-HTA, Inc) was used to investigate the pore morphology of unmodified, initiator-functionalized, and poly(DMAEMA)-modified membrane (for 12 h polymerization time). Samples from each membrane were cut into 1 cm × 1 cm pieces and shadowed with platinum to make them conductive. SEM measurements were performed at an accelerating voltage of 20.0 kV. Three SEM images at 2000×, 4000×, and 6000× magnification were taken for each membrane sample.

2.2.4.4 Ellipsometry

Poly(DMAEMA) layers grown from silicon substrates were characterized by multi-angle ellipsometry (Beaglehole Instruments Picometer[TM], He-Ne laser, λ=632.8 nm). Ellipsometric angles ψ and Δ were measured at three locations on the surface as a function of incident angle from 80º to 50º. These data were used to determine dry

polymer layer thickness. Refractive indexes of 1.437, 1.525, and 1.500 were used for PDMAEMA, PGMA and BPA to fit the data using a Cauchy model (Igor Pro Software).

2.2.5 Membrane performance testing

2.2.5.1 Flux measurements

Flux measurements were performed using 10 mM PBS buffer solution. A stirred ultrafiltration cell (model 8050, Millipore, Inc.) was modified to increase the volumetric capacity from 50 mL to 300 mL by increasing the height of the cylinder for better precision in the measurements. Each membrane sample was loaded into the ultrafiltration cell, followed by addition of 300 mL of 10 mM PBS buffer. A set of constant transmembrane pressures (66, 131, and 193 kPa) was applied from a nitrogen gas cylinder, the bottom valve of the filtration cell was opened and the time required for all 300 mL of PBS buffer to pass through the membrane was measured. Each membrane was compacted first at the highest pressure (193 kPa), and then permeability measurements were taken from lower to higher pressures. Data were averaged from three measurements taken at each applied pressure.

2.2.5.2 Static protein adsorption measurements

Static protein adsorption isotherms were measured for bovine serum albumin (BSA) on unmodified membranes and membranes modified by surface-initiated ATRP of poly(DMAEMA) for 3, 6, and 12 h. BSA concentrations were 0.4, 0.7, 1.0, 2.0, 3.0, 4.0, and 6.0 mg/mL in 10 mM PBS buffer. Each membrane (47 mm dia.) was placed in a 40 mL glass bottle (I-Chem* short, wide-mouth glass bottles, Fisher Scientific) and incubated in 10 mL protein solution for 20 h to reach equilibrium in a shaker bath at 22

°C temperature. 20, 25 and 30 h incubation time was used in one set of experiments. The static binding capacities of all three samples incubated for 20, 25 and 30 h were same suggesting that the equilibrium binding capacity was approached within 20 h. Next, membranes were removed from the glass bottles and equilibrium concentrations of the protein solutions were measured by UV-VIS spectrophotometry (Cary 50 Bio UV-VIS spectrophotometer) at 280 nm, using a calibration curve prepared in this study. Binding capacities, reported as the adsorbed mass of protein per unit volume of membrane, were calculated by mass balance using initial and equilibrium concentrations.

2.3 Results and discussion

2.3.1 Characterization of membrane physicochemical properties

Physicochemical properties of the membranes were analyzed by ATR-FTIR, AFM, and SEM. Fig. 2.1 presents typical ATR-FTIR spectra for unmodified (spectrum A), initiator-functionalized (spectrum B), and poly(DMAEMA)-modified (spectrum C) membranes. Analogous to previous work reported by our group [Singh et al., 2005], there was no distinguishable difference between the spectra for unmodified membranes and membranes after initiator functionalization, although the initiator contains a carbonyl group (C=O) that should make it distinguishable from the base membrane. The mass of initiator anchored to the membrane is low in comparison to the base material (cellulose), so signals were contributed predominantly by cellulose. The ATR-FTIR spectrum of a membrane after surface-initiated ATRP of poly(DMAEMA) for 20 hours (spectrum C) had an absorption band centered at 1728 cm^{-1} that corresponds to the carbonyl stretching

(C=O) of poly(DMAEMA) and provides evidence for successful surface-initiated

polymerization.
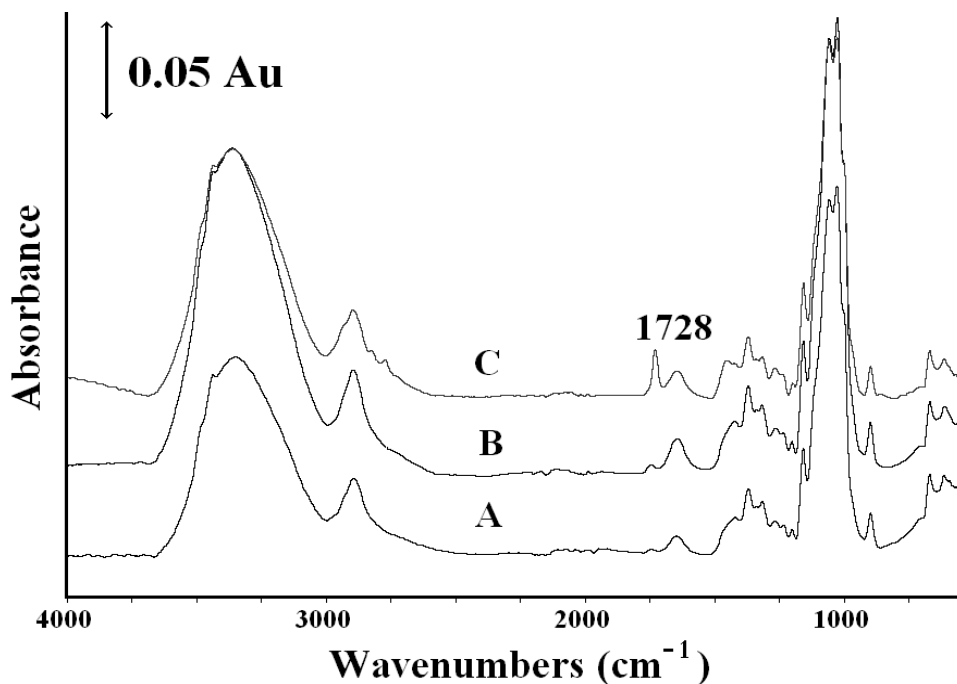
Figure 2.1 ATR-FTIR spectra for RC membranes: unmodified (spectrum A), initiator-
functionalized (spectrum B), and poly(DMAEMA)-modified (spectrum C) membranes.
Surface-initiated ATRP was done for 20 hour to produce the polymer-modified
membrane.

Atomic force microscopy was performed to examine the surface topography and

measure roughness values of unmodified and polymer-modified membrane surfaces. Fig.

2.2 presents the phase and topographical scans of unmodified and poly(DMAEMA)-

modified membranes that illustrate the significant difference in the topography of an

unmodified membrane and one that has been modified by surface-initiated ATRP of

DMAEMA for 20 hours. The unmodified membrane surface was rough with larger size

peaks and valleys (image c). Surface-modification via surface-initiated ATRP produced a

smoother and more uniform surface (image d). Significant alteration of surface

58

topography was supported by changes in the measured values of the root-mean-square (RMS) roughness; it decreased from 1.00 ± 0.01 μm to 0.83 ± 0.07 μm following polymerization. This observation that polymer grafting leads to changes in surface topography and smoothening of surface features has been cited by other research groups [Chang et al., 2008; Fujii et al., 2001; Khayet et al., 2004; Yoshida et al., 2003].
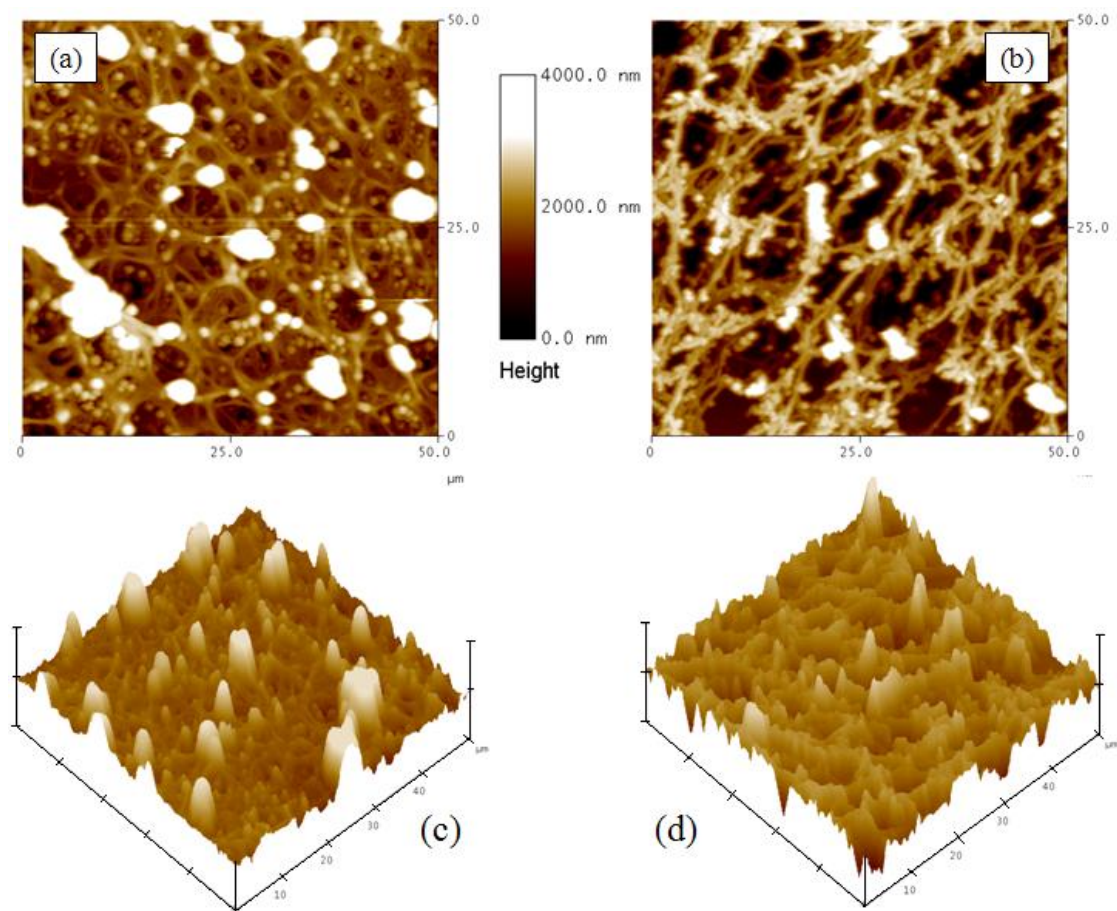
Figure 2.2 AFM micrographs for unmodified (image a) and poly(DMAEMA)-modified (image b) RC membranes. Images (c-d) are the corresponding 3-D topographical maps. Surface-initiated ATRP was done for 20 hour to produce the polymer-modified membrane. RMS roughness values for unmodified and polymer-modified membranes were 1.00 μm and 0.83 μm, respectively. AFM images represent 50 μm × 50 μm lateral area and 4.770 μm z-axis scale.

The rationalization of this phenomenon is that the grafted poly(DMAEMA) chains are collapsed in air, which is a poor solvent. Thus, the chains spread uniformly over the surface, partially filling unoccupied volume between cellulose threads, and smoothening the original surface.
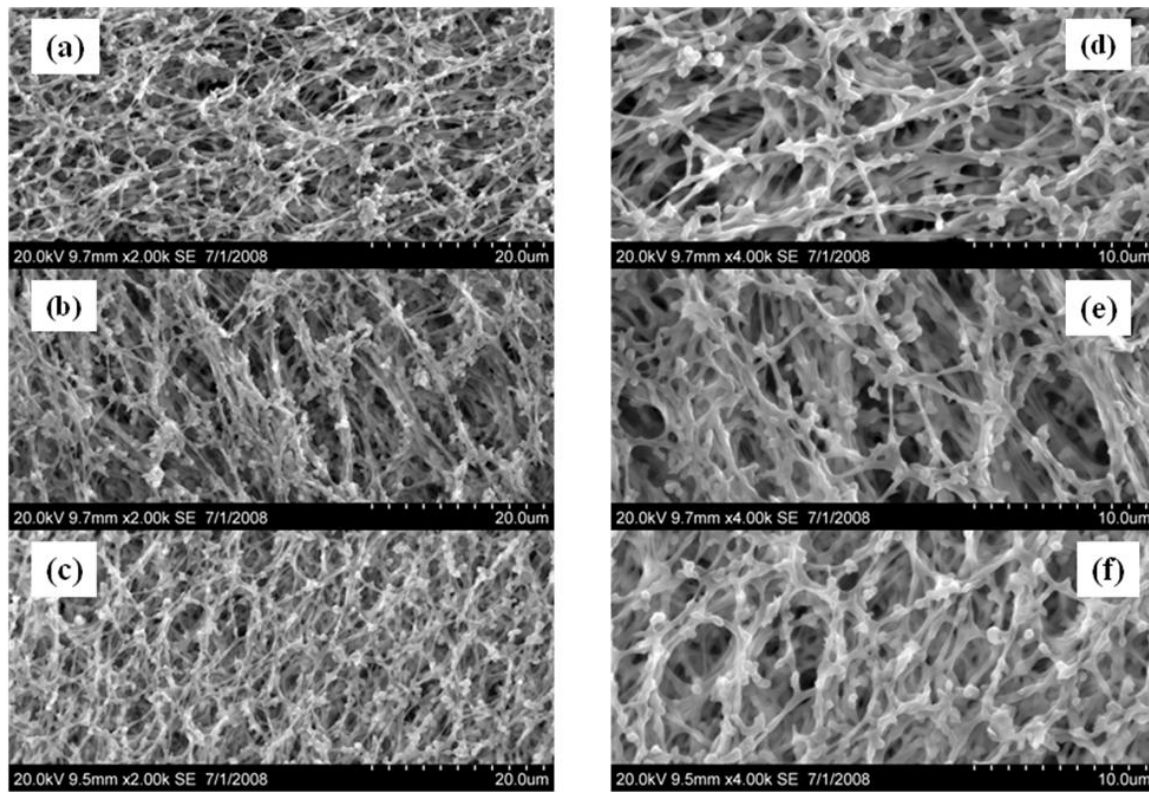
Figure 2.3 SEM images for unmodified (image a), initiator-functionalized (image b), and poly(DMAEMA)-modified (image c) RC membranes at 2000× magnification. Images (d-f) are the corresponding membranes with 4000× magnification. Surface-initiated ATRP was done for 12 hour to produce the polymer-modified membrane.

Fig. 2.3 shows SEM images for unmodified, initiator-functionalized and poly(DMAEMA)-modified membranes. Surface-initiated ATRP for 12 h was used to prepare the polymer modified membrane. SEM images (a–c) and (d–f) represent membranes at 2000× and 4000× magnification, respectively. Membrane morphology

60

remained intact following initiator attachment, which is evident from close comparison of the images (a versus b, and d versus e).
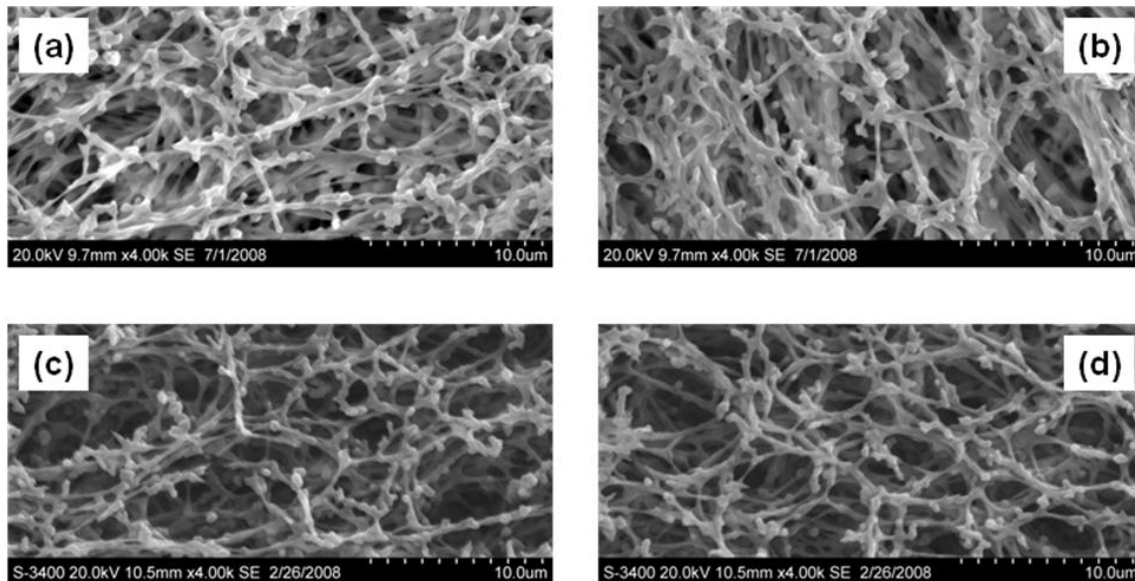
Figure 2.4 SEM images of initiator-functionalized membrane (image a), membrane after Control Experiment 1 (image b), membrane after Control Experiment 2 (image c), and membrane after Control Experiment 3 (image d) at 4000× magnification. Initiator-functionalization and all the control experiments were done at 35 °C and 2 hours reaction time.

We also conducted three control experiments to verify that this modification step does not alter the base membrane structure. In a first control experiment, unmodified membranes were placed in pure solvent, anhydrous THF, without the addition of 2-BIB. In second control experiment, unmodified membranes were placed in a solution comprised of HBr (12.2 μL, 3 mM), a neutralizing agent, TEA (15.7 μL, 3 mM), and solvent, anhydrous THF (37.5 mL). The concentration of HBr was chosen to represent the highest possible concentration that could develop during initiator functionalization, which utilized 3 mM 2-BIB. In a third control experiment, unmodified membranes were

placed in a solution comprised of HBr (12.2 μL, 3 mM) and solvent, anhydrous THF (37.5 mL). All the control experiments were done at 35 °C and 2 h reaction time. Fig. 2.4 shows the SEM images of these control experiments. Membrane morphology was unaffected during all three control experiments which can be observed from Fig. 2.4. This set of control experiments confirms that the conditions used for initiator attachment preserve the base membrane integrity.

There also was no apparent difference in the morphology of the unmodified membrane (Fig. 2.3, images a and d) and the final poly(DMAEMA)-modified membranes (Fig. 2.3, images c and f) following 12 h of polymerization. From SEM characterization, it is evident that the membrane pore morphology was intact; the micron-sized membrane pores were not blocked after 12 h of surface-initiated ATRP of DMAEMA from the regenerated cellulose membranes. This result is further confirmed by the flux measurements to be discussed.

2.3.2 Kinetics of surface-initiated ATRP of poly(DMAEMA)

ATR-FTIR, AFM and SEM characterization clearly demonstrate that the surface-initiated ATRP was successful at altering the physical and chemical properties of the base membranes. However, the success of membrane surface modification depends on the ability to control the thickness of the polymer nanolayer, and these techniques do not provide precise information about the thickness evolution of the nanolayers grown by surface-initiated ATRP. In order to determine the thickness evolution of the nanolayers, and to study how the Cu(II)/Cu(I) molar ratio and temperature influence polymer growth, a kinetic study of surface-initiated ATRP was conducted using flat silicon substrates.

Silicon substrates were coated with PGMA to achieve initiator densities representative of a three-dimensional cellulose membrane. For example, Luzinov and coworkers [Liu et al., 2004] have reported that a 6 nm thick PGMA layer on silicon substrates led to an areal initiator density of 40 molecules/nm^2, much higher than the density of 3 molecules/nm^2 for a self assembled monolayer (SAM) on the same substrate. That group [Liu et al., 2004] reported that increasing the initiator density led to an increase in the rate of polymer growth. It was demonstrated that an initiator density of 40 molecules/nm^2 yielded a 5-6 fold increase in the polymer layer thickness for a given polymerization time, relative to a surface with an initiator density of 3 molecules/nm^2. Also important is that the initiator density could be changed by varying the PGMA layer thickness, which itself could be varied easily by changing the PGMA concentration in solution during deposition onto the silicon substrates [Liu et al., 2004]. Based on prior evidence from our group [Gopireddy et al., 2002; Samadi et al., 2005; Singh et al., 2005, 2008], we submit that PGMA on silicon serves as a more appropriate model than SAMs for characterizing the polymer growth kinetics. The relatively higher areal initiator density generated by the PGMA better reflects the cellulose membrane surface, where initiator can attach throughout the 3-dimensional structure of the cellulose membrane threads. That is, the PGMA coating on the silicon substrates mimics the three dimensional nature of initiator incorporation into the membrane.
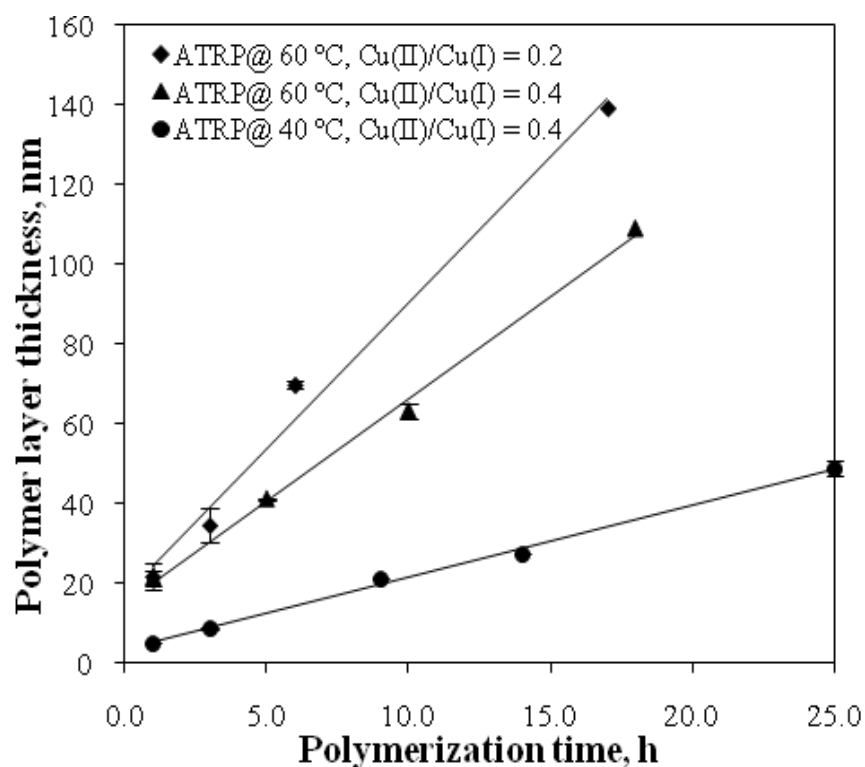
Figure 2.5 Dependence of dry polymer layer thickness on polymerization time for surface-initiated ATRP of poly(DMAEMA) from PGMA-coated silicon substrates. Symbols represent the experimental data and solid lines represent the linear fits. (♦) 60° C, molar ratio DMAEMA/Cu(I)/Cu(II)/HMTETA was 2000/1/0.2/2.4. (▲) 60 °C, molar ratio DMAEMA/Cu(I)/Cu(II)/HMTETA was 2000/1/0.4/2.8. (●) 40° C, molar ratio DMAEMA/Cu(I)/Cu(II)/HMTETA was 2000/1/0.4/2.8. Two measurements were taken at each polymerization time and data in the figure represent the average of those measurements. The error bars represent ± 1 standard deviation from the average value.

PGMA dry layer thicknesses were 8 ± 0.5 nm. Following initiator functionalization

by reaction with bromopropionic acid, the dry layer thickness increased to 10 ± 0.5 nm,

consistent with the fact that mass was added to the layer. Fig. 2.5 shows the dependence

of polymer layer thickness on polymerization time. Data represent the dry

poly(DMAEMA) layer thickness excluding PGMA and initiator layer thicknesses. A

telltale characteristic of controlled, surface-initiated ATRP is a linear relationship

between layer thickness and time [Gopireddy et al., 2002; Matyjaszewski et al., 2001; Samadi et al., 2005], as we have for the conditions presented in Fig. 2.5. One curiosity, however, was observed after 1 hour of polymerization. For all three sets of data, we observed an apparent abrupt increase in polymer layer thickness. As a result, none of the best-fit lines in Fig. 2.5 passes through the origin. To investigate the reason for this apparent abrupt increase in layer thickness, control experiments were done in which initiator-functionalized, PGMA-coated silicon wafers were placed into 2-propanol (the ATRP solvent) only at 60 °C and 40° C. After 1 hour, the wafers were removed from 2-propanol, dried, and the dry layer thicknesses were measured by ellipsometry. The result of this control study was that the thickness of the PGMA + initiator layer increased without the addition of monomer or catalyst to the solvent, 2-propanol. The reaction of residual epoxy groups of PGMA with 2-propanol was the underlying reason for the behavior observed in Fig. 2.5. Epoxy groups of PGMA can be reacted easily with the hydroxyl functionality of 2-propanol to incorporate it into the layer. Also noteworthy from Fig. 2.5 is that the layer thickness at 1 hour is similar for the two sets of data at 60 °C and much larger than the value at 40 °C. This result is logical, since increasing temperature increases the rate of reaction between epoxy groups of PGMA and hydroxyl groups of 2-propanol.

Fig. 2.5 shows data for polymerization at 40 °C and 60 °C and two values of Cu(II)/Cu(I). Increasing temperature at constant Cu(II)/Cu(I) increased the rate of polymerization. While the rate of polymerization was highest for 60 °C and the lower Cu(II)/Cu(I) value of 0.2, there does appear to be some curvature in the thickness versus

65

time data, indicative of improper control. A now classic protocol to improve control of surface-initiated ATRP was first presented by Matyjaszewski et al. [2001]; it involves a priori addition of deactivator, Cu(II), to the formulation. In our study we found that increasing the deactivator concentration at a constant temperature led to better control, albeit with an associated decrease in the rate of the polymerization.

From the kinetic study of surface-initiated ATRP of poly(DMAEMA), we developed a polymerization protocol that leads to controlled growth of grafted polymer. Also, we demonstrated that we able to grow moderately thick (~140 nm), by ATRP standards, polymer nanolayers. Furthermore, the controlled growth behavior observed in Fig. 2.5 indicates that production of thicker nanolayers is possible if we extend the time of polymerization.

2.3.3 Membrane performance properties

Performance properties of surface-modified membranes were evaluated by measurements of permeate flux and protein adsorption experiments. PBS buffer (10 mM, pH 7.4) was used to measure flux and permeability of unmodified and surface-modified membranes. Fig. 2.6 shows the flux versus pressure data for unmodified, initiator-functionalized, and polymer-modified (3 h, 6 h, 9 h, and 12 h modification times) regenerated cellulose membranes. By increasing the polymerization time, the flux decreased in a regular fashion. This result demonstrates that the controlled addition of polymer to the membrane pore surfaces was achieved by using polymerization time as the independent variable. Poly(DMAEMA) grafting from the membrane pore surfaces reduces the average effective pore size of membranes, as our group has demonstrated via

porosimetry measurements in previous work [Singh et al., 2008]. The data in Fig. 2.6 are

reported as permeabilities in Table 2.1.
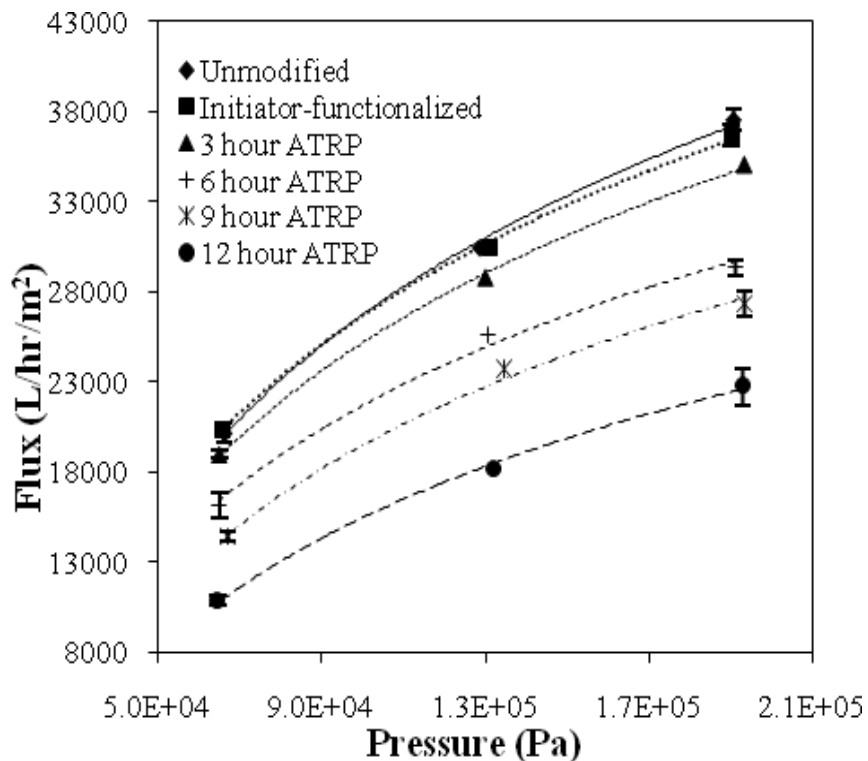
Figure 2.6 PBS buffer (10 mM, pH 7.4) flux measurements for unmodified, initiator-functionalized, and poly(DMAEMA)-modified RC membranes. Surface-initiated ATRP was done for 3 h, 6 h, 9 h, and 12 h to produce the polymer-modified membranes. By increasing polymerization time, the flux decreased in a regular fashion. Three measurements were taken at each applied pressure and data in the figure represent the average of those measurements. The error bars represent ± 1 standard deviation from the average value.

These results indicate that the permeability decreased ~40% after 12 hour

polymerization time (Table 2.1). The trade-off for the loss of permeability is that we gain

significant protein binding capacity (vide infra). Thus, there is an opportunity to design

the best membranes for chromatographic bioseparations, with optimized adsorption

capacity and permeability. Permeability and flux data were reproduced by a second batch

of polymer-modified RC membranes, and the reported uncertainties in Fig. 2.6 represent

standard deviations in the measurements between the two batches of membranes

Table 2.1 PBS buffer (10 mM, pH 7.4) permeability measurements for unmodified and poly(DMAEMA)-modified RC membranes.

Membrane	Pressure $\times 10^4$ (Pa)	Permeability $(L/m^2/bar/h)^*$
Unmodified	6.6	30500 ± 500
	12.8	23500 ± 500
	19.0	19500 ± 500
Initiator-functionalized	6.5	30500 ± 500
	13.1	23500 ± 500
	19.0	19000 ± 500
3 hour ATRP	6.5	29000 ± 500
	13.0	22000 ± 500
	19.3	18000 ± 500
6 hour ATRP	6.5	24500 ± 500
	13.0	18500 ± 500
	19.0	15500 ± 500
9 hour ATRP	6.7	21000 ± 500
	13.4	17500 ± 500
	19.3	14000 ± 500
12 hour ATRP	6.5	16500 ± 500
	13.2	13500 ± 500
	19.2	11500 ± 500

* Three measurements were taken at each applied pressure and data in the figure represent the average of those measurements. The error bars represent ± 1 standard deviation from the average value.

For protein static adsorption measurements, BSA was used in order to make

comparisons to manufacturer reported capacities of commercial membranes. BSA

solutions were made in 10 mM PBS buffer and pH was adjusted to 7.4. The pKa value for

the tertiary amine group of the DMAEMA is about 9.2−10 [Boyer et al., 2004], while the

isoelectric point (*pI*) of the BSA is about 4.7−4.9. At pH 7.4, the poly(DMAEMA)-

modified membrane surface is charged positively (weak-anion exchange membrane),

while the BSA carries a net negative charge. Fig. 2.7 shows the protein adsorption

isotherms for unmodified membrane and polymer-modified membranes (3 h, 6 h, and 12

h polymerization times). Experimental data were fitted to the Langmuir monolayer

adsorption model to evaluate the adsorption coefficient and maximum binding capacity.
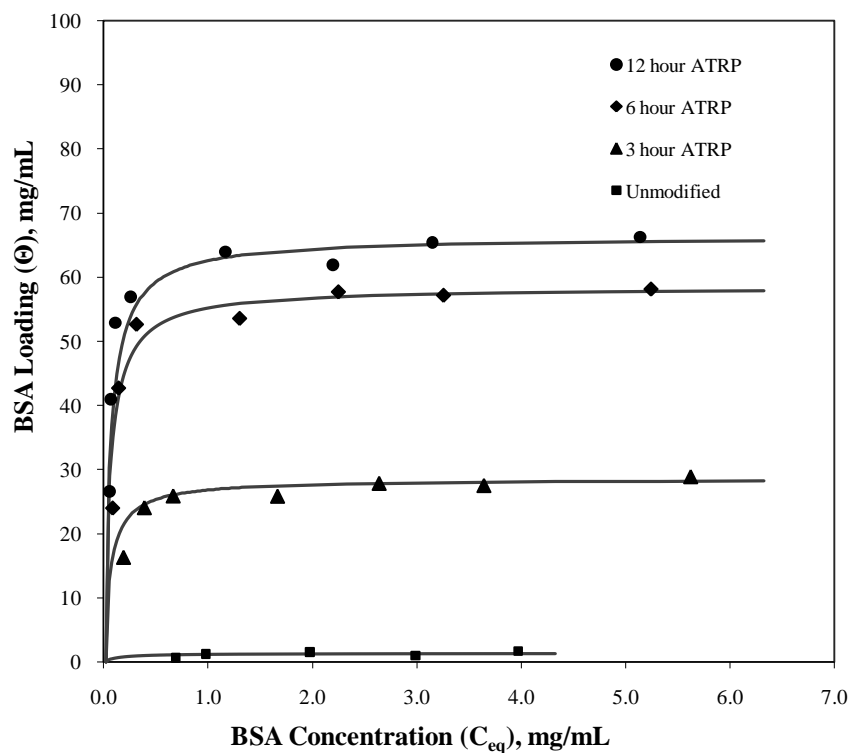
Figure 2.7 Adsorption isotherms for BSA at 22 °C on unmodified and poly(DMAEMA)-modified membranes. Surface-initiated ATRP was done for 3 h, 6 h, and 12 h to produce the polymer-modified membranes. Symbols represent experimental data, while solid curves represent the best fits to the Langmuir adsorption model. Table 2.1 gives the best-fit model parameters.

Table 2.2 Langmuir adsorption isotherm parameters for BSA static adsorption onto poly(DMAEMA)-modified RC membranes.

Membrane (h ATRP)	Adsorption coefficient K_{ads} (mL/mg)	Maximum binding capacity Θ_m (mg/mL)
3	15.9	28.5
6	17.1	58.4
12	16.8	66.3

Table 2.2 summarizes the results of the fitting. Adsorption coefficients were more or less equal for membranes modified for different polymerization times, as one would expect since the mode of interaction between protein and membrane is always the same, independent of polymerization time. By increasing the polymerization time, the adsorption capacity of the ion-exchange membranes increased regularly.

As demonstrated earlier, ATRP was controlled for this system using our established polymerization protocol. Accordingly, we anticipated a linear increase in the maximum static adsorption (ion-exchange) capacity with polymerization time. From Langmuir model fitting, maximum static adsorption capacity values were 28.5 mg/mL and 58.4 mg/mL for 3 h and 6 h polymerization times, respectively. These values agreed with our expectation that doubling the polymerization time would double the ion-exchange groups, and, thus, capacity, when using a controlled polymerization protocol. However, doubling the polymerization time from 6 h to 12 h did not yield a two-fold higher maximum ion-exchange capacity. We rationalize this behavior as follows: 1) As the mass of poly(DMAEMA) grafted from the membrane surface increases, membrane porosity decreases, and the smallest pores begin to fill with polymer, slowing and eventually ceasing polymer growth. 2) The 'thick' polymer brushes grown using longer

polymerization time may create limited accessibility of monomer to growing polymer chains in filled pores.

We compared adsorption capacities of our surface modified membranes with commercial weak-anion exchange membrane modules. The manufacturer of Sartobind D modules reports minimum static adsorption capacities ranging from 20.9 to 21.5 mg/mL for BSA. Therefore, we have measured static capacities for our surface-modified membranes that are up to 3 times higher for the same protein.

To use our surface-modified membranes for protein ion-exchange chromatographic operations, it will be necessary to have information about dynamic capacity, the impact of volumetric flow rate on dynamic capacity, separation efficiency, and reusability of the membrane module. A comprehensive set of these experiments was performed in our laboratory using an ÄKTApurifier™ chromatography system (GE Healthcare Bio-sciences) and findings of these experiments will be discussed in the Chapter 3.

2.4 Conclusions

A new method has been described to design high-capacity weak anion-exchange membranes for protein separation that uses surface-initiated atom transfer radical polymerization. AFM and SEM characterization shows that the membrane pore morphology was preserved after 20 hour surface modification. Surface-initiated ATRP from a model flat substrate that was designed to mimic the three dimensional initator distribution within a polymeric membrane surface region shows two important trends: Increasing Cu(II)/Cu(I) molar ratio improved control while slowing the growth rate of the

poly(DMAEMA) nanolayer. Increasing temperature at constant Cu(II)/Cu(I) increases the rate of polymerization. Permeability and protein static adsorption capacity measurements show that the polymerization time can be used to achieve high capacity while maintaining adequate permeability by controlling the amount of polymer grafted from the membrane surface. Protein static adsorption capacities increase with increasing polymerization time and eventually reach a plateau value of 66.3 mg/mL under the conditions studied.

2.5 References

Boyer, C., Boutevin, G., Robin, J. J., Boutevin, B., Study of the telomerization of dimethylaminoethyl methacrylate (DMAEMA) with mercaptoethanol. Application to the synthesis of a new macromonomer, Polymer 45 (2004) 7863-7876.

Chang, Y., Shih, Y., Ruaan, R., Higuchi, A., Chen, W., Lai, J., Preparation of poly(vinylidene fluoride) microfiltration membrane with uniform surface copolymerizaed poly(ethylene glycol)methacrylate and improvement of blood compatibility, J. Membr. Sci. 309 (2008) 165-174.

Endres, H. N., Johnson, J. A. C., Ross, C. A., Welp, J. K., Etzel, M. E., Evaluation of an ion-exchange membrane for the purification of plasmid DNA, Biotechnol. Appl. Biochem. 37 (2003) 259-266.

Etzel, M., Riordan, W., Membrane chromatography: Analysis of breakthrough curves and viral clearance. In Process scale bioseparations for the biopharmaceutical industry; Shukla, A., Etzel, M., Gadam, S., Eds.; Taylor & Francis: Boca Raton, FL, 2006.

Fujii, T., Yano, T., Nakamura, K., Miyawaki, O., The sol-gel preparation and characterization of nanoprous silica membrane with controlled pore size, J. Membr. Sci. 187 (2001) 171-180.

Ghosh, R., Protein bioseparation using ultrafiltration: Theory, applications and newdevelopments, Imperial college press. c (2003).

Gopireddy, D., Husson, S. M., Room temperature growth of surface-confined poly(acrylamide) from self-assembled monolayers using atom transfer radical polymerization, Macromolecules 35 (2002) 4218-4221.

Hebeish, A., Waly, A., Abdel-Mohdy, F.A., Aly, A.S., Synthesis and characterization of cellulose ion exchangers. I. Polymerization of glycidyl methacrylate, dimethylaminoethyl methacrylate, and acrylic acid with cotton cellulose using thiocarbonate–H_2O_2 redox system, J. Appl. Polym. Sci. 66 (1997) 1029–1037.

Jun, L., Min, Y., Jiuqiang, L., Hongfei, H., Preirradiation grafting polymerization of DMAEMA onto cotton cellulose fabrics, J. Appl. Polym. Sci. 81 (2001) 3578–3581.

Kawai, T., Saito, K., Lee, W., Protein binding to polymer brush, based on ion-exchange hydrophobic, and affinity interactions, J. Chromatogr. B 790 (2003) 131-142.

Khayet, M., Membrane surface modification and characterization by X-ray photoelectron spectroscopy, atomic force microscopy and contact angle measurements, Applied Surface Sci. 238 (2004) 269-272.

Knudsen, H. L., Fahrner, R. L., Xu, Y., Norling, L. A., Blank, G. S., Membrane ion-exchange chromatography for process-scale antibody purification, J. Chromatogr. A 907 (2001) 145-154.

Lee, S. B., Koepsel, R. R., Morley, S. W., Matyjaszewski, K., Sun, Y., Russell, A. J., Permanent, nonleaching antibacterial surfaces. 1. Synthesis by atom transfer radical polymerization, Biomacromolecules 5 (2004) 877–882.

Lightfoot, E. N., Moscariello, J. S., Bioseparations, Biotechnol. Bioeng. 87 (2004) 259-273.

Liu, Y., Kelp, V., Zdyrko, B., Luzinov, I., Polymer grafting via ATRP initiated from macroinitiator synthesized on surface, Langmuir 20 (2004) 6710.

Low, D., O'Leary, R., Pujar, N. S., Future of antibody purification. J. Chromatogr. B 848 (2007) 48-63.

Matyjaszewski, K., Xia, J., Atom transfer radical polymerization, Chem. Rev. 101 (2001) 2921-2990.

Pavlou, A. K., Belsey, M. J., The therapeutic antibody market to 2008, Eur. J. Pharm. Biopharm. 59 (2005) 389-396.

Pavlou, A. K., Reichert, J. M., Recombinant protein therapeutics—success rates, market trends and values to 2010, Nat. Biotechnol. 22 (2004) 1513-1519.

Roy, D., Knapp, J. S., Guthrie, J. T., Perrier, S., Antibacterial cellulose fiber via RAFT surface graft polymerization, Biomacromolecules 9 (2008) 91–99.

Samadi, A., Husson, S. M., Liu, Y., Luzinov, I., Kilbey II, S. M., Low-temperature growth of thick polystyrene brushes via ATRP, Macromolec. Rapid Commun. 26 (2005) 1829.

Singh, N., Husson, S. M., Zdyrko, B., Luzinov, I., Surface modification of microporous PVDF membranes by ATRP, J. Membr. Sci. 262 (2005) 81-90.

Singh, N., Wang, J., Ulbricht, M., Wickramasinghe, S. R., Husson, S. M., Surface-initiated atom transfer radical polymerization: A new method for the preparation of polymeric membrane adsorbers, J. Membr. Sci. 309 (2008) 64-72.

Thömmes, J., Etzel, M., Alternatives to chromatographic separations, Biotechnol. Prog. 23 (2007) 42-45.

Walsh, G., Biopharmaceutical benchmarks 2006, Nat. Biotechnol. 24 (2006) 769-776.

Yoshida, W., Cohen, Y., Topographical AFM characterization of graft polymerized silica membranes, J. Membr. Sci. 215 (2003) 249-264.

Yusof, A. H. M., Ulbricht, M., Polypropylene-based membrane adsorbers via photo-initiated graft copolymerization: Optimizing separation performance by preparation conditions, J. Membr. Sci. 311 (2008) 294-305.

CHAPTER 3

DRAMATIC PERFORMANCE IMPROVEMENT OF WEAK ANION-EXCHANGE

MEMBRANES FOR CHROMATOGRAPHIC BIOSEPARATIONS

3.1 Introduction

Chromatography is a universal unit operation in the biopharmaceutical industry for the downstream processing of protein therapeutics. As summarized in Chapter 2, the demand for protein therapeutics is increasing rapidly. Batch sizes are increasing, and costs must be reduced significantly for high dose chronic therapies [Lebreton et al., 2008]. Advances in cell culture technology have increased product titers from milligrams to multigrams per liter over the last decade or so [Wurm et al., 2004]. As production costs for protein therapeutics have shifted away from cell culture [Low et al., 2007], what remains as a bottleneck in their low-cost production is the downstream processing to purify them from crude cell culture media. There is, thus, enormous pressure on manufacturers to increase the throughput of downstream recovery and purification processes.

Historically, resin beads have been the preferred packing medium for chromatography columns due to reliability and effectiveness. Yet, conventional packed-bed chromatography is a high pressure drop, low throughput unit operation that exhibits flow rate-dependent dynamic capacities for biomacromolecules. For these reasons, membrane

chromatography has been promoted as a promising alternative to packed-bed chromatography [Knudsen et al., 2001; Lightfoot et al., 2004; Thömmes et al., 2007]. In recent years, development of new membranes and modules for membrane chromatography has been a focus for many researchers [Avramescu et al., 2008; Bhut et al., 2008; Ghosh et al., 2006; Hagiwara et al., 2005; He et al., 2008; Jain et al., 2007; Singh et al, 2005, 2008; Tatárová et al., 2009], and industrial applications of membrane chromatography have been demonstrated [Ghosh et al., 2002; Yu et al., 2008; Zhou et al., 2006]. In terms of membrane chromatography applications, ion exchange constitutes the largest market segment [Ghosh et al., 2002].

Although the potential for membrane chromatography is great, the process economy of membrane chromatography may be limiting its broad implementation; membranes often have lower binding capacity compared to packed-bed chromatography media [Van Reis et al., 2007]. Among several efforts to improve the economic viability of membrane chromatography, increasing the volumetric capacity of membranes is an obvious path forward. Therefore, a primary objective of this study was to create new weak-anion exchange membranes with ultrahigh protein binding capacities. Anion-exchange membranes were prepared by surface-initiated polymerization from macroporous membrane supports. The major advancement of this work is that we increased the density of polymerization initiation sites in a controlled way, which yielded a dramatic improvement in performance.

Incorporating functionality into commercially available base membranes via polymer grafting is an active area of research for investigators seeking to prepare membrane

77

adsorbers [Bhut et al., 2008; Hagiwara et al., 2005; He et al., 2008; Jain et al., 2007; Singh et al, 2005, 2008]. Grafted polymer chains extend into the protein solution that fills the membrane pores, providing a 3-dimensional 'scaffold' for protein molecules to adsorb and leading to relatively high protein binding capacities. A variety of micro- to macroporous membranes has been modified on the laboratory scale to produce membranes for bioseparations. Relevant to work proposed here are methods used to grow polyelectrolyte chains from the base membrane surface by monomer addition. Among the graft polymerization techniques, radiation grafting [Hagiwara et al., 2005; Kobayashi et al., 1993] and photografting [Kacar et al 2001; Ulbricht et al., 2005; Yusof et al., 2006] have been used frequently to prepare ion-exchange membranes. Among many noteworthy approaches, Yusof and Ulbricht et al. [2006] described photo-initiated, surface-selective graft polymerization to produce high capacity (~80 mg/mL) cation-exchange membranes for lysozyme purification. That same research group recently produced strong anion-exchange membranes by UV photografting from hydrophilized PP membranes using a synergistic photoinitiator immobilization method [He et al., 2008] that yielded high binding capacity for bovine serum albumin (BSA) (80 mg/mL). Hagiwara et al. [2005] used radiation-induced graft polymerization to graft glycidyl methacrylate on porous polyethylene hollow-fiber membranes and performed subsequent chemical modifications to incorporate anion-exchange groups into these membranes for bioseparations.

Membranes with a high density of accessible protein binding sites are essential for efficient chromatographic separations. While graft polymerization produces a large

78

number of binding sites, control over the modification is needed to avoid pore blocking.

Surface-initiated atom transfer radical polymerization (ATRP), a catalyst-activated

reaction, allows relatively fine control over average molecular weight and grafting

density of polymer chains [Börner et al., 2002], and yields polymer chains with low

polydispersity. Surface-initiated ATRP has been used only relatively recently by our

group and few others for the surface modification of polymeric and inorganic membranes

[Balachandra et al., 2003; Bhut et al., 2008; Singh et al., 2005, 2008; Jain et al., 2007;

Sun et al., 2006]. Pertinent to the discussion of membrane adsorbers, Husson and co-

workers have prepared high protein binding capacity weak cation-exchange [Singh et al.,

2008] and weak anion-exchange [Bhut et al., 2008] membranes using surface-initiated

ATRP from commercially available regenerated cellulose membranes. Bruening and co-

workers described the use of ATRP to incorporate immobilized metal ion affinity

functionalities within porous alumina membranes [Jain et al., 2007; Sun et al., 2006].

They achieved among the highest reported equilibrium binding capacities for BSA (150

mg/mL) and his-tagged ubiquitin (120 mg/mL). Dynamic capacities were not reported.

In work to date with ATRP, increasing membrane binding capacities has been done

by increasing polymerization time, and, thus the average M_w of the polymer chains

grafted from the membrane. However, the grafting density of the polymer chains is also

an important variable to increase the mass of grafted polymer, and, thus the protein

binding capacity. For other graft polymerization strategies, methods have been developed

to vary the initiator grafting density and to evaluate the effect of initiator grafting density

on polymer growth. Ma et al. [2000] described the use of UV irradiation time and

concentration of benzophenone in solution to increase initiation sites on porous PP membrane surfaces. Gravimetric measurements were used to estimate initiator densities. Kaur et al. [2007] used argon plasma exposure time to control the grafting density of methacrylic acid on electrospun nanofibrous PVDF membranes. The relative amount of grafted polymer was assessed by adsorption of toluidine blue dye. Ito et al. [1997] functionalized porous poly(tetrafluoroethylene) membranes by glow-discharge in the presence of ammonia in order to produce amino groups. Glow-discharge time was used to vary the amino group concentration. The work presented in this contribution focused on increasing and quantifying the density of initiation sites for ATRP by increasing the initiator precursor concentration during the membrane initiator-functionalization step.

This article describes a surface modification protocol to produce high protein binding capacity, weak anion-exchange membranes using surface-initiated ATRP from commercial regenerated cellulose membranes. Goals of this research were to increase the dynamic protein adsorption capacities significantly compared to previous works, and to characterize the performance of the newly designed weak anion-exchange membranes for protein chromatography. Grafting density and average molecular weight of polymer chains grown from the membrane pore surfaces were used as independent variables to prepare surface-modified membranes. Initiator grafting density was varied by changing the initiator precursor concentration during the membrane initiator-functionalization step. A mass balance method was used to quantify the initiator grafting density on initiator-functionalized membranes. Protein binding measurements were used to evaluate the effect of initiator grafting density at constant polymerization time. Polymerization time

was used as independent variable to increase the average molecular weight of polymer chains at constant grafting density. Dynamic and static binding capacities were measured using BSA as model protein so that we could compare results against commercial benchmarks. The effects of linear flow velocity and ionic strength on dynamic binding capacity were studied. Finally, the separation properties, protein purity and recovery, of newly designed membranes were evaluated by protein fractionation from binary protein mixtures composed of BSA and hemoglobin in phosphate buffer.

3.2 Experimental

3.2.1 Materials

Regenerated cellulose membranes (RC 60) with 70 µm thickness, 47 mm diameter, and 1.0 µm average effective pore diameter were purchased from Whatman, Inc. The following chemicals and solvents were purchased from Sigma-Aldrich, with purities given in wt.%: 2-(dimethylamino)ethyl methacrylate (DMAEMA, 98%), copper(I) bromide (98%), copper(II) chloride (99.999%), 1,1,4,7,10,10-hexamethyltriethylenetetramine (HMTETA, 97%), triethylamine (TEA, ≥99%), 2-bromoisobutyryl bromide (2-BIB, 98%), tetrahydrofuran (THF, anhydrous, ≥99.9%), 2-propanol (≥99.8%), ethanol (anhydrous, ≥99.5%), methanol (≥99.9%), water (ACS reagent grade, HPLC), and neutral, activated aluminum oxide. Prior to polymerization, DMAEMA was passed through a column of the neutral aluminum oxide to remove inhibitor compounds.

A stock solution of phosphate buffered saline (PBS) was prepared from bioreagent 1X powder concentrate (Fisher Scientific) and HPLC water (Fisher Scientific). Buffer B (10 mM PBS, pH 7.3) and buffer E (1 M NaCl in buffer B, adjusted to pH 4.0 with hydrochloric acid) were used as binding and elution buffers, respectively, for protein binding capacity measurements. Albumin from bovine serum (further purified fraction V, ~99%, M_r ~ 66 kDa) and hemoglobin from bovine blood (lyophilized powder, M_r ~ 64 kDa) were purchased from Sigma-Aldrich.

3.2.2 Membrane surface modification

Surface modification of regenerated cellulose membranes was carried out in two steps, as detailed in Chapter 2. The first step was membrane functionalization with initiator by treatment with a solution comprising the initiator precursor, 2-BIB; a neutralizing agent, TEA; and solvent, anhydrous THF. In the second step, initiator-functionalized membranes were modified by surface-initiated ATRP of DMAEMA. Polymerization time was used as the independent variable to control the molar mass of poly(DMAEMA) chains grafted from the pore surface of cellulose membrane, and, thus, the protein binding capacity of modified membranes.

3.2.3 Increasing the initiator grafting density

In order to increase the initiator grafting density systematically, the solution concentrations of 2-BIB and TEA in THF were varied from 1.8 to 18.0 mM during the initiator-functionalization step, always maintaining a 1:1 molar ratio of 2-BIB to TEA. The solution volume per membrane (50 mL) was kept constant during all of the experiments. Membranes were placed in a specially designed Teflon cage, and a

magnetic stir bar was placed on the top of membrane cage to agitate the initiator solution. Initiator grafting density was calculated from a mass balance based on the difference between initial and final concentration of 2-BIB in the solution. Initial and final concentrations of 2-BIB were determined by HPLC (HP 1100 Series) using an organic acid analysis column (Bio-Rad Aminex HPX-87H ion-exchange column, 300 mm $\times$ 7.8 mm). The mobile phase was 0.05 mM H_2SO_4 with a flow rate of 0.5 mL/min. The column was maintained at 40° C. Sample injection volumes were 10 and 20 μL. Detection was done by measuring UV absorbance at 220 nm; absorption data were collected using Chemstation B.02.01 software. Final unknown concentrations of 2-BIB were calculated from the calibration curve prepared using known concentrations of 2-BIB.

3.2.4 Performance properties of modified membranes

3.2.4.1 Protein static binding capacity

Bovine serum albumin (BSA) was used as model protein to measure static protein adsorption capacities of modified membranes. BSA concentrations of 3.0 or 4.0 mg/mL were prepared in PBS buffer B. Two high concentrations were used to ensure that the measured capacities were maximum values (i.e., in the plateau region of the adsorption isotherm) and to ensure that high precision measurements (i.e., a significant difference was observed between initial and equilibrium concentrations). Each membrane (47 mm dia.) was placed in a 40 mL glass bottle (I-Chem* short, wide-mouth, Fisher Scientific) and incubated in 10 mL protein solution for 20 h to reach equilibrium in a shaker bath at 22 °C. Work described in Chapter 2 confirmed that 20 h was sufficient to reach

equilibrium under the agitation conditions used in this study. Next, membranes were removed from the glass bottles and equilibrium concentrations of the protein solutions were measured using an ÄKTA Purifier 100 chromatography system (GE Healthcare Bio-sciences) with UV detection at 280 nm. Binding capacities, reported as the adsorbed mass of protein per unit volume of membrane, were calculated by mass balance using initial and equilibrium concentrations of protein solution determined from a calibration plot.

3.2.4.2 Reversible dynamic protein binding capacity: bind-and-elute method

Reversible dynamic adsorption capacities of modified membranes were measured using an ÄKTA Purifier 100 chromatography system. Modified membranes were cut into small diameter (12 mm) discs and equilibrated with 20 mL of buffer B in a constant-temperature shaker bath prior to loading into a membrane chromatography module. A stack of two membrane discs were placed in a CIM® module (BIA Separations, Inc.). Next, the module was attached to an ÄKTA Purifier. Buffer B and buffer E were used as binding and elution buffers, respectively.

A relatively high flow rate of 4 mL/min (linear velocity 212 cm/h, 253 bed volumes/min) was maintained during all of the dynamic binding capacity measurements. Buffer B was run through the membrane module to equilibrate the membrane bed until a stable base line was observed with UV detection at 280 nm. Then, a protein solution (3 mg BSA/ mL buffer B) was injected. A typical injection protocol for a single run was as follows: 5 mL of buffer B to equilibrate membranes, 2 mL of protein solution to load membranes, 6 mL of buffer B to remove unbound protein, 5 mL of buffer E to elute the

bound protein, and 5 mL of buffer B to prepare the membrane bed for the next run. The effluent from the membrane module was monitored continuously with UV detection at 280 nm, pH, and conductivity detectors. The pressure drop across the membrane bed was monitored by pressure transducers installed in the ÄKTA Purifier system. All data were recorded and viewed in Unicorn 5.1 software (GE Healthcare Bio-sciences). Reversible binding capacities were calculated from the mass of protein in the elution peak, as determined from an independent calibration curve, and the volume of the membrane bed. Dynamic binding capacities were measured three times for each stack of membranes, and reversible dynamic binding capacity is reported as the average of the three measurements.

3.2.4.3 Flow rate effect on reversible binding capacity

A stack of two membrane discs, modified by surface-initiated ATRP for 4 hours, was used to determine the effect of flow rate on reversible binding capacities of modified membranes. The binding and elution buffers, mass of injected protein, and injection protocol were the same as mentioned in Section 3.2.4.2, while flow rate was varied from 1 mL/min to 10 mL/min (53 to 530 cm/h, 63 to 630 bed volumes/min). Two measurements were taken at each flow rate, and reversible dynamic binding capacity is reported as the average of two measurements.

3.2.4.4 Ionic strength effect on reversible binding capacity

A stack of two membrane discs, modified by surface-initiated ATRP for 5 hours, was used to determine the effect of ionic strength on reversible binding capacities of modified membranes. Ionic strength was varied by increasing buffer concentration in binding buffer B. Binding buffers with pH 7.3 were prepared with 10, 20, 30, 50, 75, 100, 125

85

and 150 mM PBS buffer. Elution buffer E was the same as reported earlier. Protein solutions (3 mg BSA/mL) were prepared from each of the binding buffers. The flow rate was 4 mL/min (linear velocity 212 cm/h, 253 bed volumes/min). The injection protocol was the same as that used for all other dynamic binding capacity measurements. The reversible dynamic binding capacity is reported as the average of two measurements.

3.2.4.5 Protein fractionation studies

A binary protein mixture was used that comprised equal masses of BSA and hemoglobin in binding buffer B_2 (20 mM PBS, pH 7.0). The membrane chromatography module was loaded with a stack of four membrane discs that had been modified by surface-initiated ATRP for 6 hours. The flow rate was 2 mL/min (106 cm/h, 126 bed volumes/min), and 1 mL of the protein solution ((1 mg BSA + 1 mg hemoglobin)/mL buffer B_2) was used for protein fractionation measurements. Elution buffer E_2 was prepared in binding buffer B_2 by adding NaCl (1 M) and adjusting pH to 4.0. The injection protocol was the same as that used above for all other dynamic binding capacity measurements.

Indirect calculation of the composition of proteins in each peak (i.e., peaks associated with un-adsorbed protein and eluted protein) was done using data collected from individual injections of 1 mg BSA/mL buffer B_2 and 1 mg hemoglobin/mL buffer B_2. Three runs for each protein solution were made with modified membranes, and the average masses of protein observed in the un-adsorbed and eluted protein peaks were calculated from a calibration plot.

3.2.4.6 Dynamic protein binding capacity: breakthrough curve method

In order to compare our bind-and-elute method for measuring dynamic capacity with a standard method, we also determined the dynamic binding capacities for one set of modified membranes from protein breakthrough curves. A stack of five membrane discs, modified by surface-initiated ATRP for 5 hours, was used to determine the dynamic binding capacities of modified membranes by this method. The modified membranes were cut into 30 mm diameter discs and placed into a membrane module fabricated by Clemson University Machining and Technical Services. Thus, in addition to allowing comparison between measurement methods, this experiment allowed comparison between different membrane modules. Buffer B was used to equilibrate the membrane bed. A protein solution (3 mg BSA/ mL buffer B) was injected using a Superloop^{TM} (50 mL; GE Healthcare Biosciences) until the protein concentration in the effluent approached its feed concentration. Three different flow rates 10 mL/min (91 cm/h, 43 bed volumes/min), 15 mL/min (136 cm/h, 65 bed volumes/min) and 20 mL/min (183 cm/h, 87 bed volumes/min) were used to obtain breakthrough curves. The column dead volume was determined using the retention time (initial breakthrough) of protein through the bed prepared from a stack of five un-modified membranes. Dynamic binding capacities were calculated at 10% breakthrough. Two measurements were taken at each flow rate, and dynamic binding capacity is reported as the average of two measurements.

3.3. Results and discussion

3.3.1 Membrane surface modification

Husson and coworkers [Bhut et al., 2008; Singh et al., 2005; Singh et al., 2008] have demonstrated that surface-initiated ATRP can be used to control the molar mass of polymer chains grown from membrane pore surfaces. In this work, the initiator grafting density and molecular weight of poly(DMAEMA) chains were varied independently to yield surface-modified, macroporous, regenerated cellulose membranes with exceptionally high dynamic protein binding capacities under conditions of high volumetric throughput and low column pressure drop.

In the first set of experiments, the initiator grafting density was increased systematically while keeping polymerization time constant. Initiator grafting density was increased by increasing the concentration of initiator precursor, 2-BIB, in solution during the membrane initiator-functionalization reaction. In the second set of experiments, average molecular weight of poly(DMAEMA) chains was increased by increasing polymerization time at constant initiator grafting density. An optimized polymerization protocol, developed from a kinetic study of surface-initiated ATRP of poly(DMAEMA) [Bhut et al., 2008], was used to modify membranes. Static protein binding capacity measurements were used to evaluate the effects of increasing the initiator grafting density and molecular weight of poly(DMAEMA) chains.

3.3.1.1 Effect of initiator grafting density

Fig. 3.1(a) shows the dependence of static protein (BSA) binding capacity on initiator precursor concentration for surface-modified membranes prepared using two different polymerization times. For 2 hour polymerization, the static binding capacity increases

88

linearly up to the 9.0 mM initiator precursor concentration and then reaches a plateau

value of 61.0 mg/mL between 10.7–14.3 mM.
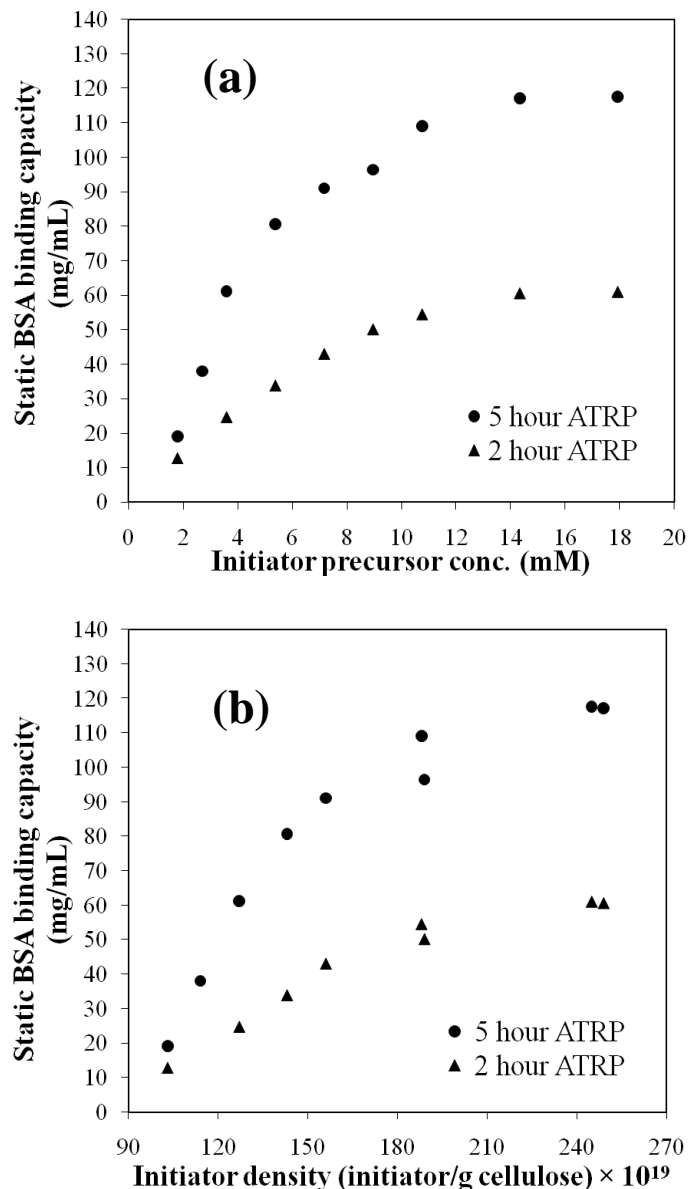
Figure 3.1 Dependence of static protein binding capacities on initiator precursor (2-BIB) concentration (a) and initiator density (b) for poly(DMAEMA)-modified membranes. Initiator-functionalized membranes were modified further by surface-initiated ATRP (DMAEMA (2M)/Cu(I)/Cu(II)/HMTETA: 2000/1/0.1/2.2). Symbols (●) and (▲) represent static BSA binding capacities of membranes modified for 5 h and 2 h, respectively.

This observation agreed with our expectation that the initiator grafting density would increase by increasing the initiator precursor concentration until all available hydroxyl groups of the base cellulose membrane were reacted. If termination of polymer chains and chain transfer are not considered, then the grafting density of polymer chains and, thus, the protein binding capacity should increase linearly with initiator grafting density. However, termination of polymer chains becomes more significant at higher initiator grafting densities, and it may impose its own limitation for the increase in polymer chain grafting density [Bao et al., 2006; Samadi et al., 2005; Singh et al., 2007]. We use a formulation in this work that yields controlled growth (i.e., minimal termination) [Bhut et al., 2008]. In order to determine whether the plateau in protein binding capacity was caused by a plateau in initiator density or a steric limitation due to pore filling by polymer chains, a second set of experiments was carried out using a constant 5 hour polymerization time. As demonstrated in Chapter 2, our established ATRP protocol yields controlled growth for this system. Accordingly, if the plateau in protein binding capacity was caused by a plateau in initiator density, then we would anticipate a 2.5 fold increase in the static protein binding capacity for the 5 hour polymerization and a similar relationship between capacity and initiator precursor concentration as observed in the first set of data. If the plateau in capacity was due to steric limitations, then increasing the polymerization time would not increase capacity further. Fig. 3.1(a) shows the data for 5 hour polymerization time. The static protein binding capacity increased linearly with initiator precursor concentration up to 3.5 mM, and increased nonlinearly with further increases in initiator precursor concentration, eventually reaching a plateau value of

117.6 mg/mL. The increase in capacity values in the linear region agrees well with our expectation, and the plateau value occurs between 10.7–14.3 mM, as was found for the 2 hour polymerization data. Both results support a conclusion that initiator density is the factor limiting capacity at short polymerization times.

While initiator density was the primary factor limiting capacity in these experiments, Fig. 3.1(a) does reveal two indicators that steric hindrance may play some role (either in protein binding or polymer growth). Firstly, the onset of nonlinearity occurs at different values of initiator precursor concentration in the two sets of data, while the capacity values where non-linearity begins are similar (ca. 50–70 mg/ml). Secondly, the increase in maximum protein binding capacity is 1.9 times, which is lower than the expected value of 2.5. We propose two reasons for this behavior: 1) As the mass of poly(DMAEMA) grafted from the membrane surface increases, membrane porosity decreases, and the smallest pores begin to fill with polymer, slowing and eventually ceasing polymer growth. 2) The 'thick' polymer brushes grown using longer polymerization time may create limited accessibility of monomer to growing polymer chains in the stagnant fluid filled pores. In our previous work [Bhut et al., 2008], as well this work (vide infra), we found that the static BSA binding capacity for this base membrane increases linearly with polymerization time up to ~60 mg/mL, indicating that the reasons mentioned above are not limiting factors at low degrees of functionalization. Steric hindrance and pore filling effects appear to depend on the mass of polymer grafted (as indicated by the protein binding capacity), not on how the polymer was deposited (e.g., short polymerization time with high graft density v. long polymerization time with low graft density). Furthermore,

91

protein access to binding sites along the polymer chains does not appear to be impeded by the highest graft densities achieved in this work. If grafting densities were too high, then protein would be excluded from the layer, and we would see the capacity go through a maximum and then begin to decrease with further increases in graft density. It therefore appears that any steric limitation to protein binding is due to pore filling, rather than increasing chain density, at least to the values achieved in this work.

In order to gain more information about the membrane initiator functionalization process, a mass balance was used to quantify how much initiator was consumed during this process. HPLC was used to measure initial ($C_{t=0}$) and final ($C_{t=2\,h}$) concentrations of 2-BIB in solution. From these measurements, conversion and total number of initiator molecules consumed per membrane were calculated. The initiator-functionalization reaction was carried out inside a moisture-free glove box (1 < ppm H2O) to prevent possible hydrolysis of 2-BIB. Even if partial hydrolysis did occur, the method used to calculate initiator grafting density accounts for possible hydrolysis of the initiator in solution. We measured UV absorbance at 220 nm and correlated this absorbance to concentration. The absorbance signal at this wavelength is associated with the carbonyl group that is present in the initiator molecule (2-BIB) and its hydrolysis product (2-bromo-2-methylpropionic acid). Therefore, the calculation of the number of 2-BIB molecules consumed during initiator-functionalization will not be affected since it is based on the difference between initial and final solution concentration. Theoretically, every repeat unit of pure cellulose contains three hydroxyl groups. Based on this information, the maximum number of hydroxyl groups per base membrane was

calculated. Combining these two sets of information, the ratio of initiator to hydroxyl group and initiator grafting density (or yield, i.e., number of initiator molecules per gram of base membrane) were calculated. Table 3.1 summarizes these results.

Table 3.1 Results of membrane initiator functionalization step.

Initiator precursor[a]		Conversion	Initiator[b]/ membrane	Initiator[b]/OH[c]	Initiator density $\times 10^{-19}$
$C_{t=0}$ (mM)	$C_{t=2h}$ (mM)	(%)	(µmol)	(%)	(g cellulose^{-1})
1.79	0.14 ± 0.03	92.2 ± 1.7	82.5 ± 3.0	9.20 ± 0.30	103 ± 4
3.58	1.54 ± 0.05	57.1 ± 1.3	102 ± 5	11.4 ± 0.6	127 ± 6
5.37	3.07 ± 0.08	42.8 ± 1.4	115 ± 8	12.8 ± 0.9	143 ± 10
7.16	4.67 ± 0.08	34.8 ± 1.1	125 ± 8	13.9 ± 0.9	156 ± 10
8.95	5.91 ± 0.22	34.0 ± 2.4	152 ± 22	17.0 ± 2.5	189 ± 27
10.74	7.73 ± 0.05	28.0 ± 0.5	151 ± 6	16.8 ± 0.6	188 ± 6
14.32	10.33 ± 0.11	27.9 ± 0.7	200 ± 11	22.3 ± 1.2	249 ± 14
17.90	13.97 ± 0.07	22.0 ± 0.4	197 ± 7	22.0 ± 0.8	245 ± 9
21.48	17.48 ± 0.01	18.6 ± 0.1	200 ± 1	22.3 ± 0.1	249 ± 1

[a]2-BIB. [b]α-bromoester attached to the membrane pore surface by reaction of 2-BIB with a hydroxyl group. [c]Calculated based on the maximum possible OH groups per membrane, assuming that the base membrane is made of pure cellulose.
Note: Two measurements were taken at each initiator precursor concentration and data in the figure represent the average of those measurements. The error bars represent ± 1 standard deviation from the average value.

The initiator grafting density increases linearly with initiator precursor concentration up to the 14.32 mM initiator precursor concentration and then becomes constant. Fig 3.1(b) shows the relationship between static BSA binding capacity and initiator density. The BSA binding capacity increases linearly with initiator density up to about 156×10^{19}/g membrane for 2 hour polymerization and eventually reaches a plateau value. For 5 hour polymerization, the static protein binding capacity increased linearly with initiator density to a lower value of about 127×10^{19}/g membrane and increased nonlinearly with

further increases in initiator density, eventually reaching a plateau value. Thus, for longer polymerization time, a lower initiator density is needed to reach the non-linear region of the diagram. This result strengthens our rationalization that the non-linear increase in protein binding capacity at higher initiator precursor concentrations (Fig.3.1a) is due to the limited accessibility of monomer and/or pore filling effects.

Overall, this part of the study showed that increasing the initiator precursor concentration leads to increased initiator grafting density. Furthermore, we observed that increasing initiator grafting density at constant polymerization time, and, thus, constant molecular weight of poly(DMAEMA) chains grafted from membrane pore surface, increased the protein binding capacity of the modified membranes. Taken together, these results indicate that increasing initiator grafting density leads to higher polymer chain density. This observation agrees with work done on the flat substrates and reported by other researchers [Bao et al., 2006; Singh et al., 2007].

3.3.1.2 Effect of molar mass of poly(DMAEMA) chains

In another set of experiments, the degree of polymerization, and, thus, molar mass of poly(DMAEMA), was increased by increasing polymerization time at constant initiator grafting density. Membranes were prepared using a high initiator precursor concentration of 18 mM. Fig. 3.2 shows that increasing polymerization time at constant initiator grafting density increases the protein binding capacity of modified membranes. As polymerization time increases, the protein binding capacity increases at a slower rate and eventually reaches the plateau value of ~140 mg/mL. Again, we submit that this behavior indicates a slowing down of polymer growth due to pore filling and/or limited

94

accessibility of monomer to growing polymer chains in the stagnant fluid filled pores at longer polymerization time. This result also was observed in our previous studies [Bhut et al., 2008; Singh et al., 2008].
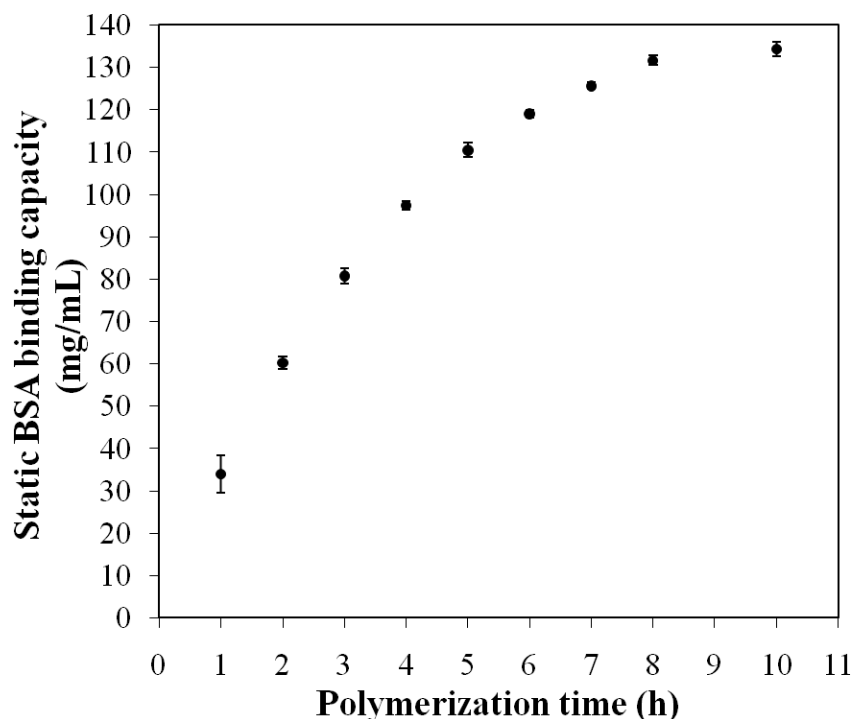
Figure 3.2 Dependence of static protein binding capacities on polymerization time for poly(DMAEMA)-modified membranes. Surface-initiated ATRP (DMAEMA (2M)/Cu(I)/Cu(II)/HMTETA: 2000/1/0.1/2.2) was used to produce the polymer-modified membranes. Two static biding measurements were perofrmed at each polymerization time and data in the figure represent the average of those measurements. The error bars represent ± 1 standard deviation from the average value.

Overall, the proposed ATRP protocol allows independent control over the grafting density and molecular weight of poly(DMAEMA) chains grown from cellulose membrane pore surface to yield very high volumetric protein binding capacity membranes for membrane-based chromatographic bioseparations.

3.3.2 Performance properties of modified membranes

Information about dynamic protein binding capacity, the impact of volumetric flow rate on dynamic capacity, separation efficiency, and reusability of the membrane module is necessary to use our newly designed, surface-modified membranes for protein ion-exchange chromatography. A comprehensive set of these experiments was carried out and will be discussed.

3.3.2.1 Reversible protein binding capacities: bind-and-elute method

The dynamic capacities of modified membranes were measured according to the chromatographic protocol shown in Fig. 3.3. Poly(DMAEMA) chains are responsive to the pH and ionic strength of the buffer. Due to charge repulsion at low ionic strength, polyelectrolyte chains extend away from the surface toward the internal pores and adjust geometric orientation according to the buffer flow [Bhut et al., 2008; He et al., 2008; Singh et al., 2008]. Therefore, binding buffer B was pumped through the membrane bed to equilibrate the poly(DMAEMA) chains prior to the protein solution injection. Thereafter, protein solution was injected into the membrane bed using a 50 mL Superloop^{TM} (GE Healthcare Biosciences). Data collection in Fig. 3.3 was started when the protein solution was injected. The pKa value for the tertiary amine group of the DMAEMA is about 8.0−9.0 [Merle et al., 1987; Uchida et al., 1993], and the isoelectric point (pI) of the BSA is about 4.7−4.9. Since buffer B has pH 7.3, the poly(DMAEMA)-modified membrane surface (weak anion-exchange membrane) is charged positively, while BSA molecules carry net negative charge. Therefore, the injected protein molecules bind to the poly(DMAEMA) chains grafted from the internal pore-wall surface of the membrane.

96
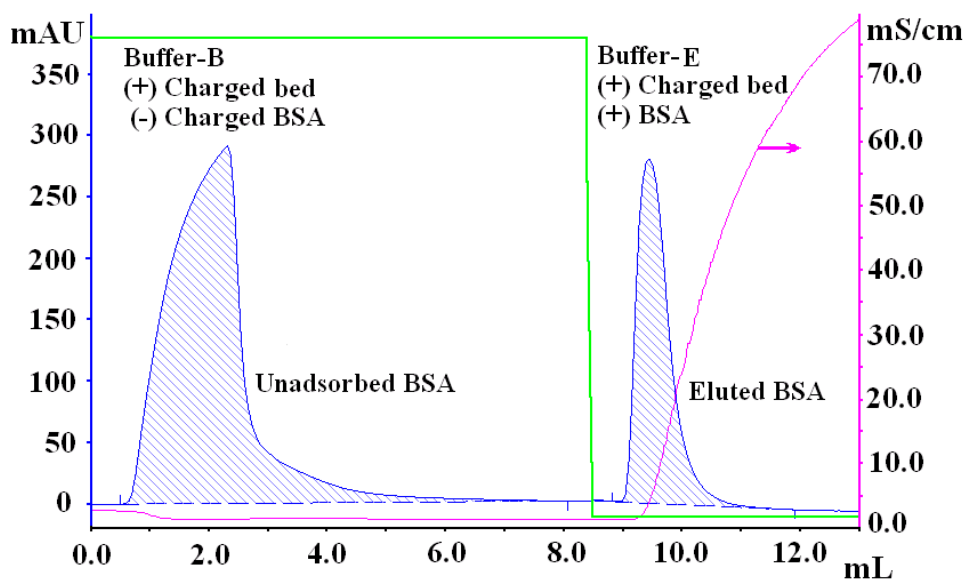
Figure 3.3 Typical chromatogram for a dynamic protein binding capacity measurement using poly(DMAEMA)-modified membranes (bed height: 140 μm; flow rate: 4 mL/min, 253 bed volumes/min; linear flow velocity: 212 cm/h; binding buffer B; elution buffer E). Surface-initiated ATRP (DMAEMA (2M)/Cu(I)/Cu(II)/HMTETA: 2000/1/0.1/2.2; polymerization time: 6 hr) was used to produce the polymer-modified membranes.

As the membrane bed capacity is approached, unadsorbed BSA molecules begin to breakthrough and appear as the first peak in Fig. 3.3. After protein injection, the binding buffer was used to rinse the bed until the UV absorbance returned to its baseline. Next, a step change was made to elution buffer E (1 M NaCl in buffer B, pH 4.0). At pH 4.0, BSA and the poly(DMAEMA) on the membrane surface both have a net positive charge, and, due to charge repulsion, the bound protein is released from the membrane bed. Furthermore, any potential Coulombic interactions between poly(DMAEMA) and localized negative charges on BSA at pH < pI of the protein will be screened by ions in the high ionic strength elution buffer E, as discussed in Section 3.3.2.3. The mass of protein bound to the membrane bed was calculated from the area under the elution peak

and a calibration curve. Protein recovery was calculated as the quotient of the sum of the

masses of BSA in the un-adsorbed and eluted protein peaks (Fig. 3.3) to the mass of

protein injected, multiplied by 100%.
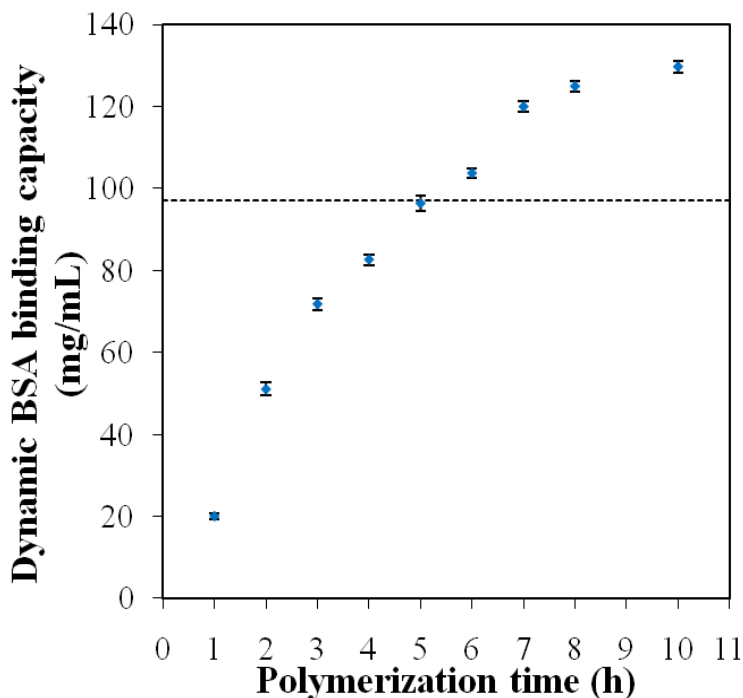
Figure 3.4 Dependence of dynamic protein binding capacities on polymerization time for
poly(DMAEMA)-modified membranes (bed height: 140 µm; flow rate: 4 mL/min,253
bed volumes/min; linear flow velocity: 212 cm/h; binding buffer B; elution buffer E).
Surface-initiated ATRP (DMAEMA (2M)/Cu(I)/Cu(II)/HMTETA: 2000/1/0.1/2.2) was
used to produce the polymer-modified membranes. Dotted line represents the dynamic
binding capacity of poly(DMAEMA)-modified membranes for 5 h polymerization time
using breakthrough curve method (Section 3.3.2.3). Dynamic binding capacities were
measured three times for each stack of membranes, and reversible dynamic binding
capacity is reported as the average of the three measurements. The error bars represent ±
1 standard deviation from the average value.

Fig. 3.4 shows that the dynamic protein binding capacity of modified membranes

increased with increasing polymerization time. The error bars represent the standard

deviation from the average of three measurements of dynamic binding capacity for a

single membrane bed. The dynamic binding capacity follows the same qualitative

behavior as static binding capacity with polymerization time (Fig. 3.2). The measured

dynamic binding capacity was 88–97% of the static binding capacity, demonstrating that

the charged anion-exchange groups are highly accessible. Micron-size membrane pores

offer convective transport of the protein molecules from the main stream to binding sites.

Therefore, the characteristic diffusion time for the protein molecule is reduced markedly

compared to resin beds and that reduces the processing times and liquid volumes for

bioseparations [Lightfoot et al., 2004; Thömmes et al., 2007; Van Reis et al., 2007]. This

point is detailed in Chapter 4.

3.3.2.2 Flow rate effect on reversible binding capacity

High protein accessibility to binding sites was supported further by increasing

volumetric flow rate through the membrane bed and measuring the dynamic binding

capacities at various flow rates. Fig. 3.5 shows the effect of linear flow velocity on

dynamic binding capacity of modified membranes. The flow rate was increased 10-fold,

and, thus, the residence time for protein molecules through the membrane bed was

decreased by the same factor. Dynamic binding capacity of the membrane did not change

significantly by increasing the linear flow velocity. These data demonstrate that the mass

transfer of protein molecules to the binding sites for macroporous membrane beds is

limited primarily by convection, not diffusion, which is the rate controlling mechanism

for resin beds [Tao et al., 2008]. However, the dynamic capacity at the lowest flow rate (1

mL/min) was about 5–6% lower than the dynamic capacity at all other flow rates studied.

We attribute this result to the non-uniform flow distribution of injected protein solution

into the membrane bed. Membrane module design affects the dynamic binding capacity of the membrane bed [Ghosh et al., 2006]. In the CIM® membrane module, the flow enters the membrane bed through a small circular channel and then distributes through a porous frit to a relatively large circular cross section of the membrane stack. At low volumetric flow rates, the central portion of the membrane bed saturates rapidly before the protein solution reaches the periphery of the membrane bed. At the lowest flow rate (1 mL/min) studied here, this non-uniform flow distribution resulted in lower dynamic binding capacity.
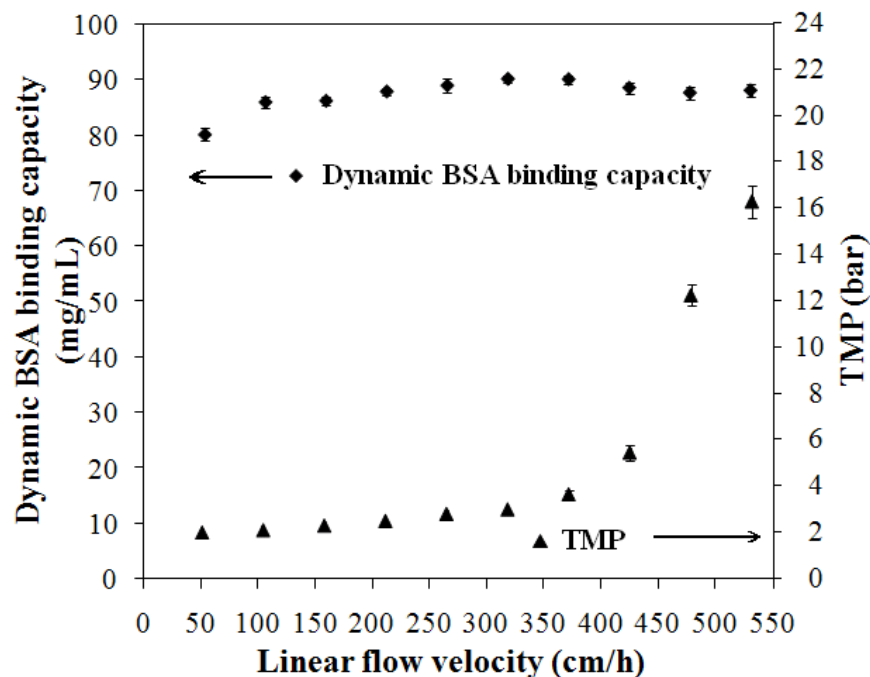
Figure 3.5 Dependence of dynamic protein binding capacities and transmembrane pressure (TMP) on linear flow velocity for poly(DMAEMA)-modified membranes (bed height: 140 μm; binding buffer B; elution buffer E). Surface-initiated ATRP (DMAEMA (2M)/Cu(I)/Cu(II)/HMTETA: 2000/1/0.1/2.2; polymerization time: 4 hr) was used to produce the polymer-modified membranes. (♦) and (▲) represent the dynamic protein binding capacities and TMP values, respectively. Two measurements were taken at each flow rate, and reversible dynamic binding capacity is reported as the average of two measurements. The error bars represent ± 1 standard deviation from the average value.

We also measured the transmembrane pressure (TMP) at various flow rates and these data are reported in Fig. 3.5. Pressure drop was measured after equilibration of membrane with binding buffer B, before injecting the protein solution. TMP remained below 3 bar up to a relatively high flow rate of 7 mL/min (371 cm/h, 442 bed volumes/min), supporting claims that membrane chromatography is a low pressure drop and high throughput operation [Ghosh et al., 2002; Lightfoot et al., 2004].
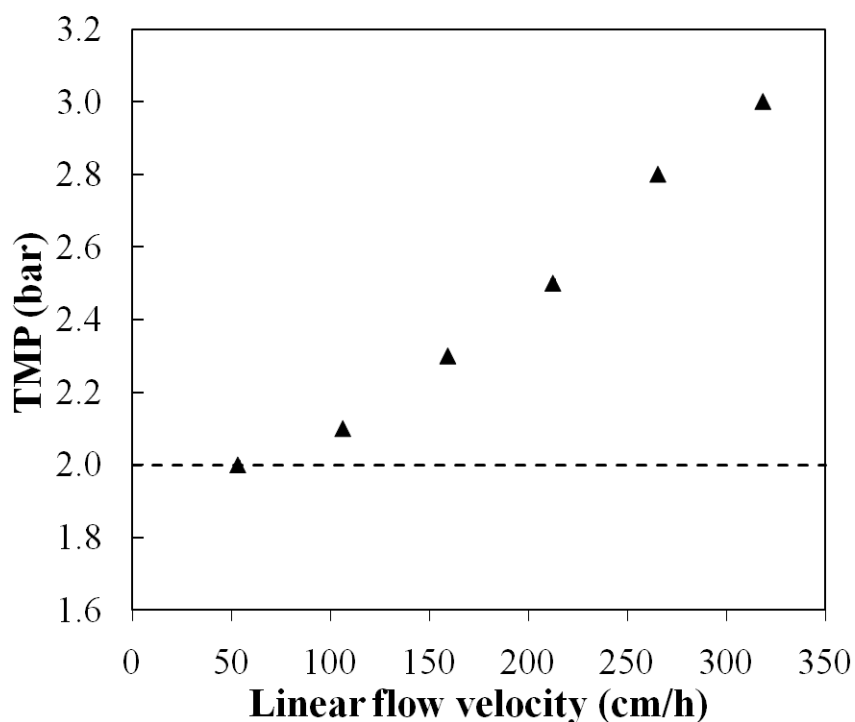
Figure 3.6 Dependence of transmembrane pressure (TMP) on linear flow velocity for poly(DMAEMA)-modified membranes (bed height: 140 μm; binding buffer B; elution buffer E). Surface-initiated ATRP (DMAEMA (2M)/Cu(I)/Cu(II)/HMTETA: 2000/1/0.1/2.2; polymerization time: 4 hr) was used to produce the polymer-modified membranes.

The nonlinear relationship between flow velocity and TMP at low flow velocity is an artifact of the system pressure measurement. The AKTA purifier maintains a minimum 2

bar (gauge) system back pressure. That is, at any flow rate, with or without column, the system pressure readout will be 2 bar or higher. Therefore, we cannot measure any TMP less than 2 bar even though it might be lower than the system recorded pressure at low flow rates (1−2 mL/min). If we expand the low TMP data of Fig. 3.5, then we see the linear behavior for values above 2 bar before the onset of membrane degradation (Fig. 3.6). The pressure drop versus flow rate was completely reversible up to 8 mL/min (424 cm/h, 505 bed volumes/min), and the membrane bed was reused over 20 times with no loss of performance. As we increased the flow rate above 8 mL/min, the pressure drop increased rapidly and was no longer completely reversible. We attribute this behavior to structural changes (i.e., damage) to the membrane bed at high flow rates (9−10 mL/min, 477−531 cm/h, 568−632 bed volumes/min). At 9 and 10 mL/min flow rates, the membrane bed had to be replaced after every single measurement.

3.3.2.3 Dynamic protein binding capacities: breakthrough curve method

The conventional method to determine dynamic binding capacity is to measure the mass of protein bound per unit bed volume at the point where the effluent concentration reaches 10% of the feed concentration. In order to compare results from our bind-and-elute measurement method with this conventional method, we measured the dynamic protein binding capacity of a modified membrane at 10% breakthrough. Fig. 3.7 shows the breakthrough curves for un-modified and surface-modified membrane beds. The curves for un-modified membrane were used to define the system dead volume. The dynamic capacity measured at 10% breakthrough (Table 3.2 and dotted line in Fig. 3.4) and the reversible protein binding capacity measured (Fig. 3.4, 5 h polymerization time)

from the bind-and-elute method (Section 3.2.4.2.) were similar in value. Also important is that the shape of the breakthrough curves for the modified membranes and, thus, the dynamic binding capacity, did not change by changing the volumetric flow rate, which is the same conclusion that we reached in Section 3.3.2.2 using the bind-and-elute method.
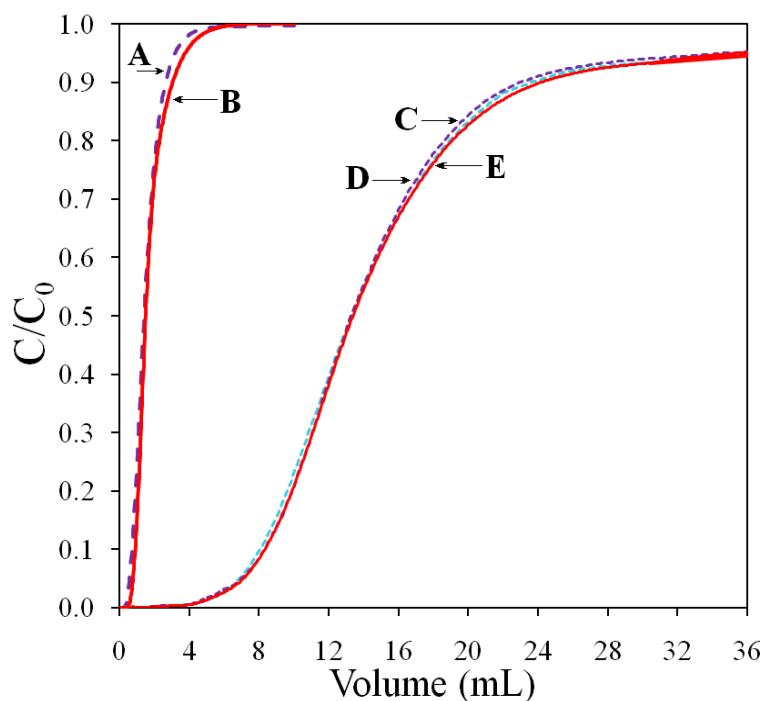
Figure 3.7 Breakthrough curves for un-modified and poly(DMAEMA)-modified membranes (bed height: 350 µm; bed diameter: 30 mm; protein feed solution: 3 mg BSA/mL; buffer B). Surface-initiated ATRP (DMAEMA (2M)/Cu(I)/Cu(II)/HMTETA: 2000/1/0.1/2.2; polymerization time: 5 hr) was used to produce the polymer-modified membranes. Breakthrough curves represent: A – module without membrane bed; B: module with un-modified membrane bed; C, D and E: module with poly(DMAEMA)-modified membranes bed for 5 hour polymerization at 91 cm/h (43 bed volumes/min), 136 cm/h (65 bed volumes /min), and 182 cm/h (87 bed volumes/min), respectively.

Table 3.2 Dynamic binding capacity measured at 10% breakthrough for poly(DMAEMA)-modified membranes prepared using a 5 hour polymerization time.

Flow rate			Dynamic capacity
(cm/h)	(bed volumes/min)	(mL/min)	(mg BSA/mL)
91	43	10	93.0
136	65	15	97.2
182	87	20	97.5
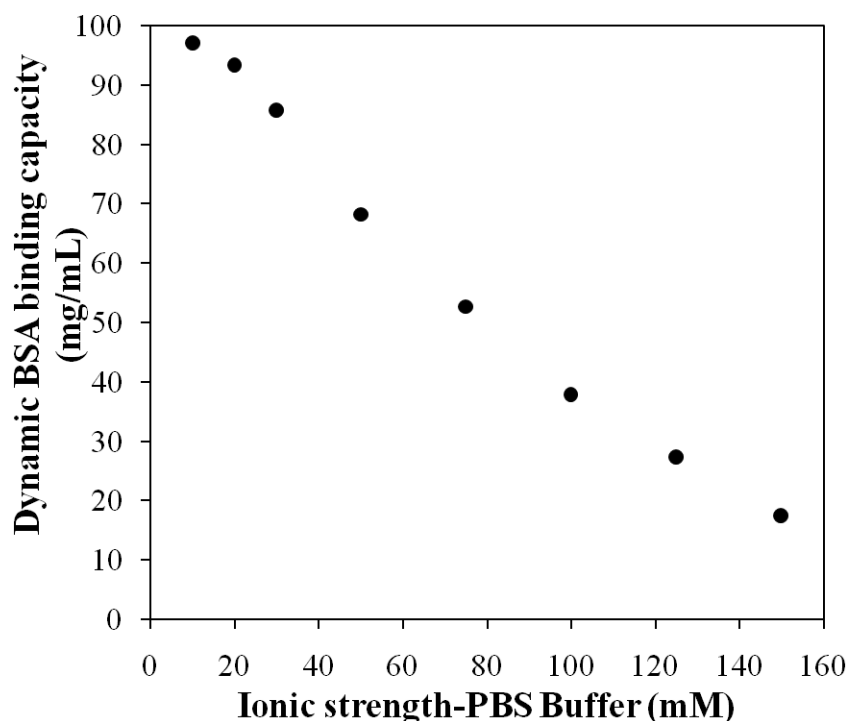
Figure 3.8 Dependence of dynamic protein binding capacities on ionic strength for poly(DMAEMA)-modified membranes (bed height: 140 μm; flow rate: 4 mL/min, 253 bed volumes/min: linear flow velocity: 212 cm/h; binding buffer B: 10−120 mM PBS; elution buffer E). Surface-initiated ATRP (DMAEMA (2M)/Cu(I)/Cu(II)/HMTETA: 2000/1/0.1/2.2; polymerization time: 5 hr) was used to produce the polymer-modified membranes.

3.3.2.4 Ionic strength effect on reversible dynamic binding capacity

Fig. 3.8 shows the effect of ionic strength on protein dynamic binding capacity of

newly designed membranes. The protein binding capacity decreases in a regular fashion

with increasing ionic strength in the loading buffer. This behavior is logical: increasing ionic strength leads to a less-expanded network of the grafted polyelectrolyte chains due to the charge screening effect of ions. Increasing ionic strength, the ions in the buffer compete with the protein molecules for binding sites. Both of these effects lead to the lower protein binding capacities.

3.3.2.5 Protein fractionation studies

Separation properties, protein purity and recovery, of newly designed membranes were evaluated by protein fractionation performance tests. BSA (pI 4.7–4.9) and hemoglobin (pI 6.8–7.0) are similar in size but different in their pI values; therefore, these proteins could be separated purely based on charge difference. A solution of 1 mg BSA and 1 mg hemoglobin dissolved in 1 mL binding buffer B_2 was injected into the membrane bed. At pH 7.0, BSA carries net negative charge, hemoglobin carries no net charge, and the membrane bed (weak anion-exchange) is charged positively. Therefore, the BSA binds to the membrane bed, while hemoglobin breaks through largely unadsorbed. Fig. 3.9 is a typical chromatogram that depicts the above described process. After the binding step, a step change was made to the elution buffer E_2. Due to high ionic strength and charge repulsion at pH 4.0, the bound BSA was released and a peak appears in Fig. 3.9 for the eluted protein. Table 3.3 summarizes the protein fractionation results. During three protein fractionation measurements, the purities of recovered protein were high (> 97%), and the recoveries also were high (> 98%). The calculated protein concentrations assume that the binding behavior was the same from the binary mixture as from the individual pure-component solutions. SDS-PAGE analysis supported this

assumption; no hemoglobin was found in the BSA product and no BSA was found in the hemoglobin product.
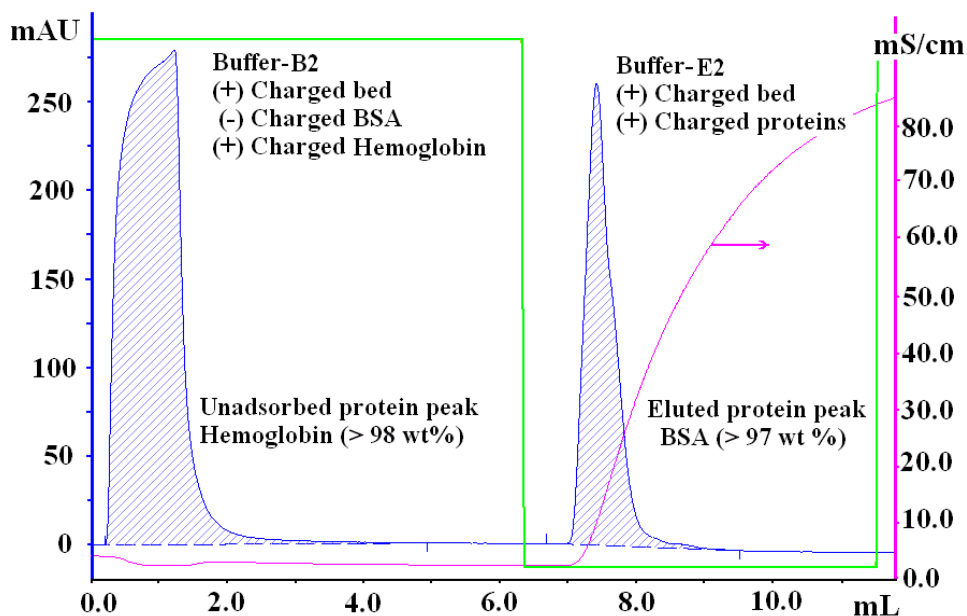
Figure 3.9 Typical chromatogram demonstrating protein fractionation from a binary protein mixture composed of equal masses of BSA and hemoglobin using ion-exchange chromatography (bed height: 280 μm; flow rate: 2 mL/min, 126 bed volumes/min: linear flow velocity: 106 cm/h; binding buffer B_2; elution buffer E_2). Surface-initiated ATRP (DMAEMA (2M)/Cu(I)/Cu(II)/HMTETA: 2000/1/0.1/2.2; polymerization time: 6 hr) was used to produce the polymer-modified membranes.

Table 3.3 Recovery and purity data for protein fractionation from a binary protein mixture composed of equal masses of BSA and hemoglobin.

Experiment No.	Composition (wt %)				Recovery (%)
	Un-adsorbed protein peak		Eluted protein peak		
	Hemoglobin	BSA	BSA	Hemoglobin	
1	98.36	1.64	97.74	2.26	98.89
2	98.35	1.64	97.72	2.27	98.53
3	98.37	1.63	97.72	2.27	98.86

Overall, the newly designed, high protein binding capacity, weak anion-exchange membranes exhibit excellent properties for protein chromatographic bioseparations. To

be assessed as viable commercially, investigations were needed to test the newly designed membranes for recovery of proteins from complex bioprocess streams. These studies are described in Chapter 4.

3.4 Conclusions

A two-step surface modification protocol involving surface-initiated atom transfer radical polymerization has been described to design high protein binding capacity weak anion-exchange membranes. The surface modification protocol shows two important trends: increasing initiator precursor concentration during membrane initiator functionalization increases the initiator grafting density and subsequently the density of grafted polymer chains, and increasing polymerization time at constant initiator grafting density increases the average molecular weight of the polymer chains grafted from membrane pore surface. Grafting density and molecular weight of the polymer chains grafted from the membrane pore surface can be tuned independently. Taken together, our results show that the protein binding capacities of membranes modified by surface-initiated ATRP can be increased by increasing initiator precursor concentration during the membrane initiator functionalization step or/and by increasing polymerization time. Newly designed membranes have very high volumetric protein binding capacities (static binding capacity ~ 140 mg BSA/mL and dynamic capacity ~ 130 mg/mL) at high linear flow velocities (> 350 cm/h) and low transmembrane pressure drop (< 3 bar). The measured dynamic binding capacities were approximately 90 % of the static binding capacities. Furthermore, the dynamic binding capacity of the newly designed membranes

is independent of the linear flow velocity. These results strengthen the argument that

membrane chromatography can reduce process times and costs for protein purifications.

3.5 References

Avramescu, M. E., Borneman, Z., Wessling, M., Particle-loaded hollow-fiber membrane adsorbers for lysozyme separation, J. Membr, Sci. 322 (2008) 306–313.

Balachandra, A. M., Baker, G. L., Bruening, M. L., Preparation of composite membranes by atom transfer radical polymerization initiated from a porous support. J. Membr. Sci. 227 (2003) 1–14.

Bao, Z., Bruening, M. L., Baker, G. L., Control of the density of polymer brushes prepared by surface-initiated atom transfer radial polymerization, Macromolecules 39 (2006) 5251–5258.

Bhut, B. V., Wickramasinghe, S. R., Husson, S. M., Preparation of high-capacity, weak anion exchange membranes for protein separations using surface-initiated atom transfer radical polymerization, J. Membr. Sci. 325 (2008) 176–183.

Börner, H. G., Duran, D., Matyjaszewski, K., Silva, M. D., Sheiko, S. S., Synthesis of molecular brushes with gradient in grafting density by atom transfer radical polymerization, Macromolecules 35 (2002) 3387–3394.

Ghosh, R., Protein separation using membrane chromatography: opportunities and challenges, J. Chromatogr. A 952 (2002) 13–27.

Ghosh, R., Wong, T., Effect of model design on the efficiency of membrane chromatographic separation processes, J. Membr. Sci. 281 (2006) 532–540.

Hagiwara, K., Yonedu, S., Saito, K., Shiraishi, T., Sugo, T., Tojyo, T., Katayama, E., High performance purification of gelsolin from plasma using anion-exchange porous hollow-fiber membrane, J. Chromatogr. B 821 (2005) 153–158.

He, D., Ulbricht, M., Preparation and characterization of porous anion-exchange membrane adsorbers with high protein-binding capacity, J. Membr. Sci. 315 (2008) 155–163.

Ito, Y., Ochiai, Y., Park, Y. S., Imanishi, Y., pH-sensitive gating by conformational change of a polypeptide brush grafted onto a porous polymer membrane, J. Am. Chem. Soc. 119 (1997) 1619–1623.

Jain, P., Sun, L., Dai, J., Baker, G. L., Bruening, M. L., High-capacity purification of his-tagged proteins by affinity membranes containing functionalized polymer brushes, Biomacromolecules 8 (2007) 3102–3107.

Kacar, Y., Arica, M. Y., Procion Green H-E4BD-immobilized porous poly(hydroxyethylmethacrylate) ion-exchange membrane: preparation and application to lysozyme adsorption. Colloids Surf. B: Biointerfa. 22 (2001) 227–236.

Kaur, S., Ma, Z., Gopal, R., Singh, G., Ramakrishna, S., Matsuura, T., Plasma-induced graft copolymerization of poly(methacylic acid) on electrospun poly(vinylidene fluoride) nanofiber membrane, Langmuir 23 (2007) 13085–13092.

Knudsen, H. L., Fahrner, R. L., Xu, Y., Norling, L. A., Blank, G. S., Membrane ion-exchange chromatography for process-scale antibody purification, J. Chromatogr. A 907 (2001) 145–154.

Kobayashi, K., Tsuneda, S., Saito, K., Yamagishi, H., Furusaki, S., Sugo, T. V., Preparation of microfiltration membranes containing anion-exchange groups. J. Membr. Sci. 76 (1993) 209–218.

Lebreton, B., Brown, A., Van Reis, R., Application of high-performance tangential flow filtration (HPTFF) to the purification of a human pharmaceutical antibody fragment expressed in *Escherichia coli*. Biotechnol. Bioeng. 100 (2008) 964–974.

Lightfoot, E. N., Moscariello, J. S., Bioseparations, Biotechnol. Bioeng. 87 (2004) 259–273.

Low, D., O'Leary, R., Pujar, N. S., Future of antibody purification. J. Chromatogr. B 848 (2007) 48–63.

Ma, H., Davis, R. H., Bowman, C. N., A novel sequential photoinduced living graft polymerization, Macromolecules 33 (2000) 331–335.

Merle, Y., Synthetic polyampholytes. 5. Influence of nearest-neighbor interactions on potentiometric curves, J. Phys. Chem. 91 (1987) 3092–3098.

Samadi, A., Husson, S. M., Liu, Y., Luzinov, I., Kilbey II, S. M., Low-temperature growth of thick polystyrene brushes via ATRP, Macromol. Rapid Commun. 26 (2005) 1829–1834.

Singh, N., Chen, Z., Tomer, N., Wickramasinghe, S. R., Soice, N., Husson, S. M., Modification of regenerated cellulose ultrafiltration membranes by surface-initiated atom transfer radical polymerization. J. Membr. Sci. 311 (2008) 225–234.

Singh, N., Cui, X., Boland, T., Husson, S. M., The role of independently variable grafting density and layer thickness of polymer nanolayers on peptide adsorption and cell adhesion, Biomaterials 28 (2007) 763–771.

Singh, N., Husson, S. M., Zdyrko, B., Luzinov, I., Surface modification of microporous PVDF membranes by ATRP, J. Membr. Sci. 262 (2005) 81–90.

Singh, N., Wang, J., Ulbricht, M., Wickramasinghe, S. R., Husson, S. M., Surface-initiated atom transfer radical polymerization: A new method for the preparation of polymeric membrane adsorbers, J. Membr. Sci. 309 (2008) 64–72.

Sun, L., Dai, J., Baker, G. L., Bruening, M. L., High-capacity, protein-binding membranes based on polymer brushes grown in porous substrates. Chem. Mater. 18 (2006) 4033–4039.

Tao, Y., Carta, G., Rapid monoclonal antibody adsorption on dextran-grafted agarose media for ion-exchange chromatography, J. Chromatorg. A 1211 (2008) 70–79.

Tatárová, I., Fáber, R., Denoyel, R., Polakovic, M., Characterization of pore structure of a strong anion-exchange membrane adsorber under different buffer and salt concentration conditions, J. Chromatogr. A 1216 (2009) 941–947.

Thömmes, J., Etzel, M., Alternatives to chromatographic separations, Biotechnol. Prog. 23 (2007) 42–45.

Uchida, E., Uyama, Y., Ikada, Y., Sorption of low-molecular-weight anions into thin polycation layers grafted onto a film, Langmuir 9 (1993) 1121–1121.

Ulbricht, M., Yang, H., Porous polypropylene membranes with different carboxyl polymer brush layers for reversible protein binding via surface-initiated graft copolymerization. Chem. Mater. 17 (2005) 2622–2631.

Van Reis, R., Zydney, A. L., Bioprocess membrane technology, J. Membr. Sci. 297 (2007) 16–50.

Wurm, F. M., Production of recombinant protein therapeutics in cultivated mammalian cells, Nat. Biotech. 22 (2004) 1393–1398.

Yu, D., McLean, M. D., Hall, J. C., Ghosh, R., Purification of a human immunoglobulin G1 monoclonal antibody from transgenic tobacco using membrane chromatographic processes, J. Chromatogr. A 1187 (2008) 128–137.

Yusof, A. H. M., Ulbricht, M., Effects of photo-initiation and monomer composition on performance of graft copolymer based membrane adsorbers. Desalination 200 (2006) 462–463.

Zhou, J. X., Tressel, T., Gottschalk, U., Solamo, F., Pastor, A., Dermawan, S., Hong, T., Reif, O., Mora, J., Hutchison, F., Murphy, M., New Q membrane scale-down model for process-scale antibody purification, J. Chromatogr. A 1134 (2006) 66–73.

CHAPTER 4

MEMBRANE CHROMATOGRAPHY: PROTEIN PURIFICATION FROM *E. COLI*
LYSATE USING NEWLY DESIGNED AND COMMERCIAL ANION-EXCHANGE
STATIONARY PHASES

4.1 Introduction

The market demand for protein therapeutics is increasing rapidly, driven by scientific advancements and the continuous growth in the biotech and biopharmaceutical industries [Low et al., 2007, Walsh et al., 2006]. In order to decrease manufacturing costs, efforts are being made to increase batch sizes and/or increase product titers [Wurm et al., 2004]. The production cost associated with upstream processing declines inversely with increasing product titer. However, the costs of downstream processing do not, and, therefore, the proportion of total production cost associated with product recovery and purification increases [Subramanian et al., 2007]. Currently, for cell-derived products, the downstream processing costs represent 50−60% of the total production cost [Ghosh et al., 2002; Low et al., 2007; Subramanian et al., 2007]. There is, thus, enormous economic pressure on manufacturers of protein therapeutics to identify and employ high-throughput and high-resolution downstream recovery and purification processes that decrease production costs.

Membrane chromatography has emerged as a promising alternative to conventional resin column chromatography for the purification of biological molecules. Predominantly convective transport of the biomolecules through the membrane pores yields several advantages over intraparticle diffusion, which is the controlling transport mechanism through the resin pores [Gebauer et al., 1996; Roper et al., 1995; Thömmes et al., 2007]. Specifically, membrane chromatography offers volumetric flow rate independent dynamic capacities, higher separation speed, and easier scale-up [Gebauer et al., 1996; Roper et al., 1995; Thömmes et al., 2007]. In this work, we dispel two common misperceptions by showing that (1) membrane chromatography can be a higher capacity process than resin chromatography in the purification of protein therapeutics and (2) membrane chromatography can be a higher resolution process than resin chromatography. In time, membrane chromatography will claim increased usage in capture and polishing steps, and decrease production cost of protein therapeutics by reducing the costs of consumables and processing time.

The advantages of membrane chromatography are being realized for polishing steps in the bioprocess separation train to remove biological macromolecules such as plasmid DNA and virus particles. The primary optimization parameter for efficient polishing step operation is the separation speed [Phillips et al., 2005]. Adsorptive capacity of the separation media is not the bottleneck for the polishing steps. Therefore, membranes with low-to-moderate binding capacity and high volumetric flow rate operability are ideal for polishing step purification. Indeed, membrane chromatography has been applied successfully at both the lab scale [Haber et al., 2004; Knudsen et al., 2001; Yu et al.,

114

2008] and large-scale [Deshmukh et al., 2000; Phillips et al., 2005; Zhou et al., 2006] to remove trace impurities (DNA, virus, host cell proteins). Teeters et al. [2003] demonstrated that the dynamic binding capacity of plasmid DNA was higher for a membrane adsorber than a resin column. Knudsen et al. [2001] proved that the anion-exchange membrane chromatography is a reasonable alternative to resin column chromatography for the removal of trace level impurities. Haber et al. [2004] studied the effects of flow velocity and feed concentration on dynamic binding capacity of plasmid DNA. Anion-exchange membranes gave base-line separation of plasmid DNA isomers and higher dynamic binding capacity than a resin column with the same quaternary amine chemistry.

Despite the success of membrane adsorbers in bioprocess polishing steps, broad implementation of membrane chromatography in bioprocess capture steps has been slow because, until now, membrane adsorbers have had lower per volume protein binding capacities than resin columns. The lower binding capacity of a membrane adsorber is attributed to lower surface area per unit bed volume. This obstacle has been cited frequently as a bottleneck for the broader implementation of membrane chromatography [Ghosh et al., 2002; Van Reis et al., 2007; Zhou et al., 2008]. In consideration of membrane chromatography as a capture step in the purification of proteins from a cell lysate, its advantages cited earlier often are overshadowed by the lower dynamic binding capacities. Thus, development of membranes with higher binding capacities is an active area of research.

Building adsorptive functionality into commercially available base membranes via polymer grafting is a common strategy to increase binding capacities [Avramescu et al., 2003; Bhut et al., 2008, 2009; Bruening et al., 2008; Wang et al., 2009]. For example, Husson and co-workers have developed a new polymer grafting protocol to design anion-exchange membranes with ultrahigh and fully reversible protein dynamic binding capacities [Bhut et al., 2008, 2009]. The literature contains many examples of new adsorptive membrane materials. While the dynamic binding capacities of these membranes are reported frequently, they often are not compared with commercial products under the same operating conditions. Yet, the operating conditions and membrane adsorber module design impact the performance of adsorptive membrane drastically [Bhut et al., 2008; Ghosh et al., 2006; Zhou et al., 2008]. In the first part of this Chapter, I compare the performance properties of our newly designed membranes with a commercial membrane product. The same membrane adsorber module and operating conditions were used to allow direct comparison. Comparison also was done with a widely used resin column. All three stationary phases had the same functional group chemistry and the same bed volume.

The literature contains a number of examples of protein purification using membrane chromatography with commercial ion-exchange membranes. Suck et al. [2006] demonstrated the application of membrane chromatography for separation of two model proteins, human serum albumin (HSA) and immunoglobulin G (IgG). That same group used anion-exchange membrane chromatography to separate enzyme penicillin acylase from the crude *E. coli* supernatant. Santarelli et al. [1998] reported the separation of IgM

from the supernatant of a human hybridoma cell culture using membrane ion-exchange chromatography. The volumetric flow rate effects on separation resolution, recovery and capacity also were studied using model binary protein mixtures.

However, comparisons of membrane and resin chromatography for separation of recombinant proteins from complex bio-mixtures (e.g., cell lysate, plant extract) are rare in the literature, particularly at the preparative scale. Deshmukh et al. [2000] compared the separation performance of a resin column and membrane adsorber for the fractionation of antisense oligonucleotides and found that the separation performance was similar for both stationary phases. The comparison was reported based on a single experiment. Kreuß et al. [2008] reported detailed comparison of a commercial membrane adsorber and resin columns and found that the membrane adsorber offers significantly higher separation speed, but the dynamic binding capacity and resolution were lower than resin columns for the fractionation of glycosylated and non-glycosylated caseinomacropeptide. In the second part of this Chapter, I report a case study on the detailed comparison of our new membrane adsorber with a commercial membrane adsorber and resin column to separate a therapeutic target protein from *E. coli* cell lysate under preparative scale conditions.

Specifically, this Chapter describes the chromatographic separation of anthrax protective antigen (PA) protein from periplasmic *Escherichia coli* lysate using three different stationary phases: a newly designed AEX membrane adsorber, the Sartobind[®] D membrane adsorber, and the HiTrap[TM] DEAE FF resin column. The newly designed AEX and Sartobind[®] D membranes were compared using the same membrane module.

Protein binding capacities were determined at three volumetric flow rates from breakthrough curve analysis. The objectives of this research were to evaluate and compare the protein separation performance of our newly designed AEX membrane with a commercial membrane product and to compare the protein separation performance of membrane adsorbers with a resin column. Anion-exchange chromatography was used under salt-gradient and pH-gradient elution to separate PA protein from *E. coli* lysate. For each elution gradient, the separation performance comparison was carried out using a bind-and-elute mode of operation, the same loading and elution buffers, and a linear elution gradient with the same slope. The membrane adsorbers were operated at 5 times higher volumetric flow rate than the resin column. Sample load volume and volumetric flow rate were varied to study their effects on separation resolution of the membrane adsorbers. The separation performance was evaluated based on visual inspection of the chromatogram, sodium dodecyl sulfate-polyacrylamide gel electrophoresis (SDS-PAGE) analysis of effluent fractions, and purity and recovery data obtained using densitometric analysis of the SDS-PAGE gels. Our design of an adsorptive membrane that offers higher dynamic protein binding capacities than resins at higher separation speed and higher resolution is a remarkable success for membrane chromatography.

4.2 Experimental

4.2.1 Materials

Albumin from bovine serum (BSA, further purified fraction V, ~99%, M_r ~ 66 kDa), piperazine (99%), 2,2'-(propane-1,3-diyldiimino)bis[2-(hydroxymethyl)propane-1,3-diol]

(bis-tris propane, $\geq$99%), triethanolamine ($\geq$98%), N-methylpiperazine ($\geq$99%),

tris(hydroxymethyl)aminomethane (Tris base, $\geq$99 %), sodium chloride (NaCl, >99.5%),

sodium hydroxide ($\geq$98%), hydrochloric acid (HCl, ACS reagent, 37%) and methanol

(CHROMASOLV® Plus, $\geq$99.8%) were purchased from Sigma-Aldrich (St. Louis, MO,

USA). Bicinchronic acid (BCA) protein assay kit, precast polyacrylamide gels (4–20%

gradient, 10-well), 20X Tris-HEPES/sodium dodecyl sulfate (SDS) buffer and Coomassie

brilliant blue R-250 dye were purchased from Pierce (Rockford, IL, USA). Spectra™

multicolor broad range prestained protein molecular weight marker was purchased from

Fermentas Life Sciences (Burlington, ON, Canada). TruSep LongLife SDS sample buffer

(BG-165) was purchased from VWR (West Chester, PA, USA).

4.2.2 Buffers and instrumentation

Loading buffer B_1 (20 mM Tris base, adjusted to pH 7.8 with HCl) was used for

protein binding capacity measurements. Loading buffer B_1 and elution buffer E_1 were

used for salt-gradient anion-exchange chromatography. Elution buffer E_1 was prepared

by adding 1 M NaCl to buffer B_1. Loading buffer B_2, elution buffer E_2, and elution buffer

E_3 were used for pH-gradient anion-exchange chromatography. Loading buffer B_2 and

elution buffer E_2 were composed of 10 mM piperazine, 10 mM triethanolamine, 10 mM

bis-tris propane and 10 mM N-methylpiperazine. The pH values of loading buffer B_2 and

elution buffer E_2 were adjusted to 8.0 and 3.5, respectively, by adding HCl. Elution

buffer E_3 was prepared by adding 1 M NaCl to buffer B_2 and adjusting the pH to 7.0 with

HCl. Buffers were prepared using distilled water that had been passed through a Milli-Q®

Ultrapure (Millipore, Bedford, MA) purification system. All buffers were degassed by ultrasonication immediately prior to use.

Protein dynamic binding capacity and anion-exchange chromatography (salt-gradient and pH-gradient) measurements were done using an ÄKTA Purifier 100 chromatography system (GE Healthcare Bio-Sciences, Uppsala, Sweden). BSA protein solution or *E. coli* lysate was injected using a 150 mL capacity Superloop^{TM} (GE Healthcare Bio-Sciences). The effluent from the chromatography column was monitored continuously with UV detection at 280 nm, pH, and conductivity detectors for online measurements. The pressure drop across the membrane bed was monitored by pressure transducers installed in the ÄKTA Purifier system. All data were recorded and viewed in Unicorn 5.1 software (GE Healthcare Bio-Sciences). The purified protein samples were collected in 15 or 50 mL polypropylene Corning$^{®}$ centrifuge tubes (Sigma-Aldrich) using a Frac-950 fraction collector (GE Healthcare Bio-Sciences) connected to the ÄKTA Purifier system.

4.2.3 Anion-exchange chromatographic stationary phases

Three weak anion-exchange (AEX) stationary phases were used in this study. The newly designed weak anion-exchange membranes (AEX membranes) were developed and prepared in our laboratory. As reported previously [Bhut et al., 2008, 2009], commercially available regenerated cellulose membranes (RC 60) with 70 μm thickness, 47 mm diameter and 1.0 μm average effective pore diameter were purchased from Whatman, Inc. and surface grafted with poly(dimethylaminoethyl methacrylate) using atom transfer radical polymerization, yielding tertiary amine functionalized anion-exchange membranes. Sartobind$^{®}$ D flat sheet membrane (275 μm thickness, 210 mm ×

297 mm and >3 μm average effective pore diameter) was purchased from Sartorius Stedim Biotech GmbH (Göttingen, Germany). In order to avoid any separation performance difference that might occur due to differences in membrane module design, our AEX membranes and the Sartobind® D membranes were cut into 30 mm diameter discs and stacked into a membrane module designed and fabricated by Clemson University Machining and Technical Services. Details of this module are given in Supplemental Information at the end of this Chapter. Multiple membranes were stacked to produce a 1 mL adsorptive bed volume. Prior to loading membranes into the module, membranes were soaked in methanol and loading buffer B_1 or buffer B_2. A widely used HiTrap^{TM} DEAE FF resin column (1 mL bed volume, 6.4 mm diameter and 30 mm height) was purchased from GE Healthcare Bio-Sciences to compare the protein separation performance of chromatographic membranes and conventional resin media. All three stationary phases used throughout this study had 1 mL adsorptive bed volume, and all have the same ion-exchange functional group chemistry (i.e., $- N(CH_3)_2$).

4.2.4 *Escherichia coli* lysate sample preparation

The *E. coli* lysate preparation process has been published elsewhere [Wigelsworth et al., 2004]. Briefly, after fermentation, *E. coli* cells were separated from the media by centrifugation. Soluble anthrax protective antigen protein (PA) was extracted from fresh *E. coli* cell paste using a periplasmic shock method in buffer B_1. The resulting biomass was centrifuged to remove cell debris, and aliquots of the supernatant, rich with cell proteins, was frozen at −80 °C in 50 mL polypropylene Corning® centrifuge tubes. For the salt-gradient anion-exchange chromatography, the aliquots were thawed and diluted

with an equal volume of loading buffer B_1 to prepare cell lysate samples. For pH-gradient anion-exchange chromatography, the aliquots were thawed and diafiltration was done to exchange buffer B_1 with buffer B_2 using an Amicon® Ultra-15, 10 kDa membrane centrifuge cassette (Millipore). The buffer exchanged samples were diluted with an equal volume of loading buffer B_2. For membrane chromatography, all samples were loaded directly into the ÄKTA Purifier. For resin chromatography, the samples had to be filtered through disposable cellulose acetate (Puradisc 30) syringe filters with 0.45 µm pore diameter (GE Healthcare Bio-Sciences) to avoid blocking of small pores and/or ghost peaks.

4.2.5 Protein binding capacity measurements

BSA was used as a model protein to measure static and dynamic protein binding capacities of all three weak anion-exchange stationary phases. BSA concentration was 3.0 mg/mL in loading buffer B_1. Immediately prior to use, the protein solution was filtered through a disposable cellulose acetate syringe filter with 0.22 µm pore diameter.

4.2.5.1 Static binding capacity

Protein static binding capacities of all three stationary phases were determined from batch adsorption experiments. AEX (47 mm diameter, 70 µm thickness) and Sartobind® D (31 mm diameter, 270 µm thickness) membranes were incubated in 10 mL protein solution for 20 h to reach equilibrium in a shaker bath at 22 °C. Equilibrium protein concentration was measured according to the method reported in Chapter 2. HiTrap™ DEAE FF resin column (1 mL bed volume) was connected to the ÄKTA Purifier and 40 column volumes (CVs) of loading buffer $B_1$was run through it to equilibrate the resin

bed. The column was disconnected from ÄKTA Purifier and wet resin bed was mixed with 60 mL BSA solution. Suspension was stirred slowly for 20 h at 22 °C to reach equilibrium and concentration was measured. Static protein binding capacities were calculated by mass balance using initial and equilibrium concentrations of protein solution.

4.2.5.2 Dynamic binding capacity

Protein dynamic binding capacities were determined from breakthrough curve analysis. For all stationary phases, equal experimental conditions were applied starting with passage of 10 CVs of loading buffer B_1 to equilibrate the column. Protein solution was injected until the protein concentration in the effluent reached its feed concentration. The bound protein was eluted with elution buffer E_1 until a stable baseline was observed with UV detection. Stationary phases were cleaned with 2 CVs of 0.3 M sodium hydroxide solution and rinsed with 20 CVs of loading buffer B_1. Three different flow rates were used to obtain breakthrough curves: 5, 10, 15 mL/min for membrane columns and 1, 2, 3 mL/min for the resin column. The column dead volume was determined using the retention time (initial breakthrough) of protein in a solution of 3 mg BSA/mL loading buffer B_1 prepared with a high NaCl concentration (2M). Dynamic binding capacities were calculated at 10% breakthrough (i.e., when $C/C_0 = 0.10$) according to following approximate equation:

$$q = \frac{C_0 \left(V_{break} - V_{dead} \right)}{V_{col}} \tag{4.1}$$

q represents the binding capacity (mg BSA/mL column volume), V_{break} is the effluent volume (mL) where the absorbance value of the breakthrough curve reached 10% of the absorbance value of the feed concentration, V_{dead} is the dead volume of the system (mL), C_0 is the feed concentration of BSA (mg/mL), and V_{col} is the stationary phase column volume (mL). Two measurements were taken at each flow rate, and protein binding capacities are reported as the average of these two measurements.

4.2.6 Salt-gradient anion-exchange chromatography

Single-step anion-exchange chromatography was used to purify the anthrax protective antigen protein (PA) from periplasmic *E. coli* lysate. The linear ionic strength gradient was generated by mixing loading buffer B_1 and elution buffer E_1 using the gradient pumps of the ÄKTA Purifier system. Weak anion-exchange stationary phases (membrane adsorbers and resin column) were connected to the ÄKTA Purifier system and equilibrated by flowing loading buffer B_1 through the column until a stable base line was observed with UV detection at 280 nm. *E. coli* lysate was loaded onto the column, followed by washing of unbound protein with loading buffer B_1. The bound proteins were eluted using a linear elution gradient over 40 CVs, starting with 100% buffer B_1 and ending with 70% (v/v) buffer B_1. Thereafter, 10 CVs of 70% loading buffer B_1 were passed through the column to achieve a stable UV base line. Finally, 10 CVs of 100% elution buffer E_1 was used to strip remaining adsorbed proteins from the anion-exchange column. The flow-through, eluted and strip fractions were collected and analyzed using sodium dodecyl sulfate-polyacrylamide gel electrophoresis (SDS-PAGE). After every

124

run, the ion-exchange bed was cleaned with 2 CVs of 0.3 M sodium hydroxide solution followed by 20 CVs of loading buffer B_1 to prepare the bed for the next run.

A set of experiments was carried out to study the effect of sample loading volume on separation performance of membrane adsorbers at constant 5 mL/min flow rate. AEX membrane adsorber was loaded with 10, 20, 30 and 40 mL of *E. coli* lysate and the Sartobind® D membrane adsorber was loaded with 5, 10, 15 and 20 mL of *E. coli* lysate.

Another set of experiments was carried out to study the effect of volumetric flow rate on separation performance of membrane adsorbers. Flow rates of 5, 10, 15 mL/min were used. During these experiments, the sample loading volume was kept constant (10 mL for Sartobind® D and 20 mL for AEX membranes).

4.2.7 pH-gradient anion-exchange chromatography

A gradient in pH from 8.0–3.5 was used to fractionate proteins from *E. coli* lysate that had been bound to the anion-exchange stationary phases during loading. The pH gradient was generated by mixing loading buffer B_2 (pH 8.0) and elution buffer E_2 (pH 3.5) using the gradient pumps of the ÄKTA Purifier. The column was equilibrated with loading buffer B_2 until a stable base line was observed with UV detection at 280 nm. The flow rates through the resin column and membrane adsorbers were 1 and 5 mL/min, respectively. Load volumes of 10 and 20 mL *E. coli* lysate were used for all three stationary phases. After sample injection, 10 CVs of loading buffer B_2 were passed through the column to wash out unbound proteins. The bound proteins were eluted using a linear elution gradient over 40 CVs, starting with 100% buffer B_2 and ending with 100% buffer E_2. Thereafter, 20 CVs of 100% elution buffer E_2 were passed through the

column to achieve a stable UV base line. In order to fractionate the remaining bound proteins, a linear ionic strength gradient was applied over 30 CVs, starting with 100% buffer E_2 and ending with 100% buffer E_3. After every run, the ion-exchange bed was cleaned with 2 CVs of 0.3 M sodium hydroxide solution followed by 20 CVs of loading buffer B_2 to prepare the bed for next run.

4.2.8 Sample analysis

4.2.8.1 SDS-PAGE

The feed cell lysate, flow-through, eluted and strip fractions from salt-gradient anion-exchange chromatography were analyzed by SDS-PAGE. In order to improve the purity profile of the recovered product, the eluted fractions were collected into PA product and non-PA product fractions. These fractions were concentrated to increase the gel image intensity of trace protein impurities present in the purified product. PA product and non-PA product fraction volumes were reduced to half using Amicon® Ultra-4, 10 kDa membrane centrifuge cassettes. Total protein content in each collected fraction (flow through, PA product, non-PA product and strip) and the feed *E. coli* lysate was determined using a bicinchoninic acid protein assay kit. Five microliters of sample buffer was mixed with 20 µL of sample prior to loading. In order to prepare a local calibration curve for densitometric analysis of each gel, 0.5 and 2.0 mg/mL BSA standard samples were loaded onto every SDS-PAGE gel. One-dimensional SDS-PAGE was performed using precast 4–20% gradient gels and 500 mL running buffer (1X Tris-HEPES-SDS) in an Xcell Sure Lock Mini-Cell (Invitrogen, Carlsbad, USA) according to the experimental procedure provided by manufacturer. All gels were run at a constant 190 V until the

126

marker and blue dye had run off the gel. Next, gels were removed from the box and stained by Coomassie brilliant blue R-250 dye.

4.2.8.2 Densitometry

SDS-PAGE gel images were captured using a Fujifilm LAS-1000 Plus Camera System (Fujifilm Life Science, Stamford, CT, USA). Densitometric analysis of the gel images was performed using ImageGauge 4.1 software (Fujifilm Life Science) to quantify protein concentrations used to evaluate the separation performance. Standard BSA protein samples were used to prepare the calibration curve of protein band absorbance versus protein mass loaded onto the gel. The concentrations of PA in the *E. coli* lysate and the purified PA fraction were calculated from the absorbance of the PA band in the gel and the local calibration curve. The volumetric flow rate was used as a throughput of the process. Recovery and purity were defined and measured using following equations.

$$\text{Recovery} = \frac{M_{PA,\text{ feed}} - M_{PA,\text{ prod.}}}{M_{PA,\text{ feed}}} \times 100\% \tag{4.2}$$

$$\text{Purity} = \frac{M_{PA,\text{ prod.}}}{M_{\text{tot. prot. prod.}}} \times 100\% \tag{4.3}$$

$M_{PA,\text{ feed}}$ and $M_{PA,\text{ prod.}}$ are the masses of PA protein in the feed lysate and the product fraction, respectively. $M_{\text{tot. prot. prod.}}$ is the mass of total protein in the product fraction.

4.3 Results and discussion

Husson and coworkers [Bhut et al., 2008, 2009] have designed weak anion-exchange membranes using surface-initiated ATRP from commercial regenerated cellulose membranes. A two-step surface modification protocol was designed to yield macroporous

membranes with exceptionally high and fully reversible dynamic protein binding capacities. In this Chapter, the protein separation performance of our newly designed weak anion-exchange membranes was evaluated and compared with commercially available and widely used weak anion-exchange products. The primary objective of this research was to compare the chromatographic protein separation performance of membrane adsorbers and a resin column. We compared the performance of our newly designed AEX membrane and the commercially available Sartobind® D membrane with the HiTrap™ DEAE FF resin column for separation of anthrax protective antigen (PA) protein from periplasmic *E. coli* lysate. The secondary objective of this research was to evaluate and compare the separation performance of our AEX membrane with the Sartobind® D membrane. Bind-and-elute anion-exchange chromatography (AEC) was performed to purify PA protein from *E. coli* lysate using all three stationary phases. Prior to the AEC experiments, the dynamic protein binding capacities of the stationary phases were determined from breakthrough curve analysis. Results of the breakthrough measurements were used to select appropriate parameters (cell lysate load volume and flow rates) for AEC separation of PA protein.

Two sets of AEC experiments were performed. In the first set of experiments, salt-gradient anion-exchange chromatography was used. A linear elution gradient of ionic strength was applied to fractionate proteins that had adsorbed to the anion-exchange media during column loading. The effects of *E. coli* lysate load volume and volumetric flow rate on PA protein separation resolution were investigated for the membrane adsorbers. The second set of experiments was carried out using pH-gradient (gradient

chromatofocusing) AEC. An externally generated 'linear' elution gradient (pH 8.0–3.5) was applied to fractionate adsorbed proteins. The effect of sample loading also was studied.
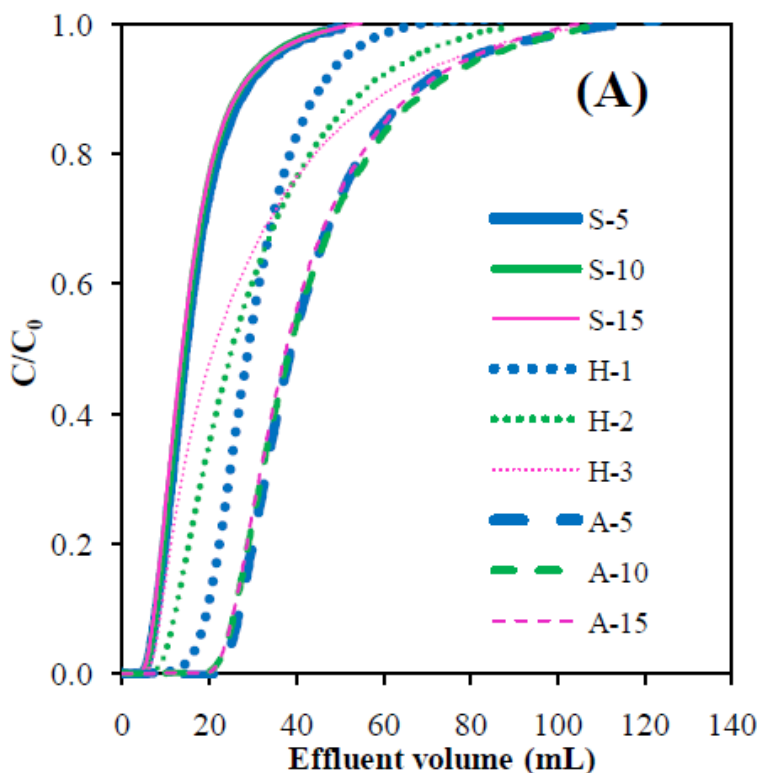
Figure 4.1(A) Effect of volumetric flow rate on the breakthrough curves for membrane adsorbers (Sartobind® D and AEX) and resin column (HiTrap^TM DEAE FF). C/C_0 is the ratio of effluent to feed BSA concentration. The feed solution was 3 mg BSA/mL buffer B_1. Absorbance was measured at 280 nm. Solid line (—) breakthrough curves labeled as S-5, S-10 and S-15 represent the Sartobind® D membrane adsorber with 5, 10 and 15 mL/min flow rate. Dotted line (⋯) breakthrough curves labeled as H-1, H-2 and H-3 represent the HiTrap^TM DEAE FF resin column with 1, 2 and 3 mL/min flow rate. Dashed line (---) breakthrough curves labeled as A-5, A-10 and A-15 represent the AEX membrane adsorber with 5, 10 and 15 mL/min flow rate.

4.3.1 Protein binding capacity measurements

Protein dynamic binding capacities of the membrane adsorbers and the resin column were determined from breakthrough curve measurements. BSA was used as the test protein. The dynamic protein binding capacities were measured under identical experimental conditions, except volumetric flow rates for the resin column were 5-fold lower than those for the membrane adsorbers. The volumetric flow rate was a test variable used to evaluate the effect of linear flow velocity on protein binding capacities.

Fig. 4.1(A) shows the breakthrough curves for BSA on all three stationary phases. Breakthrough curves for the resin column changed significantly with changes in the volumetric flow rate. Protein breakthrough occurred at lower values of effluent volume as the volumetric flow rate increased. Therefore, the dynamic capacity of the resin column depends on volumetric flow rate (residence time). As we increased the volumetric flow rate, the shape of the breakthrough curve also changed dramatically. This observation suggests that, at high enough flow rates (>1 bed volume/min), intraparticle diffusion of the protein molecules becomes the rate controlling mechanism for the resin column [Stone et al., 2007; Tao et al., 2008]. For the Sartobind® D and AEX membrane adsorbers, the breakthrough curves did not change significantly on increasing volumetric flow rates from 5 to 15 ml/min (bed volume/min). The shape of the breakthrough curves and the volume of effluent processed prior to protein breakthrough remained the same. Thus, the membrane adsorbers offer volumetric flow rate independent protein binding capacities. The breakthrough curves were self-sharpening, indicating highly favorable sorption isotherms under the conditions used for loading [Bhut et al., 2008]. Self-

sharpening occurs for a favorable isotherm because the velocity of solute moving through

the column depends on concentration. Low concentrations at the solute front yield lower

velocity, and higher concentrations within the solute wave yield higher velocity. The net

effect is to sharpen the velocity profile of the solute wave. These results suggest that the

transport of protein molecules from solution to binding sites is dominated by convective

transport in macropores of the membrane adsorbers [Gebauer et al., 1996; Roper et al.,

1995; Thömmes et al., 2007]. Yang et al. [2002] reached the same conclusion from

analysis of breakthrough curves obtained using two proteins with significantly different

molar mass.
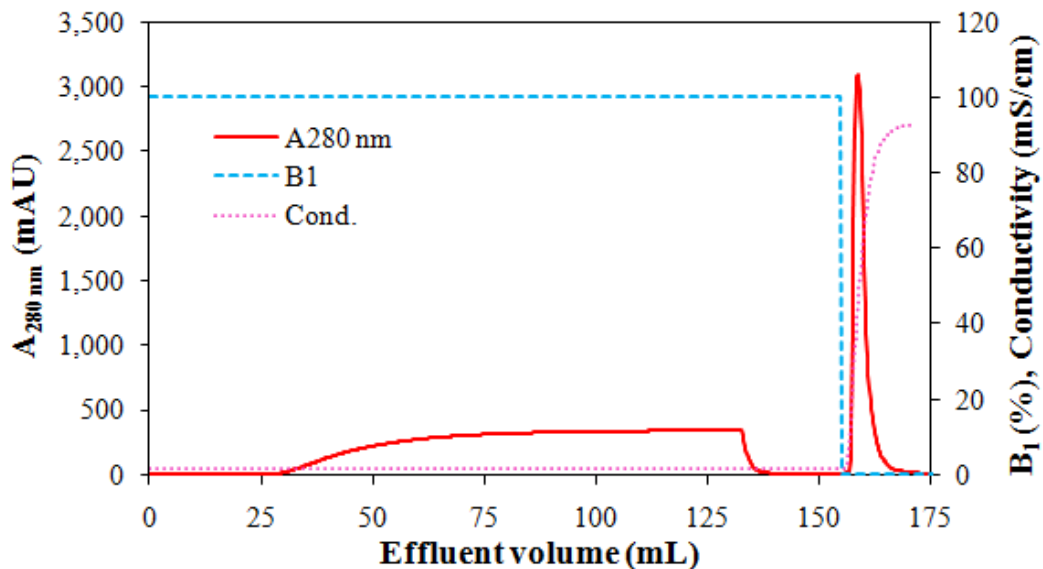
Figure 4.2 Bind-and-elute curve for AEX membrane adsorber (loading buffer B_1: 20 mM Tris-HCl, pH 7.8; elution buffer E_1: 1 M NaCl in loading buffer B_1; flow rate: 15 mL/min; sample load volume: 130 mL). The feed solution was 3 mg BSA/mL buffer B_1. Solid line represents the absorbance at 280 nm. Dotted line represents conductivity. Dashed line represents the % of loading buffer B_1.

Fig. 4.2 shows bind-and-elute chromatogram for newly designed AEX membrane adsorber. Protein solution was injected until the protein concentration in the effluent reached its feed concentration. The bound protein was eluted with elution buffer E1 until a stable baseline was observed with UV detection. Elution yields full recovery of the BSA, and more than 95% of the area under the elution curve can be collected in a volume fraction of 10 mL (10 CV). The mass of BSA protein (130 ± 5 mg) in the elution peak was estimated from the area under the elution curve and an independent calibration curve. Taken together, the concentration of the eluted protein was > 12 mg/mL, a 4-fold increase relative to the feed concentration.

Though governed primarily by convective transport, breakthrough curves are S-shaped and not perfect step functions. One reason for such behavior is the non-uniform pore structure of the membrane bed. Large diameter pores have higher volumetric throughput than small diameter pores and, therefore, experience earlier saturation of binding sites. This phenomenon creates a distribution of site saturation times among pores of different diameters and results in broadening of adsorptive breakthrough curves. Surface crowding of adsorbed proteins and convective dispersion in the flow system also may contribute to the asymmetry of the breakthrough curves [Roper et al., 1995; Yang et al., 2002]. Advanced module design can decrease non-uniform flow, column back mixing and convective dispersion in the module and, therefore, improves scalability and separation performance of membrane adsorbers [Ghosh et al., 2006]. The membrane module used in our study was designed and fabricated specifically to reduce such effects. Multiple flow channels were placed equidistant from each other at the module entrance

and exit to enhance the feed flow distribution and effluent collection. Both membrane types, Sartobind® D and AEX, when stacked in our custom module, gave residence time independent dynamic capacities over a broad range of volumetric flow rates. Membrane adsorbers with flow rate independent dynamic capacities offer relatively linear scalability and flexibility of design parameters for large-scale operations. For example, Knudsen et al. [2001] found nearly linear scalability on increasing the number of membrane discs from 10 to 60 in an adsorptive bed.

Table 4.1 Static protein binding capacity of HiTrap[TM] DEAE FF resin column, Sartobind® D membrane adsorber and newly designed AEX membrane adsorber.

Stationary phases	Static binding capacity (mg BSA/mL)
HiTrap[TM] FF DEAE	95 ± 3
Sartobind® D membrane	55 ± 2
AEX membrane	135 ± 4

Note: Two measurements were taken for each stationary phase, and protein binding capacities are reported as the average of these two measurements. The error bars represent ± 1 standard deviation from the average value.

Table 4.1 shows the static protein binding capacities of all three stationary phases. Our newly designed membrane adsorber has higher static protein binding capacity than HiTrap[TM] FF DEAE resin column and Sartobind® D membrane adsorber. However, the surface area of the AEX membrane adsorber (0.53 ± 0.02 m^2/mL measured by BET method) is much lower than the surface area of Sepharose resin (literature reported value ~ 50 m^2/mL [Barrande et al., 2009; DePhillips et al., 2000]). Therefore, the higher protein binding capacity is attributed to the polymer chains grafted from the membrane pore surface, and depends on both grafting density and degree of polymerization [Bhut et al., 2008, 2009]. During protein adsorption, these chains extend into the protein solution,

providing a 3-dimensional 'scaffold' for protein molecules to adsorb and leading to high

protein binding capacities.
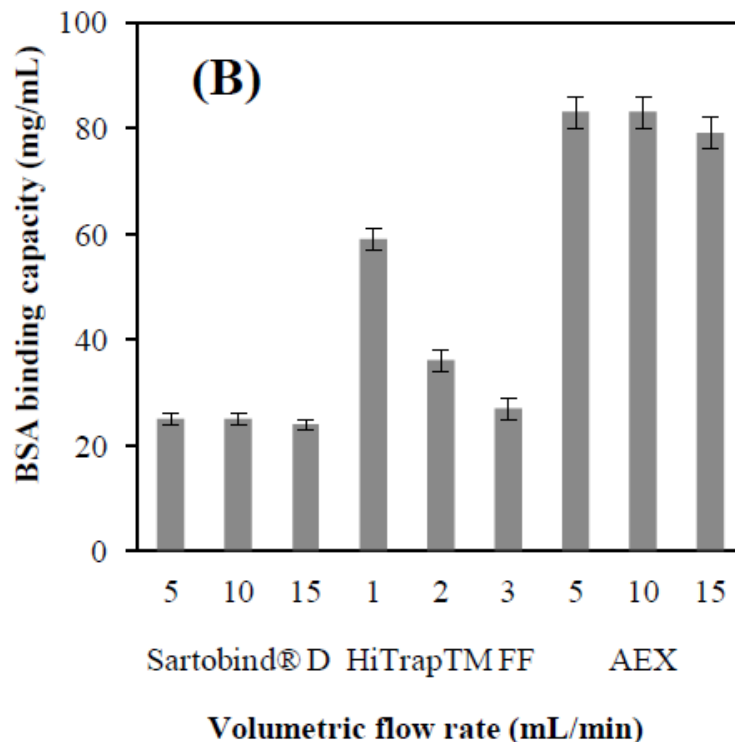
Figure 4.1(B) Effect of volumetric flow rate on the protein dynamic binding capacities for membrane adsorbers (Sartobind® D and AEX) and resin column (HiTrap™ DEAE FF). Dynamic protein binding capacities were calculated using breakthrough curves from the Fig. 4.1(A) and equation (4.1). Two measurements were taken at each flow rate, and protein binding capacities are reported as the average of these two measurements. The error bars represent ± 1 standard deviation from the average value.

Fig. 4.1(B) shows the dynamic binding capacities of all three stationary phases.

Dynamic binding capacities were calculated according to equation (4.1). In all cases,

dynamic capacities are lower than static capacities, as expected from peak broadening

described earlier. Calculated dynamic binding capacities of the membrane adsorbers did

not change significantly with increasing volumetric flow rate, which was expected from

examination of Fig. 4.1(A). For the resin column, the dynamic binding capacities decreased regularly as the volumetric flow rate increased. Again, the explanation is that the resin column operates under a diffusion-controlled rate process. In comparison, Sartobind® D membranes have the lowest binding capacities and AEX membranes have the highest binding capacities among the three stationary phases. The AEX membrane has higher binding capacities than the resin column at 15 times higher volumetric flow rate (in bed volumes/min). Traditionally, the dynamic protein binding capacities of membrane adsorbers have been lower than conventional resin columns, and the relatively lower capacities have hindered the broader implementation of membrane chromatography in the biopharmaceutical industry [Bhut et al., 2008, 2009]. This obstacle has been pointed out frequently in the bioseparations community [Ghosh et al., 2002; Van Reis et al., 2007; Zhou et al., 2008]. Therefore, our design of an anion-exchange membrane with higher, fully reversible dynamic protein binding capacity and with *at least* 15 times higher volumetric throughput than one of the most widely used resin columns is a highly significant milestone for membrane chromatography.

4.3.2 Salt-gradient anion-exchange chromatography

4.3.2.1 Separation performance comparison of stationary phases

Salt-gradient AEC was used to purify anthrax protective antigen (PA) protein from *E. coli* lysate. Performance metrics of the AEX membrane adsorber, Sartobind® D membrane adsorber and HiTrap™ FF resin column were defined as the percentage recovery and purity of PA protein from *E. coli* lysate. The performance comparison was carried out using a bind-and-elute mode of operation, the same loading and elution

buffers, and a linear ionic strength elution gradient with the same slope. Sample load

volume and volumetric flow rate were varied to study their effects on separation

resolution. Separation performance was evaluated based on visual inspection of the

chromatogram, SDS-PAGE analysis of effluent fractions, and purity and recovery data

obtained using densitometric analysis of the SDS-PAGE gels. The reported isoelectric

point (pI) of PA protein is 5.4–5.9 [Ahuja et al., 2001; Powell et al., 2007]. Therefore, pH

7.8 was selected for the loading buffer to generate a positively charged stationary phase

and net negatively charged PA protein.
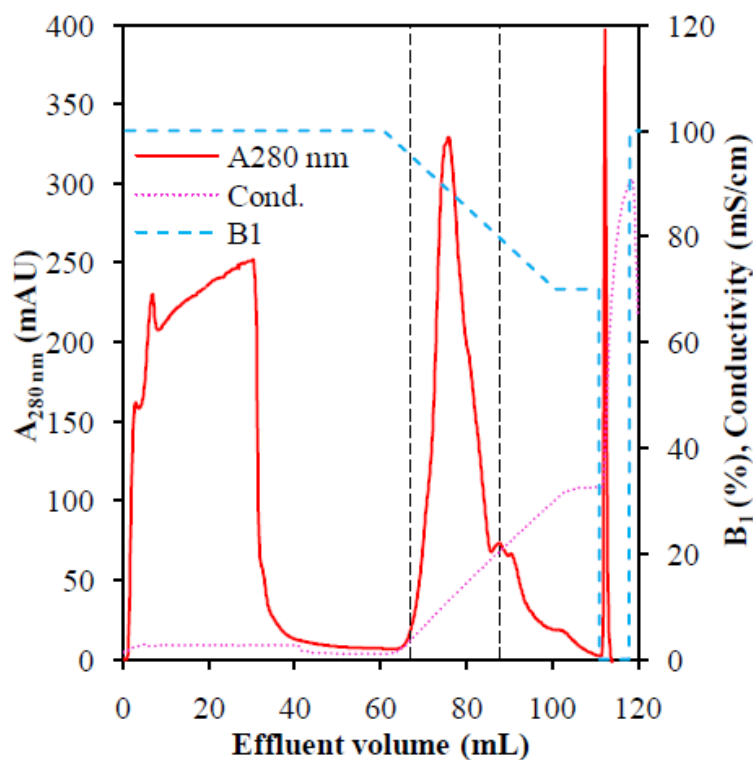
Figure 4.3 Single step purification of PA protein from *E. coli* lysate using HiTrap^{TM}
DEAE FF resin column (loading buffer B$_1$: 20 mM Tris-HCl, pH 7.8; elution buffer E$_1$: 1
M NaCl in loading buffer B$_1$; flow rate: 1 mL/min; sample load volume: 30 mL). Solid
line represents the absorbance at 280 nm. Dotted line represents conductivity. Dashed
line represents the % of loading buffer B$_1$. The effluent volume between the two vertical
long dashed lines was collected as the PA product fraction.
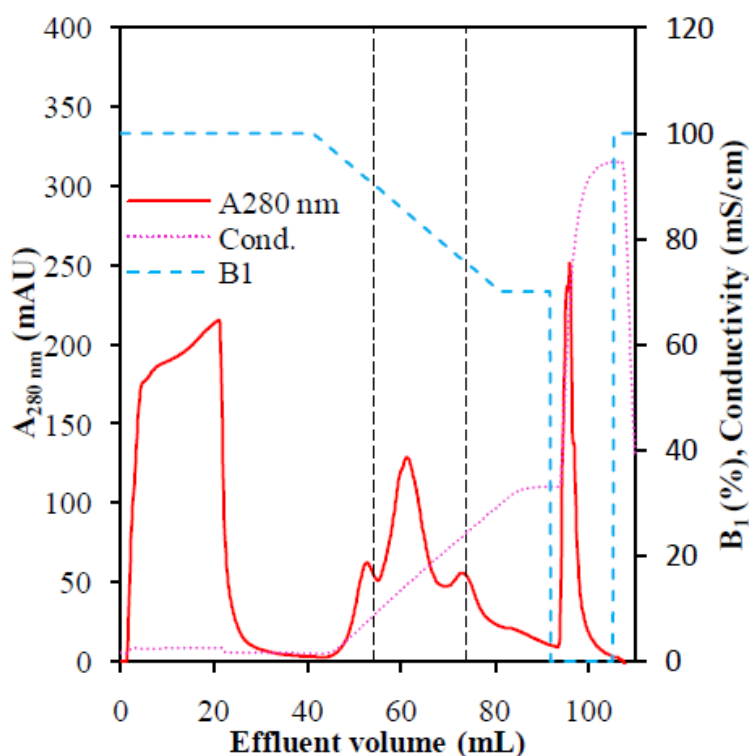
Figure 4.4 Single step purification of PA protein from *E. coli* lysate using Sartobind® D membrane adsorber (loading buffer B_1: 20 mM Tris-HCl, pH 7.8; elution buffer E_1: 1 M NaCl in loading buffer B_1; flow rate: 5 mL/min; sample load volume: 20 mL). Solid line represents the absorbance at 280 nm. Dotted line represents conductivity. Dashed line represents the % of loading buffer B_1. The effluent volume between the two vertical long dashed lines was collected as the PA product fraction.

Figs. 4.3–4.5 present the chromatograms for PA purification from *E. coli* lysate using the HiTrap™ FF resin column, Sartobind® D membrane adsorber and AEX membrane adsorber. For the HiTrap™ FF resin column, 30 mL of *E. coli* lysate was loaded onto the column after equilibrating the bed with loading buffer B_1. Bound proteins were eluted with a linear ionic strength gradient, producing a large peak from 67 to 88 mL effluent volume that was assigned as the PA product peak, followed by several smaller, unresolved peaks. Fractions from 67 to 88 mL effluent volume were collected

and pooled for SDS-PAGE analysis. Fractions for all non-PA protein peaks from 88 to 105 mL effluent volume also were collected and pooled for SDS-PAGE analysis. Proteins eluted using 100% elution buffer E_2 were collected as the strip fraction.

Fig. 4.6(A) shows the SDS-PAGE gels for the samples collected. Comparing the *E. coli* lysate (lane 2) with the PA product fraction (lane 3), the single-step purification using the HiTrap^{TM} FF resin column was quite successful at removing several impurities. The intensity of protein bands in the flow through fraction (lane 5) is relatively lower, but the volume of the flow through fraction was significantly higher than other fractions. The non-PA product fraction (lane 4) indicates that the proteins eluted in the small non-resolved peaks (Fig. 4.3) were different than PA protein. However, the non-PA product fraction (lane 4) also shows a significant amount of PA is present. We attribute the presence of PA product in the non-PA fraction to poor separation resolution during elution with this resin column.
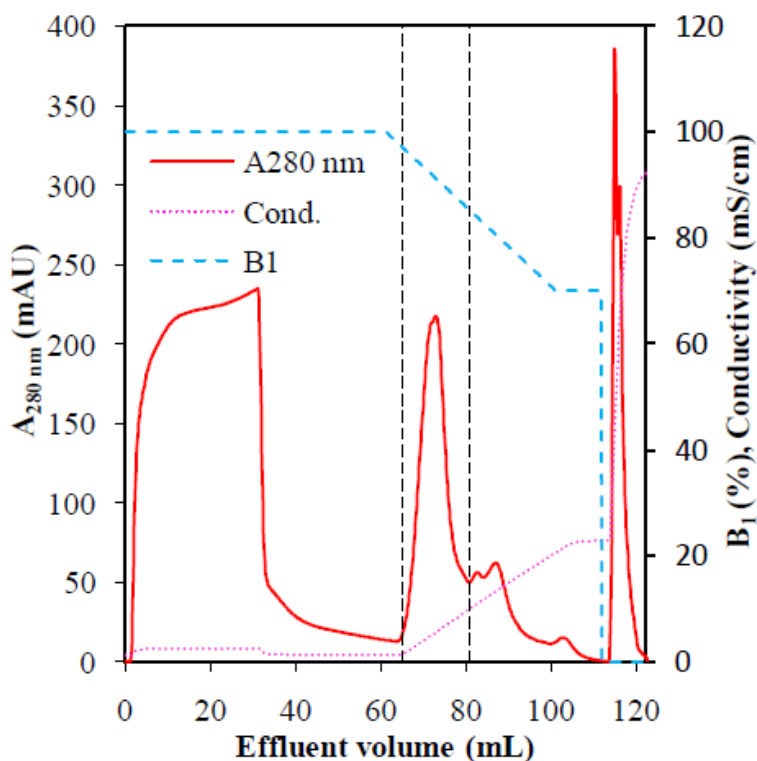
Figure 4.5 Single step purification of PA protein from *E. coli* lysate using newly designed AEX membrane adsorber (loading buffer B_1: 20 mM Tris-HCl, pH 7.8; elution buffer E_1: 1 M NaCl in loading buffer B_1; flow rate: 5 mL/min; sample load volume: 30 mL). Solid line represents the absorbance at 280 nm. Dotted line represents conductivity. Dashed line represents the % of loading buffer B_1. The effluent volume between the two vertical long dashed lines was collected as the PA product fraction.

The same AEC protocol was applied to purify PA protein from *E. coli* lysate using the Sartobind® D membrane adsorber. From the protein binding capacity measurements (Fig. 4.1), it was determined that the dynamic protein binding capacity of Sartobind® D membranes was the lowest among the three stationary phases; therefore, a 20 mL sample load volume was used. A five-fold higher flow rate (5 mL/min) was used for the membrane adsorbers, relative to that used for the resin column. Fig. 4.4 presents the chromatogram obtained using Sartobind® D membranes. Surprisingly, the elution profile

of proteins was markedly different than what was observed for the resin column (Fig. 4.3). Using the same elution gradient, three unresolved but distinct peaks were observed between 45 and 80 mL effluent volume. From comparison of Figs. 4.3 and 4.4, the peak separation resolution was higher when Sartobind® D membrane adsorber was used as stationary phase. Initial SDS-PAGE analysis indicated that the second elution peak in Fig. 4.4 was the PA product and that the first and third elution peaks were non-PA proteins. Therefore, collected fractions from 54 to 75 mL effluent volume were pooled to form the PA product fraction, and all remaining effluent fractions were pooled to form the non-PA product fraction. Fig. 4.6(B) shows the SDS-PAGE gel of these samples.
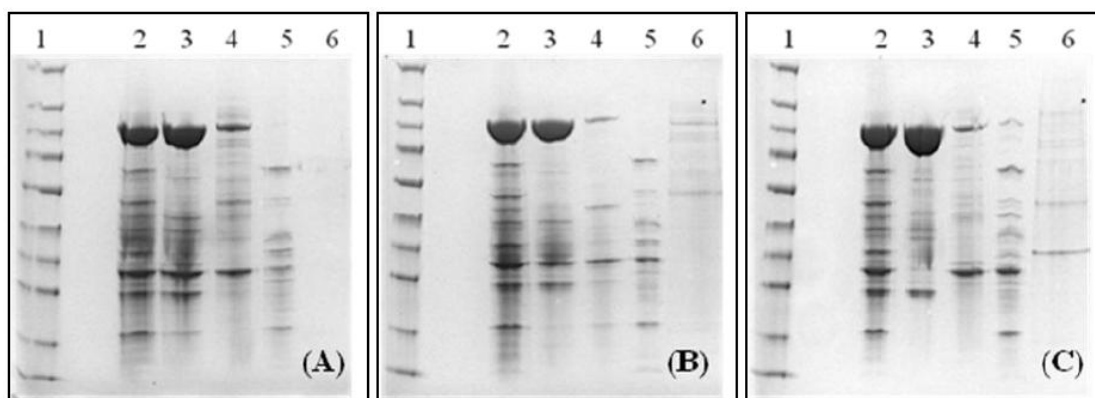
Figure 4.6 SDS-PAGE images obtained from single step anion-exchange chromatographic purification of PA protein from *E. coli* lysate using HiTrap[TM] DEAE FF resin column (A), Sartobind® D membrane adsorber (B) and newly designed AEX membrane adsorber (C). Staining was done with Coomassie blue. Lane 1, high-range M_w marker; lane 2, *E coli.* lysate load (lysate); lane 3, pool of PA product fractions collected between vertical long dashed lines in Figs. 3–5; lane 4, pool of non-PA product fractions; lane 5, pool of flow through fractions; and lane 6, strip fraction.

140

Visual comparison of the *E. coli* lysate (lane 2) with PA product fraction (lane 3) of Figs. 4.6(A) and 4.6(B) suggests that the purity of the PA product fraction using the Sartobind® D membrane adsorber was significantly higher than that obtained using the HiTrap™ FF resin column. This result strengthens the earlier conclusion derived from visual inspection of the chromatograms (Figs. 4.3 and 4.4) that the Sartobind® D membrane adsorber gives higher peak separation resolution than the resin column for the purification of PA protein from *E. coli* lysate. Importantly, resolution is higher for the membrane adsorber at five times higher volumetric flow rate.

Finally, our newly designed AEX membranes were used to purify PA protein from *E. coli* lysate using the same AEC protocol. Fig. 4.5 presents the chromatogram obtained using AEX membranes. After equilibration, 30 mL of lysate was loaded onto the AEX membrane adsorber. For this stationary phase, the protein peak elution profile was similar to what we observed for the resin column. However, resolution is better (i.e., the ratio of height to half width is larger) for the newly designed AEX membrane adsorber. Proteins eluted in four unresolved but easily distinguishable peaks. The largest elution peak was identified as the PA protein; therefore, fractions collected between 65 and 81 mL effluent volume were pooled to form the PA product fraction. Fig. 4.6(C) shows the SDS-PAGE gel of the samples collected. Comparing the PA product fraction (lane 3) for Figs. 4.6(A−C), the purity of the PA protein obtained using the AEX membrane adsorber appears to be similar to the purity obtained using the Sartobind® D membrane adsorber. Also, the purity of PA protein obtained using membrane adsorbers was higher than that obtained using the resin column. Again, this result is even more significant because the

membrane adsorbers were operated at a volumetric flow rate that was five times higher than the resin column.
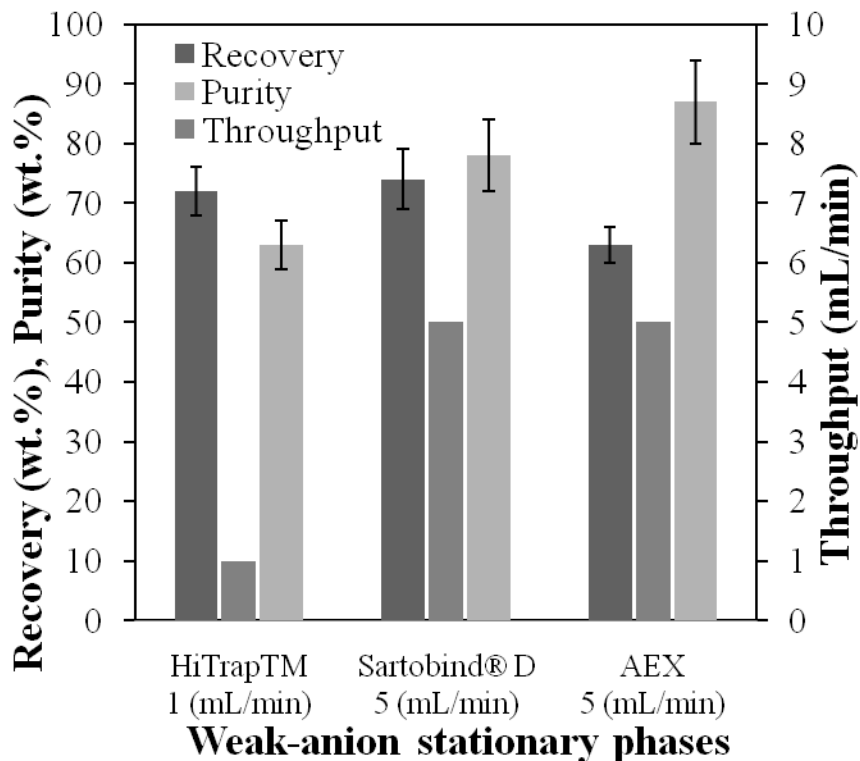
Figure 4.7 Percentage recovery and purity of PA protein recovered from *E. coli* lysate using HiTrap[TM] DEAE FF resin column and Sartobind[®] D and newly designed AEX membrane adsorbers. The purity and recovery data were obtained using densitometric analysis of SDS-PAGE images. Two gels were prepared for each stationary phase and two images of each gel were used for densitometric measurements. The purity and recovery data represent the average of these four measurements. The error bars represent ± 1 standard deviation from the average value.

In order to strengthen the conclusions derived from visual analysis of the chromatograms and SDS-PAGE gels, densitometric measurements were done on the SDS-PAGE gel images to quantify the purities and recoveries of PA protein. Fig. 4.7 compares all three stationary phases based on PA purity and recovery. Two gels were prepared for each stationary phase and two images of each gel were used for

densitometric measurements. An internal standard was used on every gel. The purity and recovery data shown in Fig. 4.7 represent the average of these four measurements; error bars represent ± 1 standard deviation from the average value. Fig. 4.7 confirms that the mass percentage purity of PA protein was higher for membrane adsorbers than the resin column.

Overall, results from single-step AEC purification of PA protein from *E. coli* lysate indicate that peak separation resolution was better for membrane adsorbers than the resin column. Visual inspection of SDS-PAGE gels showed that the purity of PA protein obtained using a single-step AEC purification was higher for membrane adsorbers than the resin column and was similar for the membrane adsorbers. This conclusion was supported quantitatively by densitometric measurements of SDS-PAGE images. Taken all together, the results clearly demonstrate that membrane chromatography is a high-resolution separation technique, and resolution in membrane chromatography is as high as or higher than resin column chromatography, even at much higher volumetric throughput. Traditionally, advantages of membrane chromatography have been overshadowed by lower binding capacity and lower separation resolution [Kreuß et al., 2008; Van Reis et al., 2007; Zhou et al., 2008]. Here, we demonstrate that under preparative conditions, membrane chromatography can be a higher capacity, higher resolution, *and* higher throughput technique.

The higher peak resolution of membrane adsorbers may be explained from the transport profile of protein molecules inside the membrane pores. In surface-functionalized membranes, adsorptive sites are in direct contact with the flowing product

stream; therefore, the maximum effective diffusion path length is roughly equal to the average effective pore radius of the membranes (<3 µm). During elution, protein molecules desorb from the binding sites directly into the main flow stream and are carried through the membrane bed by convective flow. In resin columns, intraparticle diffusion is the rate controlling mechanism. The maximum intraparticle diffusion path length for resin media corresponds roughly to the particle radius (>40 µm), multiplied by a tortuosity factor of typically 2.0–2.6 [Lipin et al., 2009; Natarajan et al., 2000]. Due to the long diffusion path lengths in resins (relative to the membrane pore dimensions), a broader distribution of residence times exists for protein elution, particularly for a fully loaded resin bed where all adsorption sites are occupied [Gebauer et al., 1996; Roper et al., 1995; Tao et al., 2008; Thömmes et al., 2007]. For example, during loading, some proteins adsorb at the entrance of the pore, while others may travel tens of microns to reach unoccupied binding sites. During elution, protein molecules desorb from the binding sites and must travel by intraparticle diffusion back through the resin pores before entering the main flow stream. Therefore, the broad distribution of diffusion path lengths during elution results in a broad elution profile.

4.3.2.2 Impact of volumetric flow rate

From the breakthrough curve analysis described in Section 4.3.1, it was determined that the dynamic binding capacity of membrane adsorbers is independent of the flow rate over the range studied. However, separation resolution also depends on volumetric flow rate. In order to investigate the effect of flow rate on separation resolution of membrane

adsorbers, three flow rates were studied. Fig. 4.8 shows the effect of volumetric flow rate on separation resolution for Sartobind® D and AEX membranes. By increasing the flow rate from 5 to 15 mL/min, the separation resolution decreased only slightly. Except for minor peak broadening, the peak elution profile remained un-changed by increasing flow rates. Peak broadening is attributed largely to convective dispersion within the membrane bed; however, the overall effect comes from the membrane bed and the module system (pump, tubing, fittings and holder) [Gebauer et al., 1996; Roper et al., 1995; Thömmes et al., 2007].
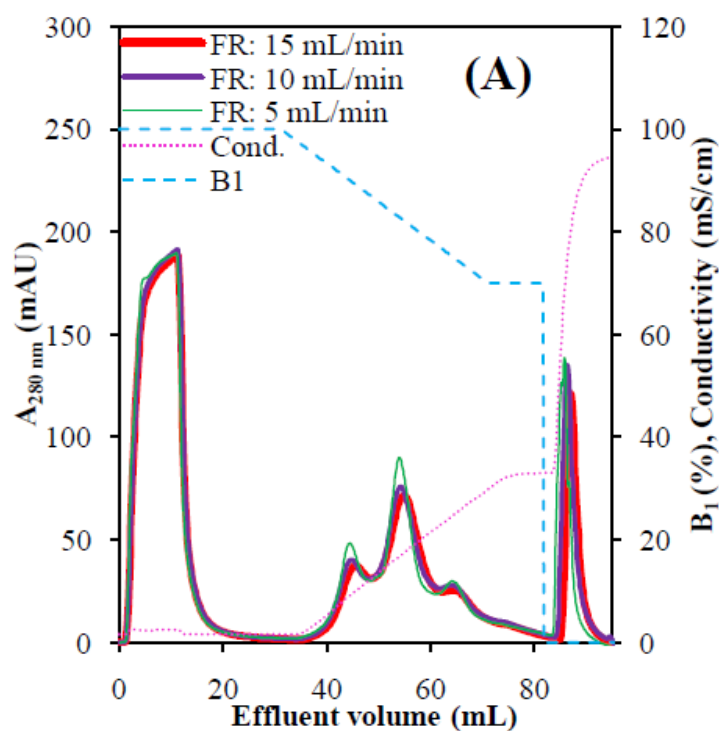
Figure 4.8(A) Effect of volumetric flow rate on the separation resolution of PA from *E. coli* lysate using Sartobind® D membrane adsorber (loading buffer B_1: 20 mM Tris-HCl, pH 7.8; elution buffer E_1: 1 M NaCl in loading buffer B_1; flow rate: 5, 10 and 15 mL/min; sample load volume: 10 mL). Solid line represents the absorbance at 280 nm. Dotted line represents conductivity. Dashed line represents the % of loading buffer B_1.
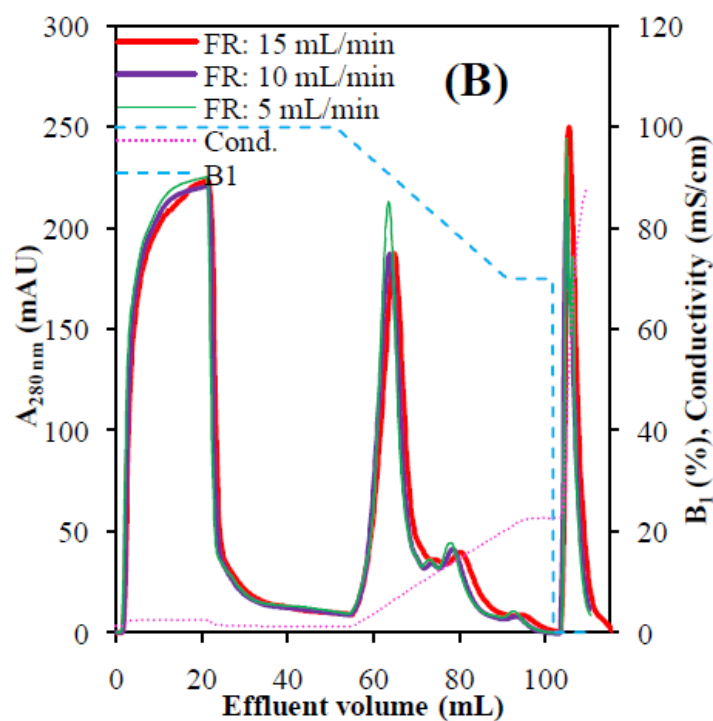
Figure 4.8(B) Effect of volumetric flow rate on the separation resolution of PA from *E. coli* lysate using newly designed AEX membrane adsorbers (loading buffer B_1: 20 mM Tris-HCl, pH 7.8; elution buffer E_1: 1 M NaCl in loading buffer B_1; flow rate: 5, 10 and 15 mL/min; sample load volume: 20 mL). Solid line represents the absorbance at 280 nm. Dotted line represents conductivity. Dashed line represents the % of loading buffer B_1.

4.3.2.3 Impact of sample load volume

Fig. 4.9 shows the effect of sample load volume on the separation profile obtained using Sartobind® D and AEX membranes. The sample load volume was increased by 4-fold in each case. Increases in the sample load volume led to increased peak widths. However, the total number of distinguishable peaks remained the same, and peak resolution decreased only slightly even under conditions where >75% of the total protein dynamic binding capacity of the membrane bed had been utilized.
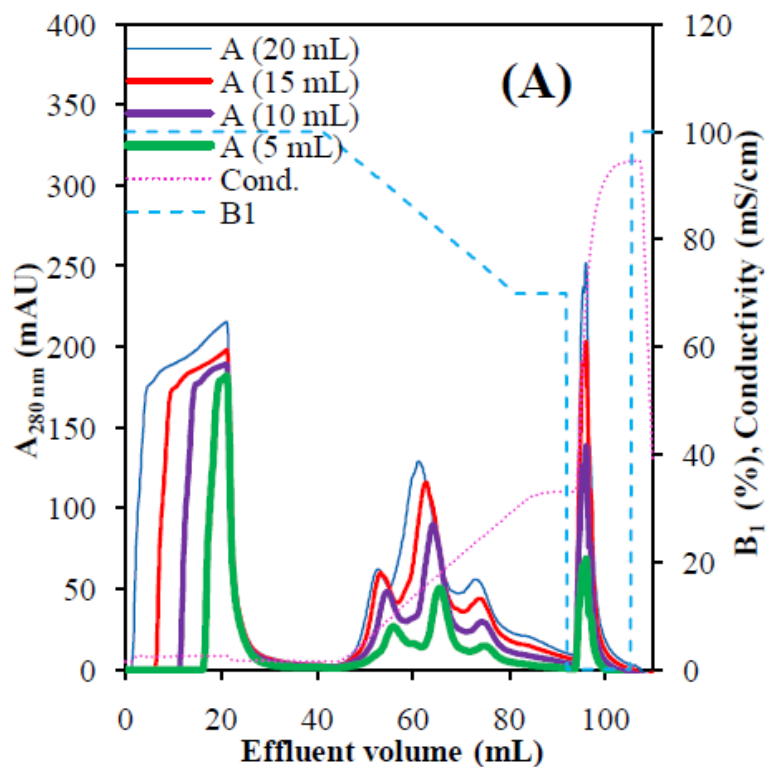
Figure 4.9(A) Effect of load volume on the separation resolution of PA from *E. coli* lysate using Sartobind® D membrane adsorber (loading buffer B_1: 20 mM Tris-HCl, pH 7.8; elution buffer E_1: 1 M NaCl in loading buffer B_1; flow rate: 5 mL/min; sample volume: 5, 10, 15 and 20 mL). Solid line represents the absorbance at 280 nm. Dotted line represents conductivity. Dashed line represents the % of loading buffer B_1.
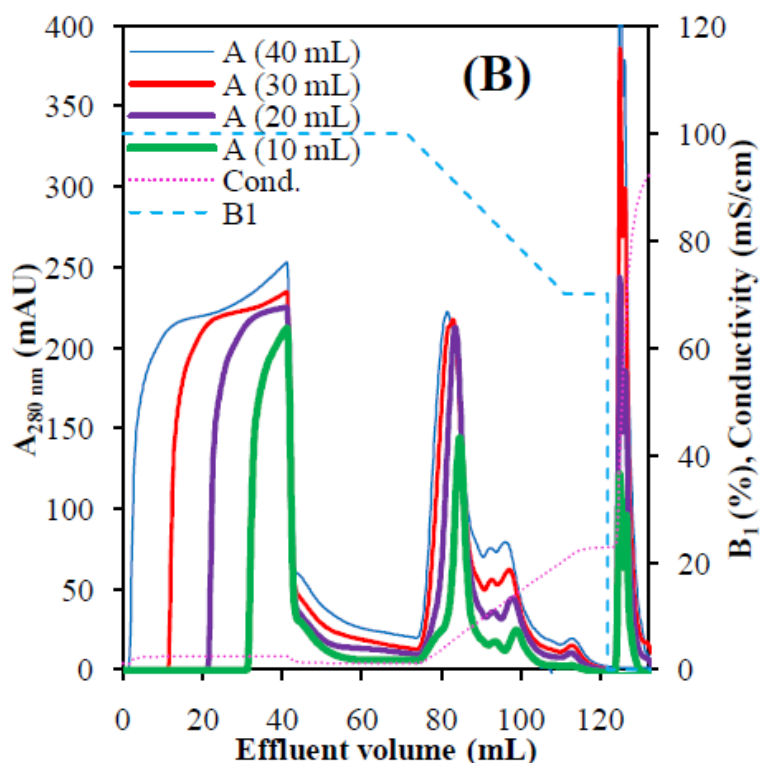
Figure 4.9(B) Effect of load volume on the separation resolution of PA from *E. coli* lysate using newly designed AEX membrane adsorber (loading buffer B_1: 20 mM Tris-HCl, pH 7.8; elution buffer E_1: 1 M NaCl in loading buffer B_1; flow rate: 5 mL/min; sample volume: 10, 20, 30 and 40 mL). Solid line represents the absorbance at 280 nm. Dotted line represents conductivity. Dashed line represents the % of loading buffer B_1.

4.3.3 pH-gradient anion-exchange chromatography

Increasing mobile phase ionic strength is used commonly to elute bound proteins from stationary phases in large scale IEC bioseparations. Nevertheless, pH-gradient elution, albeit a relatively recent concept, has some prominent advantages over salt-gradient IEC. Proteins are focused in narrower bands, resulting in higher separation resolution than generally achieved by ionic strength gradient IEC [Shan et al., 2001]. During pH-gradient elution, bound proteins typically are eluted in order of their isoelectric points [Andersen et al., 2004; Pepaj et al., 2006; Shan et al., 2001]. pH-

gradient IEC has been applied to analytical scale separations and has great potential as an analytical tool for the design and optimization of IEC protein separations [Ahamed et al., 2007; Andersen et al., 2004; Pepaj et al., 2006].

Two standard approaches have been employed to generate pH gradients: internal generation of the pH gradient by exploiting the buffering capacity of stationary phase functional groups [Pabst et al., 2007, 2008] and external generation of the pH gradient by mixing two or more buffers with different pH values at the entrance of the column [Ahamed et al., 2007; Andersen et al., 2004; Pepaj et al., 2006]. In this study, externally generated pH-gradient AEC was used to purify PA protein from *E. coli* lysate using all three stationary phases. A gradient in pH from 8.0 to 3.5 was applied. The upper value of pH was kept at 8.0 to ensure that the polyelectrolyte functional groups remained charged positively. The lower value of pH was kept at 3.5 because applications of AEC are rare at pH < 3.5. Also, at pH < 3.5, protein precipitation may occur. Four buffering species with pK_a values in regular intervals (piperazine, $pK_{a2} = 9.7$, $pK_{a1} = 5.3$; bis-tris-propane, $pK_{a2} = 9.0$, $pK_{a1} = 6.8$; triethanolamine, $pK_a = 7.7$; and N-methylpiperazine, $pK_a = 4.7$) were used to prepare loading and elution buffers. Generating a linear and controllable external pH gradient at the end of the column is quite difficult for weak ion-exchange media because of the proximity of loading buffer pH to the pK_a of the functional groups. Several groups [Ahamed et al., 2007; Andersen et al., 2004; Pepaj et al., 2006] have used strong ion-exchange media for pH-gradient IEC separations, but the use of weak ion-exchange media is limited in the literature.

The same AEC protocol was applied to the three stationary phases and a nearly linear pH gradient was generated in each case. Each stationary phase was equilibrated with buffer B_2 (pH 8.0), followed by loading of the *E. coli* lysate. Proteins that had adsorbed to the anion-exchange media during column loading were eluted using pH-gradient elution. Figs. 4.10−4.12 present the chromatograms for pH-gradient AEC separation of PA protein using the HiTrap[TM] FF resin column, Sartobind[®] D membrane and AEX membrane adsorbers. For all three stationary phases, four easily distinguishable elution peaks were generated using pH-gradient elution. The first peak was the largest and eluted around pH 5.8−6.0 for all three stationary phases. The reported p*I* of PA protein is 5.4−5.9 [Ahuja et al., 2001; Powell et al., 2007]. From previous SDS-PAGE and total protein assays, it was known that PA protein is the largest fraction of the total protein in the *E. coli* lysate. Therefore, the largest peak eluted during pH-gradient is PA protein. In order to recover and fractionate any remaining adsorbed proteins at pH 3.5, a salt gradient was applied. Application of the salt gradient generated two protein elution peaks when the resin column was used as stationary phase (Fig. 4.10). In contrast, four or five distinguishable protein peaks were generated by application of the salt gradient when membrane adsorbers were used as stationary phases. This observation strengthens the previous conclusion that the membrane adsorbers offer higher resolution than the resin column.
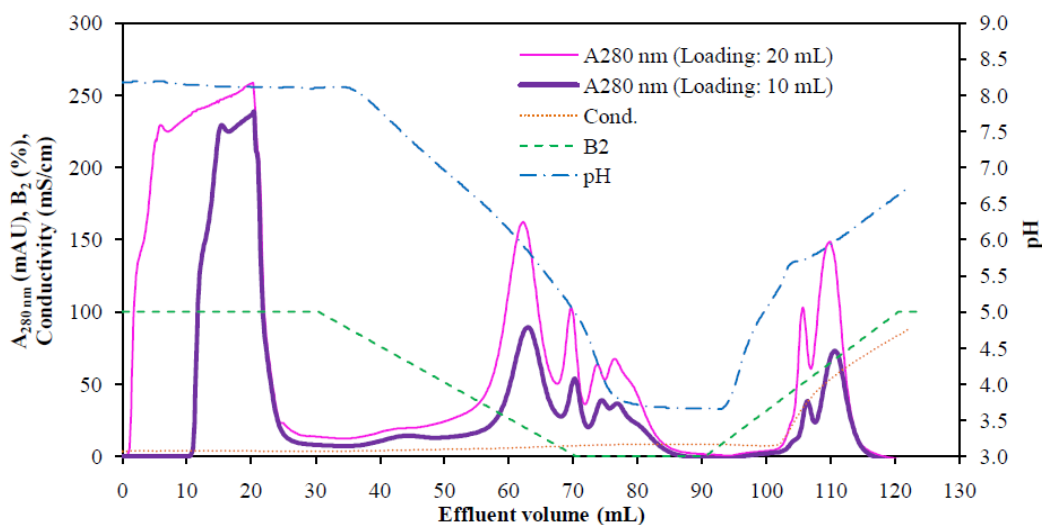
Figure 4.10 pH-gradient anion-exchange chromatographic separation of PA protein from *E. coli* lysate using HiTrap^{TM} DEAE FF resin column (loading buffer B$_2$: pH 8.0; elution buffer E$_2$: pH 3.5; elution buffer E$_3$: 1 M NaCl in loading buffer B$_2$, pH 7.0; flow rate: 1 mL/min; sample load volume: 10 and 20 mL). Solid line represents the absorbance at 280 nm. Dotted line represents conductivity. Dashed line represents the % of loading buffer B$_1$. Long dash-dot line represents effluent pH.
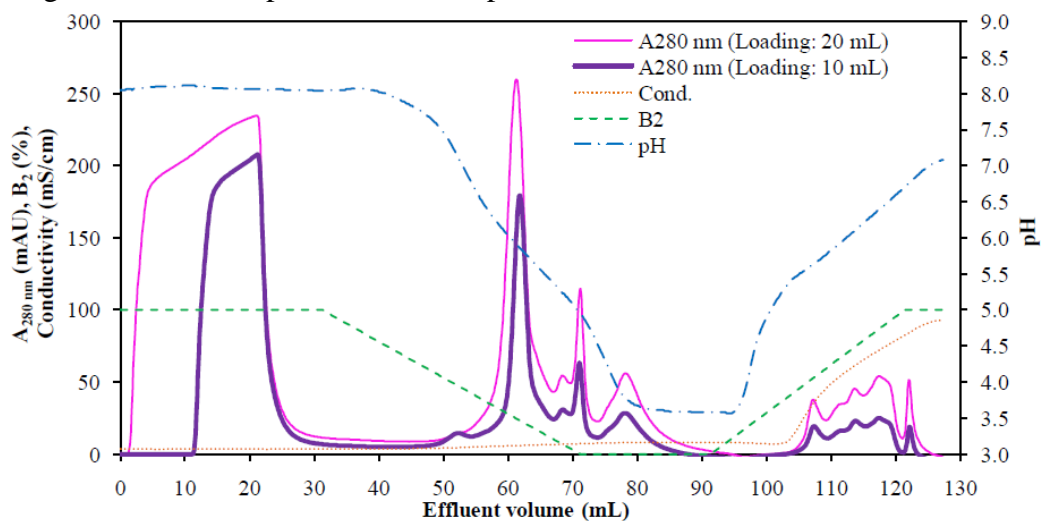
Figure 4.11 pH-gradient anion-exchange chromatographic separation of PA protein from *E. coli* lysate using Sartobind$^{®}$ D membrane adsorber (loading buffer B$_2$: pH 8.0; elution buffer E$_2$: pH 3.5; elution buffer E$_3$: 1 M NaCl in loading buffer B$_2$, pH 7.0; flow rate: 5 mL/min; sample load volume: 10 and 20 mL). Solid line represents the absorbance at 280 nm. Dotted line represents conductivity. Dashed line represents the % of loading buffer B$_1$. Long dash-dot line represents effluent pH.
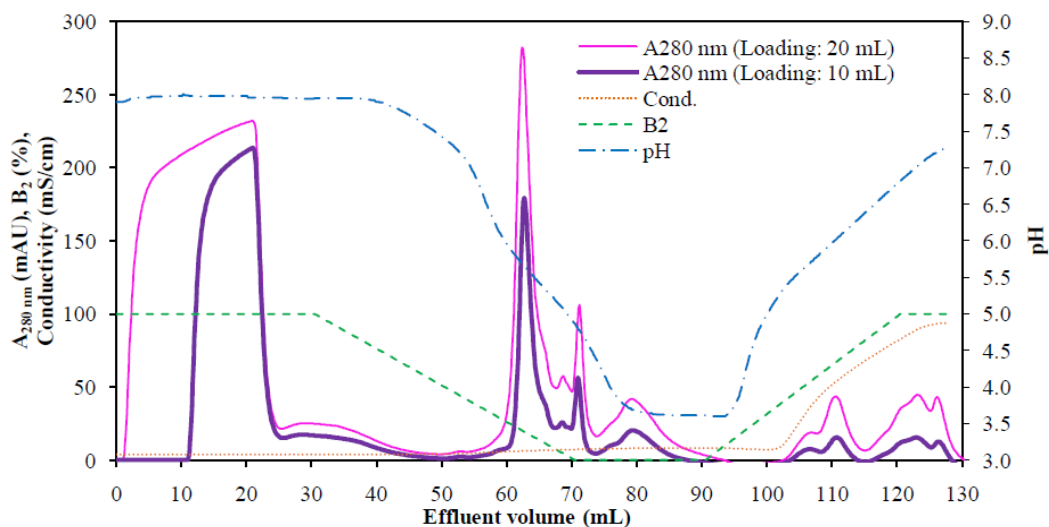
Figure 4.12 pH-gradient anion-exchange chromatographic separation of PA protein from *E. coli* lysate using newly designed AEX membrane adsorber (loading buffer B_2: pH 8.0; elution buffer E_2: pH 3.5; elution buffer E_3: 1 M NaCl in loading buffer B_2, pH 7.0; flow rate: 5 mL/min; sample load volume: 10 and 20 mL). Solid line represents the absorbance at 280 nm. Dotted line represents conductivity. Dashed line represents the % of loading buffer B_1. Long dash-dot line represents effluent pH.

On visual inspection, the protein separation resolution obtained using pH-gradient AEC (Figs. 4.10−4.12) was significantly better compared to that obtained using ionic strength gradient AEC (Figs. 4.3−4.5). The important characteristic of pH-gradient IEC is that the focusing effect eliminates any peak broadening caused by high sample loading [Andersen et al., 2004]. Figs. 4.10−4.12 illustrate this point; increasing sample load volume by 2-fold did not affect the peak resolution. On comparison of the stationary phases, the PA protein elution peak resolution was higher (i.e., the ratio of height to half-width was larger) for membrane adsorbers than the resin column. Noteworthy is that the membrane adsorbers were operated at 5 times higher volumetric flow rate than the resin column. Again, we submit that the better separation resolution with membrane adsorbers results from a shorter diffusion path length between the main flow stream and stationary

phase binding sites. In the absence of diffusion-limited mass transfer, the characteristic time for desorbed molecules to reach the main flow stream is much shorter in membranes than resins. Plate efficiency of membrane adsorbers is higher than resin columns at higher volumetric flow rates due to the absence of diffusive mass-transfer limitations [Roper et al., 1995].

Surprisingly, the elution profiles of the Sartobind® D and AEX membranes were exactly the same under pH-gradient elution, even through the materials differ in physical structure (e.g., pore size and perhaps polymer chain grafting density and M_w). This observation suggests that the rate-controlling mechanism for protein binding/elution is similar for membranes with average effective pore diameters between 1−5 μm. As long as the residence time in the membrane bed is greater than the characteristic diffusion time to travel from the main flow stream to binding sites on the stationary phase, convective transport becomes the primary mode of mass transfer [Shukla et al., 2007]. In order to check whether this condition holds for the membrane beds used in this study, the following requirement was tested:

$$\frac{L}{v} >> \frac{d_p^2}{4D}$$

(4.4)

L is the thickness of the membrane bed, v is the interstitial velocity, d_p is the average pore diameter of the membrane, D is the external diffusion coefficient of protein. The diffusion coefficient of BSA in phosphate buffer was used as a standard for the calculation. The L.H.S. of equation (residence time in the bed) is an order of magnitude greater than the R.H.S (characteristic diffusion time to reach a binding site located inside

the circular pore) for Sartobind® D and AEX membranes. This calculation suggests that the external diffusion of protein molecules to the binding sites is not the rate-limiting mechanism.

The protein elution profile obtained by pH-gradient AEC can be used to optimize the conditions for PA purification from periplasmic *E. coli* lysate. The PA elution peak maximum occurs at $pH = 5.8 \pm 0.1$ for all three stationary phases (Figs. 4.10–4.12). This pH at which the protein elutes during pH-gradient elution is called the experimental isoelectric point (p*I*) of that protein. The experimental p*I* agrees closely with the p*I* values reported in the literature [Ahuja et al., 2001; Powell et al., 2007]. As a rule of thumb, the optimum operational pH for bind-and-elute AEC to separate PA protein would be roughly $0.5-1.0$ pH units higher than the experimental p*I*. Any pH value greater than 6.8 would bind practically all of the PA protein from the lysate under appropriate loading. However, using pH greater than 6.8 would increase the binding of protein impurities that are more basic than the PA protein. Minimizing the binding of non-product impurities in the bind-and-elute mode of AEC increases the product binding capacity of the column and improves the purity profile of the recovered product. Therefore, the optimum operational pH of the loading buffer should be between $6.3-6.8$ for bind-and-elute AEC to purify PA from periplasmic *E. coli* lysate.

4.4 Conclusions

Protein separation performance of our newly designed AEX membrane adsorber was evaluated and compared with the commercial Sartobind® D membrane adsorber, and the

protein separation performance of membrane adsorbers was compared with the HiTrap[TM] DEAE FF resin column. The protein binding capacities measured using breakthrough curve analysis showed that the dynamic binding capacities of membrane adsrorbers were independent of volumetric flow rate, while the dynamic binding capacity of the resin column decreased regularly as the volumetric flow rate increased. The newly designed AEX membrane adsorber showed higher dynamic binding capacities than the commercial membrane adsorber at the same volumetric throughput and higher capacities than the resin column at 15 times higher volumetric throughput. Higher volumetric throughputs may be used for the membranes, since no decline in performance was observed at the highest value tested in this study. Thus, 15 times higher throughput is a conservative value.

Anion-exchange chromatography performed using linear ionic strength gradient elution showed the following results: The separation performance evaluated based on visual inspection of the chromatogram and quantitative SDS-PAGE analysis of effluent fractions showed that the purity of PA protein was higher for membrane adsorbers than the HiTrap[TM] DEAE FF resin column at 5 times higher volumetric flow rate and was similar for our newly designed AEX membrane and Sartobind[®] D membrane adsorbers. The effects of *E. coli* lysate load volume and volumetric flow rate on PA protein separation resolution of membrane adsorbers were minor, and the peak elution profile remained un-changed. Results obtained from pH-gradient anion-exchange chromatography showed that the PA protein elution peak resolution was higher for

155

membrane adsorbers than the resin column at 5 times higher volumetric flow rate than the resin column.

Overall, the results clearly demonstrate that membrane chromatography is a high-capacity, high-throughput, high-resolution separation technique and that resolution in membrane chromatography is as high as or higher than resin column chromatography under preparative conditions and at much higher volumetric throughput.

4.5 References

Ahamed, T., Nfor, B. K., Verhaert, P. D. E. M., Van Dedem, G. W. K., Van der Wielen, L. A. M., Eppink, M. H. M., Van de Sandt, E. J. A. X., Ottens, M., pH-gradient ion-exchange chromatography: An analytical tool for design and optimization of protein separations, J. Chromatogr. A (2007) 181-188.

Ahuja, N., Kumar, P., Bhatnagar, R., Rapid purification of recombinant Anthrax-Protective Antigen under nondenaturing conditions, Biochem. Biophys. Res. Comm. 286 (2001) 6-11.

Andersen, T., Pepaj, M., Trones, R., Lundanes, E., Greibrokk, T., Isoelectric point separation of proteins by capillary pH-gradient ion-exchange chromatography, J. Chromatogr. A 1025 (2004) 217-226.

Avramescu, M. E., Borneman, Z., Wessling, M., Dynamic behavior of adsorber membranes for protein recovery, Biotech. Bioeng. 84 (2003) 564-572.

Barrande, M., Beurroies, I., Denoyel, R., Tatarova, I., Gramblička, M., Polakovič, M., Joehnck, M., Schulte, M., Characterisation of porous materials for bioseparation, J. Chromatogr. A 1216 (2009) 6906-6916.

Bhut, B. V., Husson. S. M., Dramatic performance improvement of weak anion-exchange membranes for chromatographic bioseparations, J. Membr. Sci. 337 (2009) 215-223.

Bhut, B. V., Wickramasinghe, S. R., Husson, S. M., Preparation of high-capacity, weak anion-exchange membranes for protein separations using surface-initiated atom transfer radical polymerization, J. Membr. Sci. 325 (2008) 176-183.

Bruening, M. L., Dotzauer, D. M., Jain, P., Ouyang, L., Baker, G. L., Creation of functional membranes using polyelectrolyte multilayers and polymer brushes, Langmuir 24 (2008) 7663-7673.

DePhillips, P., Lenhoff, A. M., Pore size distributions of cation-exchange adsorbents determined by inverse size-exclusion chromatography, J. Chromatogr. A 883 (2000) 39-54.

Deshmukh, R. R., Warner, T. N., Hutchison, F., Murphy, M., Leitch II, W. E., Leon , P. D., Srivatsa, G. S., Cole, D. L., Sanghvi, Y. S., Large-scale purification of antisense oligonucleotides by high-performance membrane adsorber chromatography, J. Chromatogr. A 890 (2000) 179-192.

Gebauer, K. H., Thömmes, J., Kula, M. R., Breakthrough performance of high-capacity membrane adsorbers in protein chromatography, Chem. Eng. Sci. 52 (1996) 405-419.

Ghosh, R., Protein separation using membrane chromatography: opportunities and challenges, J. Chromatogr. A 952 (2002) 13-27.

Ghosh, R., Wong, T., Effect of module design on the efficiency of membrane chromatographic separation processes, J. Membr. Sci. 281 (2006) 532-540.

Haber, C., Skupsky, J., Lee, A., Lander, R., Membrane chromatography of DNA: Conformation-induced capacity and selectivity, Biotech. Bioeng. 88 (2004) 26-34.

Knudsen, H. L., Fahrner, R. L., Xu, Y., Norling, L. A., Blank, G. S., Membrane ion-exchange chromatography for process-scale antibody purification, J. Chromatogr. A 907 (2001) 145-154.

Kreuß, M., Krause, I., Kulozik, U., Separation of a glycosylated and non-glycosylated fraction of caseinomacropeptide using different anion-exchange stationary phases, J. Chromatogr. A 1208 (2008) 126-132.

Lipin, D. I., Raj, A., Lua, L. H. L., Middelberg, A. P. J., Affinity purification of viral protein having heterogeneous quaternary structure: Modeling the impact of soluble aggregates on chromatographic performance, J. Chromatogr. A, 1216 (2009) 5696-5708.

Low, D., O'Leary, R., Pujar, N. S., Future of antibody purification, J. Chromatogr. B 848 (2007) 48-63.

Natarajan, V., Cramer, S. M., A Methodology for the characterization of ion-exchange resins, Sep. Sci. Technol. 35 (2000) 1719-1742.

Pabst, T. M., Antos, D., Carta, G., Ramasubramanyan, N., Hunter, A. K., Protein separations with induced pH gradients using cation-exchange chromatographic columns containing weak acid groups, J. Chromatogr. A 1181 (2008) 83-94.

Pabst, T. M., Carta, G., pH transitions in cation exchange chromatographic columns containing weak acid groups, J. Chromatogr. A 1142 (2007) 19-31.

Pepaj, M., Wilson, S. R., Novotna, K., Lundanes, E., Greibrokk, T., Two-dimensional capillary liquid chromatography: pH Gradient ion exchange and reversed phase chromatography for rapid separation of proteins, J. Chromatogr. A 1120 (2006) 132-141.

Phillips, M., Cormier, J., Ferrence, J., Dowd, C., Kiss, R., Lutz, H., J. Carter, Performance of a membrane adsorber for trace impurity removal in biotechnology manufacturing, J. Chromatogr. A 1078 (2005) 74-82.

Powell, B. S., Enama, J. T., Ribot, W. J., Webster, W., Little, S., Hoover, T., Adamovicz, J. J., Andrews, G. P., Multiple asparagine deamidation of Bacillus anthracis protective antigen causes charge isoforms whose complexity correlates with reduced biological activity, PROTEINS: Struc. Func. Bioinform. 68 (2007) 458-479.

Roper, D. K., Lightfoot, E. N., Separation of biomolecules using adsorptive membranes, J. Chromatogr. A 702 (1995) 3-26.

Santarelli, X., Domergue, F., Clofent-Sanchez, G., Dabadie, M., Grissely, R., Cassagne, C., Characterization and application of new macroporous membrane ion exchangers, J. Chromatogr. B 706 (1998) 13-22.

Shan, L., Anderson, D. J., Effect of buffer concentration on gradient chromatofocusing performance separating proteins on a high-performance DEAE column, J. Chromatogr. A 909 (2001) 191-205.

Shukla, A. A., Etzel, M. R., Gadam, S., Process scale bioseparations for the biopharmaceutical industry, CRC Press, Boca Raton, FL, 2007, p. 281.

Stone, M. C., Carta, G., Protein adsorption and transport in agarose and dextran-grafted agarose media for ion exchange chromatography, J. Chromatogr. A 1146 (2007) 202-215.

Subramanian, G., Bioseparation and bioprocessing, 2nd ed., Wiley-VCH, Weinheim, 2007.

Suck, K., Walter, J., Menzel, F., Tappe, A., Kasper, C., Naumann, C., Zeidler, R., Scheper, T., Fast and efficient protein purification using membrane adsorber systems, J. Biotechnol. 121 (2006) 361-367.

Tao, Y., Carta, G., Rapid monoclonal antibody adsorption on dextran-grafted agarose media for ion-exchange chromatography, J. Chromatogr. A 1211 (2008) 70-79.

Teeters, M. A., Conrardy, S. E., Thomas, B. L., Root, T. W., Lightfoot, E. N., A dsorptive membrane chromatography for purification of plasmid DNA, J. Chromatogr. A 989 (2003) 165-173.

Thömmes, J., Etzel, M., Alternatives to chromatographic separations, Biotechnol. Prog. 23 (2007) 42-45.

Van Reis, R., Zydney, A., Bioprocess membrane technology, J. Membr. Sci. 297 (2007) 16-50.

Walsh, G., Biopharmaceutical benchmarks 2006, Nat. Biotechnol. 24 (2006) 769-776.

Wang, J., Faber, R., Ulbricht, M., Influence of pore structure and architecture of photo-grafted functional layers on separation performance of cellulose-based macroporous membrane adsorbers, J. Chromatogr. A 1216 (2009) 6490-6501.

Wigelsworth, D. J., Krantz, B. A., Christensen, K. A., Lacy, D. B., Juris, S. J., Collier, R. J., Binding stoichiometry and kinetics of the interaction of a human Anthrax toxin receptor, CMG2, with protective antigen, J. Biol. Chem. 279 (2004) 23349-23356.

Wurm, F. M., Production of recombinant protein therapeutics in cultivated mammalian cells, Nat. Biotechnol. 22 (2004) 1393-1398.

Yang, H., Viera, C., Fischer, J., Etzel, M. R., Purification of a large protein using ion-exchange membranes, Ind. Eng. Chem. Res. 41 (2002) 1597-1602.

Yu, D., McLean, M. D., Hall, J. C., Ghosh, R., Purification of a human immunoglobulin G1 monoclonal antibody from transgenic tobacco using membrane chromatographic processes, J. Chromatogr. A 1187 (2008) 128-137.

Zhou, J. X., Tressel, T., Gottschalk, U., Solamo, F., Pastor, A., Dermawan, S., Hong, T., Reif, O., Mora, J., Hutchison, F., Murphy, M., New Q membrane scale-down model for process-scale antibody purification, J. Chromatogr. A 1134 (2006) 66-73.

Zhou, J. X., Tressel, T., Yang, X., Seewoester, T., Implementation of advanced technologies in commercial monoclonal antibody production, Biotechnol. J. 3 (2008) 1185-1200.

4.6 Supplemental information

4.6.1 Membrane module design

The membrane module was made of upper and lower housings, screw cap for each housing and a cylinder body that holds housings. Each housing consisted of a polytetrafluoroethylene (PTFE) porous filter disc (Interstate Specialty Products Inc., thickness: 1.5 mm, pore diameter: 5-9 μm) and an ethylene propylene diene monomer (EPDM) rubber O-ring (O-Rings West Inc.). A stack of membranes was sandwiched between the upper and lower housings. Fig. 4.6.1 represents the cross-section view of the housing. Process fluid enters the housing through a main channel (1.6 mm diameter) and distributes to 9 sub-channels (0.5 mm ø center, 0.6 mm diameter on periphary). Each of these sub-channels delivers flow to the PTFE porous disk that further distributes flow uniformly before it reaches the stack of membranes. Nine sub-channels were placed equidistant from each other at the entrance and exit of the membrane stack to enhance the feed flow distribution and effluent collection. Fig. 4.6.2 shows the top view of the housing and the dimensions of sub-channels. Figures are not scaled to the dimensions. The dimensions are given in mm.
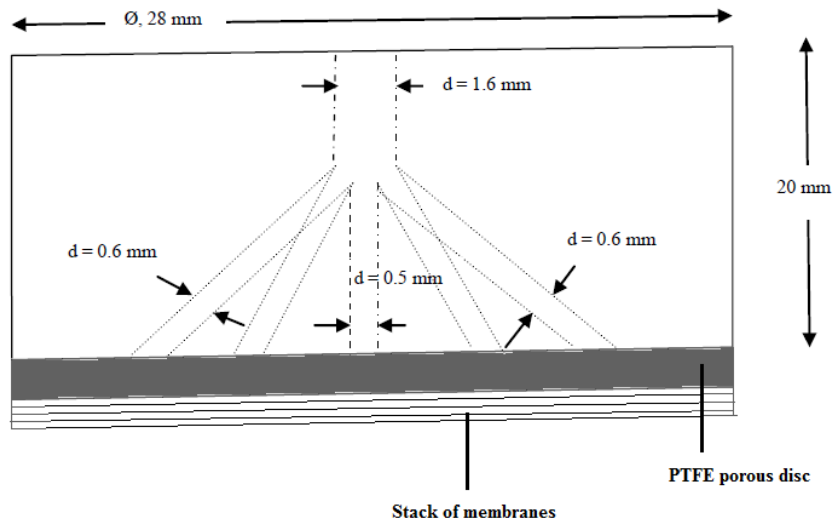
Figure 4.6.1 Side view of upper housing, porous PTFE disc and membrane stack.
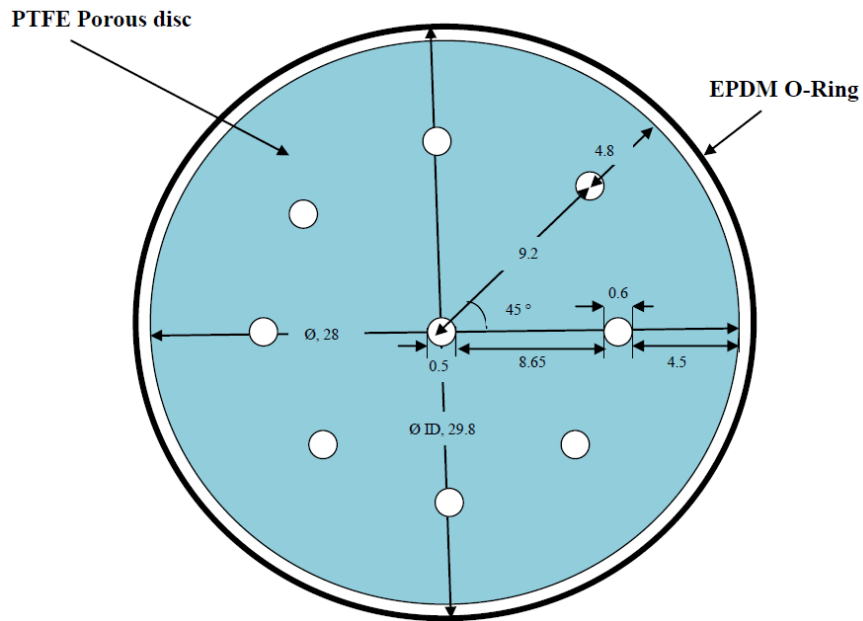
Figure 4.6.2 Top view of housing. Small circle represents cross-sectional area of sub-channels.

163

CHAPTER 5

THE ROLE OF POLYMER NANOLAYER ARCHITECTURE ON THE

SEPARATION PERFORMANCE OF ANION-EXCHANGE MEMBRANE

ADSORBER

5.1 Introduction

The market demand for protein therapeutics such as recombinant proteins,

monoclonal antibodies, viral vaccines and plasmid DNA is increasing rapidly [Gottschalk

et al., 2005; Langer et al., 2007; Pavlou et al., 2004]. With the advent of molecular

biotechnology and engineered cell lines, upstream production processes have made

unprecedented progress in the last decade. Therapeutic proteins with titer >5 g/L have

become feasible in recent years [Langer et al., 2007; Subramanian et al., 2007; Wurm et

al., 2004]. However, this success shifts the production burden to the downstream

processing because the cost of downstream processing increases in proportion with the

mass of product in the feed stream. Currently, for cell-derived products, the downstream

processing costs represent 50−80% of the total production cost [Ghosh et al., 2002;

Shukla et al., 2007; Subramanian et al., 2007]. Therefore, focus is needed to improve the

process economics of downstream separations by employing high-productivity and high-

resolution separation techniques in the biopharmaceutical industry.

Along these lines, membrane chromatography has become a promising alternative to

the more conventional resin chromatography [Charcosset et al., 1998; Gebauer et al.,

1996; Ghosh et al., 2002; Gottschalk et al., 2004; Zeng et al., 1999; Zhou et al., 2006].

Predominantly convective transport of biologics through macroporous membranes yields higher separation speed and flow rate-independent dynamic capacities. These features lead to faster processing time, reduction in the cost of consumables, and economically favorable scale-up [Ghosh et al., 2002; Gottschalk et al., 2004; Zhou et al., 2006]. However, enthusiasm for membrane chromatography has been tempered by the historically lower per volume protein binding capacities of membranes than resin beads [Ghosh et al., 2002; Van Reis et al., 2007; Zhou et al., 2008]. Therefore, an overall goal of this study was to develop advanced strong anion-exchange membranes with higher reversible protein binding capacities than the best resins.

Building "tentacles" on the support matrix is a widely used technique to increase the protein adsorption capacity of chromatography materials [Bowes et al., 2009; Müller et al., 1986; Tsuneda et al., 1995]. Polymeric tentacles with adsorptive functionality extend into the protein solution that fills the porous volume, providing a scaffold for protein molecules to adsorb and leading to relatively high protein binding capacities. A wide variety of resin beads for column chromatography [Bowes et al., 2009; Franke et al., 2010; Ghose et al., 2007; Langford Jr. et al., 2007; Müller et al., 1986; Tao et al., 2008; Zhang et al., 2002] and macroporous membranes for membrane chromatography [Balachandra et al., 2003; Bhut et al., 2008, 2009; He et al., 2008; Singh et al., 2008; Tsuneda et al., 1995] have been modified with adsorptive polymeric tentacles. Incorporating polymeric tentacles into the macroporous membrane has even greater importance since the surface area per volume of a macroporous membrane is much lower than a bed of resin particles [Bhut et al., 2010; Wang et al., 2009]. A focus of this study

165

was to optimize the architecture of polyelectrolyte nanolayers grafted from the pore surfaces of cellulose macroporous membranes.

The separation performance of a membrane adsorber depends primarily on the chemistry and architecture of the adsorptive polymer layer, physical properties of the base membrane and membrane module design [Charcosset et al., 1998; Ghosh et al., 2002; Roper et al., 1995; Singh et al., 2008; Thömmes et al., 1995; Zeng et al., 1999; Wang et al., 2009]. Membranes with a high density of adsorptive sites are essential for high-throughput chromatography. However, the accessibility of binding sites and mass transfer characteristics of the adsorptive polymer layer must be good to enable the full utilization of these adsorptive sites. In an early study, Gebauer et al. [1996] conducted a theoretical analysis of the mass-transfer behavior for ion-exchange membranes with different degrees of grafting. They showed that differences in degree of grafting affect the rate of mass transfer. However, the study was conducted using small size proteins and membranes with only two grafting densities. Camperi et al. [1999] demonstrated that adsorption capacity of lysozyme increases with increasing sulfonate group density for tentacle cation-exchange hollow-fiber membranes. In their study, the sulfonate group density was varied by controlling the extent of reaction during the conversion of epoxy functionality into sulfonate groups; polymer chain graft density was not varied. However, the spacing between the polymer chains grafted from the membrane pore surface is a critical parameter in determining the accessibility of protein to binding sites. Therefore, the primary focus of our research was to evaluate the impact of polymer chain density on

166

the mass-transfer resistance and accessibility of binding sites in the 3-dimensional adsorptive polymer layer for large size bimolecules.

Methods to modify membrane substrates with adsorptive polymer films can be divided into two general categories: 1) coating [Dileo et al., 2007; Hou et al., 2006; Kozlov et al., 2009; Wu et al., 2008] and 2) graft polymerization [Balachandra et al., 2003; Bhut et al., 2008, 2009; Friebe et al., 2007; Singh et al., 2008; Tsuneda et al., 1995]. Though convenient and used widely, coating methods offer limited control over final nominal pore size, pore-size distribution and film thickness. Among graft polymerization methods, ultraviolet (UV)-assisted photochemical grafting is used widely. Ulbricht and co-workers [He et al., 2008; Wang et al., 2009] carried out an extensive study on the effect of grafting density on the protein adsorption capacities of anion-exchange [He et al., 2008] and cation-exchange membrane adsorbers [Wang et al., 2009] prepared by UV grafting. Because conventional photografting methods offer no control mechanism for chain growth, significant irreversible termination may occur, and the grafted polymer chains have relatively higher polydispersity and reduced mobility (e.g., bimolecular termination yields polymer chains with both ends tethered to the surface). Thus, the impact of polymer chain density may be different for this case than for the case when polymer grafting is done using a controlled radical polymerization technique that minimizes chain termination. In order to minimize the effects of chain termination, a controlled polymerization technique was used in this work to graft anionic polyelectrolytes. Our objective was to modify macroporous membranes by grafting polymer chains with uniform and high molar mass and varying the spacing between them

167

to maximize the number of accessible binding sites for large biologics. Grafting was done by surface-initiated atom transfer radical polymerization (ATRP).

Surface-initiated ATRP allows relatively fine and independent control over grafting density and average molecular weight of polymer chains grafted from the surface of base membranes [Balachandra et al., 2003; Bhut et al., 2008, 2009; Friebe et al., 2007; Singh et al., 2008]. Among several noteworthy efforts, Husson and co-workers [Bhut et al., 2008, 2009] prepared weak anion-exchange membranes with ultrahigh and fully reversible protein dynamic binding capacities using surface-initiated ATRP. Bruening and co-workers described the use of ATRP to incorporate immobilized metal ion affinity functionalities within porous alumina membranes [Balachandra et al., 2003; Jain et al., 2007]. In our work, surface-initiated ATRP was used to graft polyelectrolytes from the membrane substrate to prepare strong anion-exchange membrane adsorbers. The ATRP formulation that was used in this study has been shown to yield controlled growth from surfaces [Samadi et al., 2009]. We show that this method leads to membranes with exceptionally high protein binding capacities, and capacities that scale linearly with mass of grafted polymer.

The objectives of this study were to design a surface-initiated graft polymerization protocol to prepare quaternary amine (i.e., Q-type) anion-exchange membranes with high protein binding capacities and to evaluate the impact of polymer nanolayer architecture on the adsorption properties of large biomolecules. Surface-modified adsorptive membranes with different polymer chain graft density, and, thus, different chain spacing, were prepared using surface-initiated ATRP. Dynamic binding capacities of IgG and

168

salmon sperm DNA (SS-DNA) were measured to evaluate the impact of polymer chain density on the accessibility of these large biomolecules to binding sites within the polyelectrolyte nanolayer. Volumetric flow rate was used as an independent variable to study the effect of polymer chain density on mass transfer resistance of IgG and SS-DNA. This research provides clear evidence that the dynamic binding capacities of large biomolecules can be much higher for well-designed macroporous membrane adsorbers than commercial ion-exchange adsorbers and resin columns. Using controlled polymerization and high polymer chain density leads to anion-exchange membrane adsorbers with high binding capacities and the capacities are independent of flow rate, enabling high throughput.

5.2 Materials and methods

5.2.1 Materials

Regenerated cellulose macroporous membranes (RC 60) with 70 µm thickness, 47 mm diameter, and 1.0 µm average effective pore diameter were purchased from Whatman, Inc. The following chemicals and solvents were purchased from Sigma–Aldrich (St. Louis, MO, USA), with purities given in wt.%: [2-(Methacryloyloxy)ethyl]trimethylammonium chloride solution (METAC, 80 wt.% in H_2O), copper(I) chloride (99.995+%), copper(II) chloride (99.99%), 2,2'-bipyridyl (≥99%), 2-bromoisobutyryl bromide (2-BIB, 98%), 1-bromocarbonyl-1-methylethyl acetate (1-BCMEA, 96%), tetrahydrofuran (THF, anhydrous, ≥99.9%), ethanol (anhydrous, ≥99.5%), methanol (≥99.9%), water (ACS reagent grade, HPLC),

tris(hydroxymethyl)aminomethane (Tris–base, ≥99 %), sodium chloride (NaCl, >99.5%), sodium hydroxide (≥98%) and hydrochloric acid (HCl, ACS reagent, 37%) . UltraPure™ Salmon Sperm DNA Solution in a stock concentration of 10 mg/mL (SS-DNA, ≤ 2 kbp size range) was purchased from Life Technologies (Gaithersburg, MD, USA). Albumin from bovine serum (further purified fraction V, ≅99%, M_r ≅ 66 kDa) and IgG from bovine serum (reagent grade, ≥95% (SDS-PAGE), M_r ≅150 kDa) were purchased from Sigma–Aldrich.

5.2.2 Buffers and instrumentation

Loading buffer B_1 (20 mM Tris–base, adjusted to pH 8 with HCl) was used for BSA static protein binding capacity measurements. Loading buffer B_2 (25 mM Tris–base with 50 mM NaCl, adjusted to pH 8.0 with HCl) and elution buffer E_2 (prepared by adding 1.15 M NaCl to loading buffer B_2) were used for SS-DNA dynamic binding capacity measurements. Loading buffer B_3 (25 mM Tris–base, adjusted to pH 9.0 with HCl) and elution buffer E_3 (prepared by adding 1 M NaCl to loading buffer B_3) were used for IgG dynamic binding capacity measurements. Buffers were prepared using distilled water that had been passed through a Milli-Q® Ultrapure purification system (Millipore, Bedford, MA). All buffers were degassed by ultrasonication immediately prior to use.

Dynamic binding capacities of IgG and SS-DNA were measured using an ÄKTA Purifier 100 chromatography system (GE Healthcare Bio-Sciences). Membranes that had been surface modified with anionic polyelectrolytes were cut into small diameter (16 mm) discs and equilibrated with 20 mL of loading buffer in a constant-temperature shaker bath prior to loading them into a membrane holder. A stack of 6−10 membrane

discs was placed in a Mustang® Coin Unit (Pall Corporation, Port Washington, NY) to prepare a membrane adsorber. The effective filtration diameter of membranes stacked into this module is 14 mm; however, the sample diameter of 16 mm was used for calculation of the membrane bed volume because radial distribution of the adsorbing species within the membrane stack is likely to happen during adsorption. The effective filtration diameter (14 mm) was used to calculate the linear flow velocities. Next, the membrane adsorber was attached to the ÄKTA Purifier. Loading samples (IgG and SS-DNA) were injected using a 50 mL capacity Superloop™ (GE Healthcare Bio-Sciences). The effluent from the membrane adsorber was monitored continuously using UV detection (280 nm for IgG and 260 nm for SS-DNA) and pH and conductivity meters installed in the ÄKTA Purifier system for online measurements. The pressure drop across the membrane bed was monitored by pressure transducers. All data were recorded and viewed in Unicorn 5.1 software (GE Healthcare Bio-Sciences).

5.2.3 Preparation of strong anion-exchange membranes

5.2.3.1 Membrane surface modification

Strong anion-exchange membranes were prepared by modifying the surface of commercial regenerated cellulose membranes. The surface-modification process was carried out in two steps, as detailed in our previous publications [Bhut et al., 2008, 2009]. In the first step, membranes were activated by covalent anchoring of an initiator precursor. Membrane activation was carried out in solution at 35 ± 2 °C for 2 hours. A typical solution comprised an ATRP initiator precursor, 2-BIB (28−111 µL, 4.5−18.0 mM), a non-ATRP analogue molecule, 1-BCMEA (0−99 µL, 0−13.5 mM), and solvent,

anhydrous THF (50 mL). The membrane was placed in a specially designed Teflon cage, and a magnetic stir bar was placed on the top of the cage to agitate the reaction mixture. Next, the membrane was removed from the solution, washed thoroughly with THF, HPLC water and ethanol, and dried in the oven at 80 ºC for 30 min.

Surface-functionalized membranes were modified further by surface-initiated ATRP. Grafting of polymer with quaternary amine functionality was carried out from the membrane pore surfaces. A typical polymerization solution was composed of monomer, METAC (10.4 g, 2.0 M); a catalyst system composed of activator, copper(I) chloride (2.0 mg, 1.0 mM), deactivator, copper(II) chloride (0.3 mg, 0.1 mM), and ligand, 2,2'-bipyridyl (8.1 µL, 2.2 mM); and a mixture of solvents composed of methanol (8.7 mL) and HPLC water (1.8 mL). Here, the values of mass and volume are given per membrane sample, along with the final solution concentration of each component. In order to increase measurement accuracy for the small masses and volumes used, one large volume of solution was prepared for each set of 5−10 membranes. To ensure high accuracy for the small volumes used, syringes (Hamilton, Inc.) with range of 0–50 µL or 0–100 µL and a precision of ±1 µL were used for dispensing. In a typical experiment, monomer and solvents were mixed in a flask and this mixture was de-oxygenated by three cycles of freeze–pump–thaw according to a procedure reported earlier [Bhut et al. 2008, 2009]. The solution flask was isolated under nitrogen gas and transferred to an oxygen-free glove box. Catalyst components were added to this flask inside the glove box. Next, this mixture was placed onto a magnetic stir plate for 15 min until it became homogeneous, indicating the formation of a fully soluble catalyst complex. The temperature of the

reaction mixture was raised to 50 °C by placing the flask into a constant-temperature

glass bead bath (ISOTEMP 145D, Fisher). To start polymerization, an initiator-

functionalized membrane was placed into the reaction mixture. The entire procedure was

carried out inside the glove box to avoid oxidation of the copper catalyst.

5.2.3.2 Systematic control of polymer chain density

The density of polymer chains grafted from the membrane pore surface was

controlled by varying the concentration ratio of 2-BIB to 1-BCMEA during the

membrane activation reaction. The concentration ratio of 2-BIB to 1-BCMEA was varied

in the range of 0.25 to 1.0 by keeping the total concentration of 2-BIB + 1-BCMEA at 18

mM. In our previous study [Bhut et al., 2009], 18 mM initiator concentration was found

to be sufficient to activate the maximum number of –OH groups possible. The solution

volume per membrane (50 mL) was kept constant during all of the experiments.

The initiator degree of grafting (DG_{init}) and polymer degree of grafting (DG_{poly}) were

determined by weighing the membrane before and after each modification step using the

following equations:

$$DG_{init} = \frac{w_1 - w_0}{w_0} \times 100\% \tag{5.1}$$

$$DG_{poly} = \frac{w_2 - w_0}{w_0} \times 100\% \tag{5.2}$$

DG represents the degree of grafting for initiator or polymer, w_0, w_1 and w_2 are the

masses of unmodified, initiator-functionalized, and polymer-grafted membranes,

respectively. A set of 5−10 membranes was weighed for each measurement to increase

accuracy.

5.2.4 Performance properties of surface-modified anion-exchange membranes

5.2.4.1 Effect of grafting density and polymerization time on protein binding capacity

Bovine serum albumin (BSA) was used as a model protein to measure static protein adsorption capacities of poly(METAC)-modified membranes. BSA concentrations of 1.0, 1.5, 2.0 and 3.0 mg/mL were prepared in loading buffer B_1. Four concentrations were used to measure adsorption isotherms. An anion-exchange membrane (47 mm dia.) was placed in a glass bottle and incubated in 10 mL of BSA solution for 20 h to reach equilibrium in a shaker bath at 22 °C. Previous studies indicate that this length of time is sufficient to attain equilibrium. After 20 h, membranes were removed from the protein solutions and equilibrium concentrations of the protein solutions were measured as reported earlier [Bhut et al., 2008]. Binding capacities, reported as the adsorbed mass of protein per unit volume of membrane, were calculated by mass balance using initial and equilibrium concentrations of protein solution.

5.2.4.2 Dynamic binding capacity of IgG and SS-DNA

IgG from bovine serum and SS-DNA were used to measure dynamic binding capacities of surface-modified anion-exchange membranes. IgG was dissolved into loading buffer B_2 to prepare a 1.0 mg/mL solution. The protein solution was placed into a shaker bath at 18 °C and agitated overnight. Prior to loading onto the membrane adsorber, solutions were pre-filtered through disposable cellulose acetate syringe filters with 0.2 μm pore diameter (Puradisc 30, GE Healthcare Bio-Sciences) to remove any protein aggregates. The IgG concentration after pre-filtration was measured using UV

absorbance at 280 nm. For studies with SS-DNA, a 10 mg/mL stock solution of SS-DNA was mixed with loading buffer B_3 to prepare a 60 µg/mL sample solution.

The dynamic binding capacities were determined from breakthrough curve analysis. For all the measurements, equal experimental conditions were applied starting with passage of 10 column volumes (CVs) of loading buffer to equilibrate the membrane adsorber bed. Next, IgG or SS-DNA solution was injected. The bound IgG or SS-DNA was eluted with an elution buffer until a stable baseline was observed with UV detection. After every run, the membrane bed was cleaned and regenerated with 5 CVs of 0.5 M sodium hydroxide solution, followed by 10 CVs of 1 M NaCl solution, and finally rinsed with 20 CVs of loading buffer to prepare the bed for the next run. Three different volumetric flow rates (1, 3 and 5 mL/min; equivalent to 39, 117 and 195 cm/h) were used to study the effect of linear flow velocity on the dynamic binding capacities of the anion-exchange membranes. The system dead volume was determined using the retention time (initial breakthrough) of IgG or SS-DNA through the bed prepared from a stack of equivalent un-modified membranes. Dynamic binding capacities were calculated at 10% breakthrough (i.e., when $C/C_0 = 0.10$) and 50% breakthrough ($C/C_0 = 0.50$) according to following approximate equation:

$$q = \frac{C_0 \left(V_{break} - V_{dead}\right)}{V_{col}} \tag{5.3}$$

q represents the dynamic binding capacity (mg IgG or SS-DNA/mL column volume), V_{break} is the effluent volume (mL) where the absorbance value of the breakthrough curve reached 10 or 50% of the absorbance value of the feed concentration, V_{dead} is the dead

volume of the system (mL), C_0 is the feed concentration of IgG or SS-DNA (mg/mL), and V_{col} is the stationary phase column volume (mL).

5.3 Results and discussion

Husson and co-workers [Bhut et al., 2008, 2009] have demonstrated that surface-initiated ATRP can be used to prepare weak anion-exchange membranes for chromatographic bioseparations. They showed that the initiator grafting density and molecular weight of poly(dimethylaminoethyl methacrylate) chains can be varied independently to prepare weak anion-exchange membranes with exceptionally high and completely reversible BSA binding capacities. In this work, the impact of polymer nanolayer architecture on the separation performance of strong anion-exchange membranes was investigated for large biomolecules. For these surface-modified adsorptive membranes, the binding capacity derives exclusively from the polymer nanolayer [Bhut et al., 2008]. Therefore, the objectives of this study were to design a surface-initiated graft polymerization protocol to prepare strong anion-exchange membranes with high protein binding capacities and to evaluate the impact of nanolayer architecture on the adsorption properties of large size biomolecules. The primary focus of the research was to study the effect of polymer chain graft density on the mass transfer resistance and accessibility of IgG and DNA molecules to binding sites within the 3-dimensional polymer nanolayer scaffold.

5.3.1 Preparation of strong anion-exchange membranes

Anion-exchange membranes with different polymer chain grafting densities were prepared using a two-step surface-modification protocol. In the first step, the surfaces of commercial regenerated cellulose macroporous membranes were activated with ATRP initiator groups. In the second step, surface-initiated ATRP was performed to graft poly(METAC) chains from the initiator groups, yielding quaternary amine (i.e., Q-type) anion-exchange membranes. In our previous study [Bhut et al., 2009], the grafting density was manipulated by using sub-stoichiometric amounts (relative to the number of active –OH groups) of the initiator precursor, 2-BIB, during the membrane-activation step. This method may lead to an uneven distribution of initiator immobilized onto the membrane surface. For example, at low initiator precursor concentration, all of the initiator precursor molecules may react near the external surface of the membrane or at pore entrances, resulting in a high density of initiators at the surface and low density farther into the membrane. As we increase initiator precursor concentration, the reactive front may move deeper into the membrane/pores. In this work, the grafting density of polymer chains, and, thus, the spacing between them, was varied using different concentration ratios of an ATRP initiator precursor (2-BIB) and a non-ATRP analogue (1-BCMEA) during the surface-activation step. We hypothesize that by keeping a fixed number of reactive molecules ([2-BIB] + [1-BCMEA] = 18 mM) well above the stoichiometric amount relative to the membrane –OH groups, the distribution of ATRP initiators immobilized onto the membrane surface will be uniform, leading to better control over polymer chain density and eventually higher binding capacities. During this

177

reaction, the acid bromide group of the 2-BIB and 1-BCMEA reacts with the –OH functionality of the cellulose membrane. The hypothesis was that the 1-BCMEA will compete with 2-BIB for –OH groups during surface activation and, thereby, will ensure variable spacing between the ATRP initiator groups throughout the membrane. Surface-initiated ATRP requires immobilized initiator with halogen functionality to initiate the polymer chain growth; therefore, poly(METAC) chains only grow from the immobilized ATRP initiator precursor (2-BIB), while the non-ATRP analogue (1-BCMEA) works as a site blocker to create space between polymer chains. 1-BCMEA was selected as the non-ATRP analogue because we wanted the reactivity of the non-ATRP analogue to be similar to 2-BIB so that both compounds compete effectively for –OH groups. Bromine and acetate are both electron-withdrawing substituents, with similar impacts on reactivity [McMurray et al., 1988]. Thus substituting bromine (in 2-BIB) with acetate (in 1-BCMEA) should yield similar reactivity of the acid bromide group with –OH.
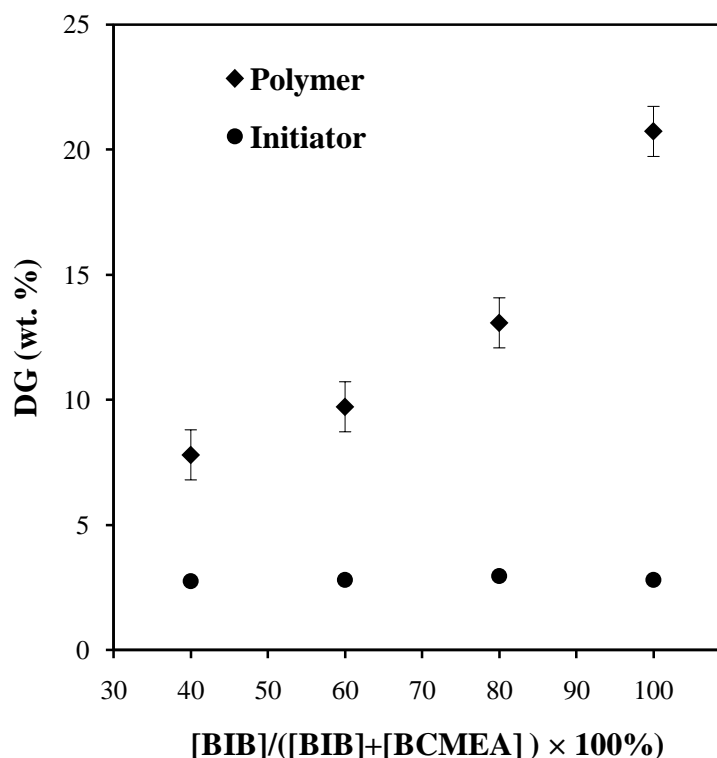
Figure 5.1 Dependence of degree of grafting on the concentration ratio of an initiator precursor, 2-BIB, to a non-ATRP analogue, 1-BCMEA, during membrane activation. Surface-activated membranes were modified further by surface-initiated ATRP (METAC (2M)/Cu(I)/Cu(II)/2,2'-bipyridyl: 2000/1/0.1/2.2) for 20 h. Symbols represent degrees of grafting for poly(METAC) (♦) and initiator (2-BIB or 2-BIB + 1-BCMEA) (●). Two sets of membranes were surface-modified and DG data represent the average of these two measurements. The error bars represent ± 1 std. deviation from the average value.

5.3.1.1 Degree of grafting (DG)

Fig. 5.1 shows the dependence of initiator degree of grafting (DG_{init}) and polymer

degree of grafting (DG_{poly}) on the concentration ratio of an ATRP initiator precursor (2-

BIB) to a non-ATRP analogue (1-BCMEA). The percentage of 2-BIB in solution was

increased from 25 to 100 mol% during the membrane surface-activation step. Surface-

activated membranes were modified further with poly(METAC) using surface-initiated

ATRP for 20 hours. The degrees of grafting were calculated from equations (5.1) and

179

(5.2). Fig. 5.1 shows that DG_{init} did not change significantly by increasing the fraction of 2-BIB during the membrane activation step. This observation agreed with our expectation. Since the concentration of 2-BIB + 1-BCMEA always exceeded that needed to react fully with all –OH groups in the membrane, and since the two reactive species have similar molecular weight, replacing 2-BIB with 1-BCMEA should not change DG_{init} significantly. However, by increasing the molar fraction of 2-BIB, DG_{poly} increased in a regular fashion. This observation validates our hypothesis that by changing the concentration ratio of ATRP-initiator (2-BIB) to non-ATRP analogue (1-BCMEA), the mass of poly(METAC) grafted from the internal pore surface of the membrane can be varied without changing polymerization time. If termination of polymer chains and chain transfer are negligible, as we expect for controlled ATRP and as suggested by the results for protein adsorption (vide infra), then the poly(METAC) chains grafted from the membrane surface should have the same molecular weight. Therefore, differences in DG_{poly} result only from differences in the grafting density of poly(METAC) chains. Another observation from Fig. 5.1 is that the relationship between the molar fraction of 2-BIB and DG_{poly} is not linear as one would expect if 2-BIB and 1-BCMEA had equal reactivity. We rationalize this behavior as follows: there is a higher reaction rate between –OH groups in the membrane and 1-BCMEA compared to 2-BIB. Nevertheless, our newly introduced method provides relatively precise control over polymer chain density.
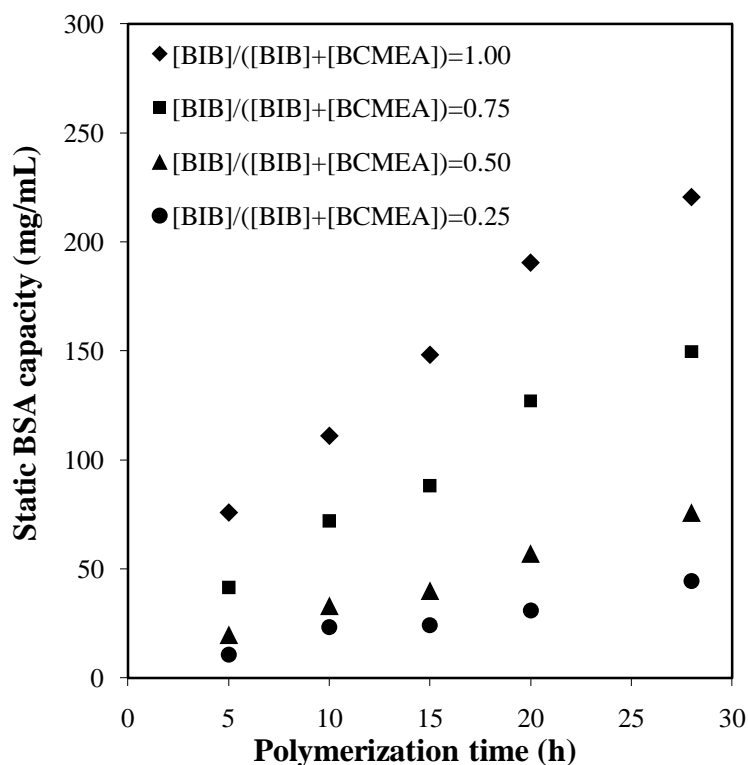
Figure 5.2 Dependence of static protein (BSA) binding capacities on (i) the concentration ratio of an initiator precursor, 2-BIB, and a non-ATRP analogue, 1-BCMEA, used for membrane activation and (ii) polymerization time. Surface-initiated ATRP (METAC (2M)/Cu(I)/Cu(II)/2,2'-bipyridyl: 2000/1/0.1/2.2) was used to produce the poly(METAC)-modified membranes. Symbols represent 2-BIB:1-BCMEA molar concentration ratios of 1.00 (♦), 0.75 (■), 0.50 (▲) and 0.25 (●).

5.3.1.2 Effect of degree of grafting and polymerization time on static BSA binding capacity

If the incidence of irreversible termination of polymer chains and chain transfer are low, then the molecular weight of the poly(METAC) chains grafted from the membrane surface should increase linearly with increasing polymerization time. Fig. 5.2 shows the dependence of BSA static (equilibrium) binding capacity on the polymerization time and concentration ratio of 2-BIB to 1-BCMEA. As polymerization time increases, the protein

binding capacity of poly(METAC)-modified anion-exchange membranes increases

relatively linearly at any given concentration ratio of 2-BIB to 1-BCMEA. These results

demonstrate clearly that the mass of poly(METAC) grafted from the membrane surface,

and, thus, the average molecular weight of polymer chains increases with increasing

polymerization time. Another observation is that, for a constant polymerization time, the

BSA static binding capacity increases with increasing molar fraction of ATRP initiator

molecule (2-BIB) used in the membrane activation step. Taken together, the newly

proposed membrane activation method allows control over the grafting density and

surface-initiated ATRP allows control over the average molecular weight of the grafted

poly(METAC) chains.

Overall, the newly designed two-step graft polymerization protocol offers

independent and nearly linear control of grafting density and average molecular weight of

poly(METAC) chains grown from cellulose macroporous membranes. The result is

anion-exchange membranes with very high per volume BSA binding capacities for

membrane chromatographic bioseparations.

5.3.2 Effect of poly(METAC) chain density on the dynamic binding capacity of IgG and SS-DNA

The separation performance of a membrane adsorber depends primarily on the

chemistry and architecture of the adsorptive polymer layer, physical properties of base

membrane and membrane module design [Charcosset et al., 1998; Ghosh et al., 2002;

Roper et al., 1995; Thömmes et al., 1995; Zeng et al., 1999; Zhou et al., 2006]. In this

work, the polymer chemistry, base membrane and membrane module were kept the same

for all experiments so that the role of polymer nanolayer architecture could be studied. The accessibility of binding sites and mass transfer characteristics of the adsorptive polymer layer are important for the full utilization of the membrane bed capacity. As an example, an adsorptive bed with predominantly convective mass transfer characteristics yields a sharp breakthrough curve and offers flow rate-independent dynamic binding capacities. Therefore, the primary focus of this research was to study the effect of polymer chain density on the accessibility and mass transfer resistance of large size biomolecules. The effect of polymer grafting density on the dynamic binding capacity of IgG and DNA were measured for our newly designed, surface-modified membranes. The isoelectric point (pI) of IgG is about 5.8–7.5 [Baruah et al., 2006; Hahn et al., 1998; Hemmings et al., 1974]. Working at a pH value 1 unit greater than pI, the IgG carries a net negative surface charge and will bind to an anion-exchange stationary phase [Staby et al., 2000, 2001]. Anion-exchange membranes with four different polymer chain densities, and, thus, different spacing between polymer chains, were prepared using surface-initiated ATRP for 20 hours. Volumetric flow rate was used as process variable to study the effect of linear flow velocity on the dynamic binding capacities.

5.3.2.1 Dynamic binding capacity of IgG

Table 5.1 shows the dependence of dynamic binding capacity on DG_{poly}. Dynamic binding capacity was measured at 10 and 50% breakthrough using equation (5.3). The dynamic binding capacity of this large antibody protein increases nearly linearly with increasing DG_{poly}. This observation suggests that the accessibility of IgG to the binding sites along the polymer chains is not impeded by the highest graft densities achieved in

this work. If grafting densities were too high, then IgG molecules would be excluded from the polymer layer, and we would expect to see the capacity go through a maximum and then begin to decrease with further increases in polymer chain density (here indicated by increasing DG_{poly} since polymerization time was constant). We do not see such behavior; therefore, it appears that the spacing between polymer chains is enough for IgG to access binding sites all along the poly(METAC) chains grafted from the membrane pore surface. This trend contrasts that for resin particles. Franke et al. [2010] discussed the effects of ligand density on the dynamic protein binding capacity for linear polymer chain grafted Fractogel EMD SO3⁻ (strong cation-exchange resin, Merck, Darmstadt, Germany) chromatography media. They reported that, at higher grafting densities, the number of overall available sites increases but the number of accessible sites decreases, and, therefore, the dynamic binding capacity increases with increasing ligand density up to a certain value and then it decreases with further increases in ligand density. The maximum dynamic binding capacity of Fractogel EMD SO3⁻ media with optimized ligand density was reported to be about 60 mg/mL at 181 cm/h for IgG. Our values are significantly higher. Ghose et al. [2007] studied the effect of ligand density on the dynamic binding capacities of antibodies and Fc-Fusion proteins on various commercial protein A chromatographic media. They demonstrated that ligand utilization decreases with increasing amounts of ligand immobilized on the surface. They attribute this behavior to the spacing limitation and inter-ligand steric hindrance at high ligand density.

184

Table 5.1 Dynamic binding capacity measured at 10 and 50% breakthrough for poly(METAC)-modified membranes (bed height: 420 μm; loading buffer B_3: 25 mM Tris–HCl, pH 9; elution buffer E_3: 1 M NaCl in loading buffer B_3; feed solution: 1 mg IgG/mL buffer B_3). Surface-initiated ATRP (METAC (2M)/Cu(I)/Cu(II)/2,2'-bipyridyl: 2000/1/0.1/2.2) was used for 20 h to produce the anion-exchange membranes.

Membrane	Flow rate			IgG dynamic binding capacity (mg/mL)	
	mL/min	cm/h	CVs/min	10% breakthrough	50% breakthrough
A: DG − 9.52	1	39	12	50	73
	3	117	36	52	74
	5	195	59	49	71
B: DG − 11.20	1	39	12	72	96
	3	117	36	73	96
	5	195	59	72	99
C: DG − 14.01	1	39	12	87	120
	3	117	36	90	118
	5	195	59	89	116
D: DG − 21.92	1	39	12	135	180
	3	117	36	138	184
	5	195	59	134	176

Table 5.1 summarizes the effect of linear flow velocity on the dynamic binding capacities of IgG. Volumetric flow rate was used as an independent variable to investigate the impact of residence time on the dynamic binding capacities of our newly designed anion-exchange membranes. The volumetric flow rate was increased 5-fold, and, thus, the residence time for IgG molecules through the membrane bed was decreased by the same factor. The dynamic binding capacities calculated at 10 and 50% ($C/C_0 = 0.1$ and 0.5) breakthrough did not change by increasing linear flow velocity. The shape of the breakthrough curves remained un-changed despite increasing volumetric flow rate 5-fold. These data demonstrate that the mass transfer of IgG molecules to the binding sites for our newly designed anion-exchange membranes is primarily via convection, not

diffusion, which is the rate controlling mechanism for resin beds [Carta et al., 2008; Franke et al., 2010; Ghose et al., 2007]. If the diffusion of IgG to the binding sites was the rate limiting step, then the dynamic binding capacity of adsorptive material should have varied with residence time inside the adsorptive bed. For example, Franke et al. [2010] demonstrated that the dynamic binding capacity of polymer chain-grafted resin decreases with increasing volumetric flow rate. They concluded that the optimization of ligand density in resins becomes complicated since it is a function of volumetric flow rate. Our membranes do not have such complication.

The contrasting effect of grafting density for resin and membrane substrates may be explained by their structural differences: for membranes, the polymer chains with adsorptive functionalities (binding sites) are grafted from the surface of macropores; thus, controlled grafting of longer polymer chains (100−200 nm) [Bhut et al. 2008; Singh et al. 2008] in a macroporous membrane substrate does not reduce the pore diameter drastically. The result is that the mass transfer of molecules inside the pores remains predominantly convective. As long as the spacing between grafted polymer chains is sufficient, the accessibility of proteins to the binding site is not hindered. While for the resin, the grafting of longer polymer chains in the cylindrical and closed-end, nanometer-sized pores hinders the accessibility to binding sites and slows mass transfer, even for smaller size proteins such as BSA [Zhang et al., 2002] and lysozyme [Langford Jr. et al., 2007]. This effect is exacerbated at high graft densities, when chains stretch from the surface to avoid overlap.

Overall, our results indicate clearly that the spacing between grafted polymer chains is sufficient for IgG to access binding sites all along the polymer chains. Our newly designed membrane operates under predominantly convective mass transfer mode and, as a result, the dynamic binding capacity is independent of the residence time of IgG inside the membrane bed. More importantly, the newly designed anion-exchange membrane has unusually high and completely reversible protein dynamic binding capacities. These results are remarkable since we have used a globular protein with size of about 150 kDa as the model protein in our measurements. Historically, the lower dynamic protein binding capacity of membranes has been pointed out as the bottleneck for implementation of membrane adsorbers in the capture step of protein therapeutics [Charcosset et al., 1998; Ghosh et al., 2002; Roper et al., 1995; Thömmes et al., 1995; Van Reis et al., 2007; Zeng et al., 1999; Zhou et al., 2006]. Based on our current results and those from recent studies [Bhut et al., 2009, 2010; Singh et al., 2008], we feel that dynamic capacity is no longer the bottleneck. Our design of a strong anion-exchange membrane with unprecedented, fully reversible and flow rate-independent dynamic binding capacity for a model antibody is a highly significant milestone for membrane chromatography.

5.3.2.2 Dynamic binding capacity of DNA

Strong anion-exchange chromatography is the most widely used unit operation for polishing stage purification to remove trace levels of DNA, virus, host cell protein (HCP) and endotoxins [Ghosh et al., 2002; Zhou et al., 2006]. The efficiency of trace impurity removal is measured using log removal value (LRV). LRV is related directly to the volume of process fluid and, thereby, the adsorption capacity of the membranes. Anion-

exchange membranes with high binding capacity provide higher process capacity.

Membrane anion-exchange chromatography in bind-and-elute mode also is under

investigation to purify large quantities of plasmid DNA for vaccine and gene therapy

applications [Eon-Duval et al., 2004; Knudsen et al., 2001; Syrén et al., 2007]. Therefore,

a comprehensive set of experiments was conducted to evaluate the effect of polymer

chain density on the dynamic binding capacity of DNA for our newly designed Q-

membranes. Salmon sperm DNA (SS-DNA) was used as model nucleic acid to measure

the dynamic binding capacities at 10% breakthrough using equation (3).
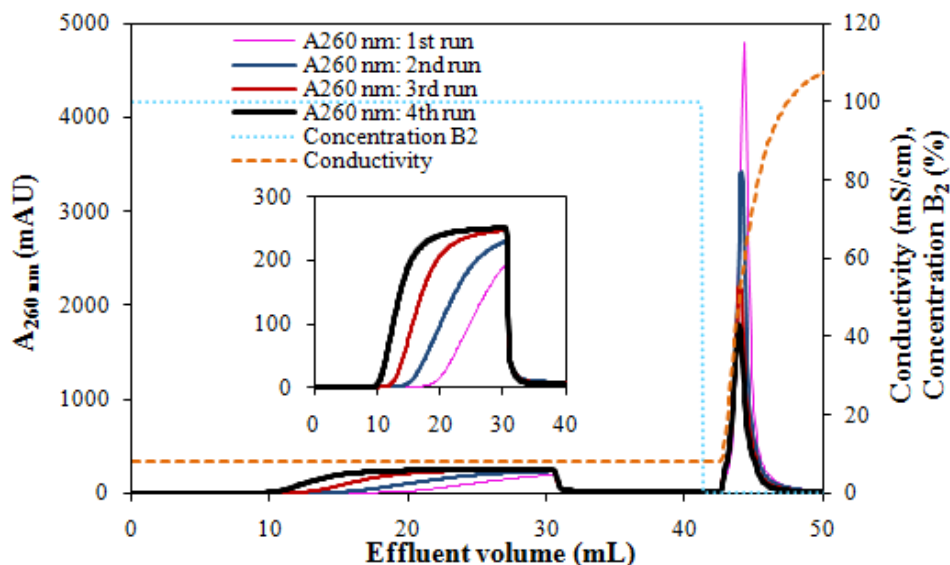
Figure 5.3 Bind-and-elute breakthrough curves of Salmon Sperm DNA obtained using the newly designed strong anion-exchange membrane adsorber (loading buffer B_2: 25 mM Tris-HCl + 50 mM NaCl, pH 8; elution buffer E_2: 1.15 M NaCl in loading buffer B_2; flow rate: 5 mL/min; sample load volume: 30 mL). The feed solution was 60 µg SS-DNA/mL buffer B_2. Surface activation ([2-BIB]/([2-BIB]+[1-BCMEA]) = 0.80) and surface-initiated ATRP (METAC (2M)/Cu(I)/Cu(II)/2,2'-bipyridyl: 2000/1/0.1/2.2) for 20 h were used to produce the poly(METAC) modified membranes. Solid line (—) breakthrough curves represent the UV absorbance at 260 nm. Dotted line (···) represents the conductivity. Dashed line (---) represents the % of loading buffer B_2. The same membrane adsorber bed was used to obtained the four breakthough curves, labeled as 1st, 2nd, 3rd and 4th run.

Fig. 5.3 shows the bind-and-elute chromatogram for SS-DNA obtained using a newly

designed Q-type anion-exchange membrane adsorber. The set of breakthrough curves in

Fig. 5.3 correspond to multiple runs using the same membrane bed. The breakthrough

curves were self-sharpening, indicating highly favorable sorption isotherms under the

conditions used for loading. Using an adsorptive material with a self-sharpening

breakthrough curve is highly advantageous for large-scale industrial application because

it offers maximum utilization of binding capacity before the sorptive breaks through.

Elution of bound DNA yielded a sharp peak, and more than 95% of the area under the

elution curve can be collected in a volume fraction of 2 mL (20 CV). The mass of SS-

DNA (1.60 ± 0.05 mg) in the elution peak was estimated from the area under the elution

curve and an independent calibration curve. Taken together, the concentration of the

eluted SS-DNA was > 0.8 mg/mL, a 13-fold increase relative to the feed concentration.

This concentration effect further demonstrates the highly favorable transport properties of

our newly designed Q-membranes.
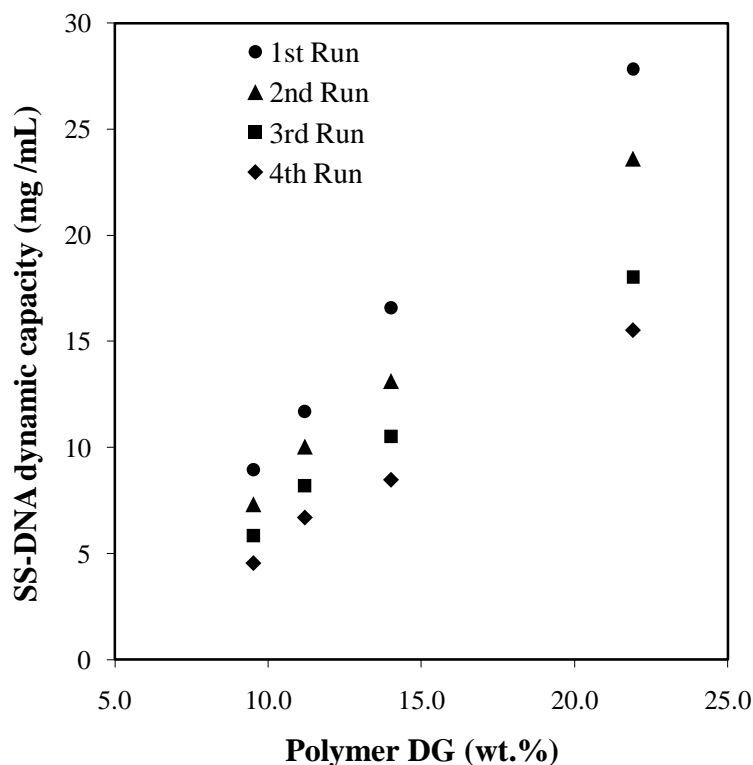
Figure 5.4 Dependence of SS-DNA dynamic binding capacities on the degree of polymer grafting for poly(METAC)-modified membranes (loading buffer B_2: 25 mM Tris-HCl + 50 mM NaCl, pH 8; elution buffer E_2: 1.15 M NaCl in loading buffer B_2; flow rate: 5 mL/min; sample load volume: 20−30 mL). The feed solution was 60 μg SS-DNA/mL buffer B_2. Surface activation ([2-BIB]/([2-BIB]+[1-BCMEA]) = 0.40, 0.60, 0.80 and 1.00) and surface-initiated ATRP (METAC (2M)/Cu(I)/Cu(II)/2,2'-bipyridyl: 2000/1/0.1/2.2) for 20 h were used to produce the poly(METAC) modified membranes. Symbols represent the 1st (●), 2nd (▲), 3rd (■) and 4th run (♦) using the same membrane bed.

Fig. 5.4 shows the effect of DG_{poly} (chain density) on the dynamic binding capacity of

SS-DNA. The dynamic binding capacity increases linearly with increasing

poly(METAC) chain density up to the highest chain density used in this study. This

observation again suggests that the accessibility of SS-DNA molecules to the binding

sites along the polymer chains is not impeded by the highest graft densities achieved in

this work. Given the large size of the DNA, it appears, perhaps, that insertion of the linear

DNA chains in a parallel orientation to the grafted polymer chains allows access to binding sites all along the polymer chains. Considering the large size of DNA (radius of gyration >50 nm for 2.0 kbp size [Latulippe et al., 2007]) and the available adsorptive surface area of membrane (0.53 ± 0.02 m^2/mL [Bhut et al., 2010]), the parallel orientation of DNA is most likely. This orientation is consistent with the findings of Tarmann et al. [2008], who demonstrated using a correlation between theoretical calculations and DNA uptake experiments that the binding of DNA to an ion-exchange resin surface occurred preferential in an upright position. Here again, the dynamic binding capacity of our newly designed anion-exchange membrane is remarkably high. The literature reports that the DNA dynamic binding capacity of the commercial Sartobind® Q membrane is much higher than the widely used resins [Eon-Duval et al., 2004; Knudsen et al., 2001; Syrén et al., 2007]. Knudsen et al. [2001] reports that the dynamic capacity of Sartobind® Q membrane was about 9 ± 1 mg/mL under the same process conditions used in our study. Therefore, our newly designed membrane has 3-fold higher SS-DNA binding capacity than the Sartobind® Q membrane. The same membrane bed was used repeatedly to generate the reversible dynamic capacity data and it was found that the dynamic capacity was not completely reversible. This observation is common for strong anion-exchange media [Eon-Duval et al., 2004; Syrén et al., 2007]. The negatively charged DNA strands bind strongly to the strong anion exchangers and are difficult to elute with a salt gradient.

Once again, volumetric flow rate was used as an independent variable to investigate the impact of residence time on the DNA dynamic binding capacities. The volumetric flow rate was increased 5-fold. Table 5.2 shows the results. Surprisingly, the dynamic

191

binding capacity of DNA increased slightly with increasing volumetric flow rate. We attribute this behavior to the molecular structure of DNA molecules and flow-induced shear forces. Zydney and co-workers [Latulippe et al., 2007, 2009] have done extensive studies on the effect of volumetric flow rate on the flux of DNA through UF membranes. They reported that DNA elongates due to high shear caused by increased flow rate at the pore entrance and that, in turn, DNA flux increases with increasing flow velocity. As mentioned earlier, insertion of linear DNA chains appears to occur in a parallel orientation to the grafted polymer chains. Thus, at higher volumetric flow rate, the DNA elongates, which may lead to easier insertion and packing into the polymer nanolayer network. In any case, these data demonstrate that the mass transfer of DNA molecules to the binding sites of our macroporous membrane beds is limited primarily by convection; diffusional limitations are minimal [Teeters et al., 2003].

Table 5.2 Dynamic binding capacity measured at 10 % breakthrough for poly(METAC)-modified membranes (bed height: 420 μm; loading buffer B_2: 25 mM Tris–HCl + 50 mM NaCl, pH 8; elution buffer E_2: 1.15 M NaCl in loading buffer B_2; feed solution: 60 μg SS-DNA/mL buffer B_2). Surface activation ([2-BIB]/([2-BIB]+[1-BCMEA]) = 1.00) and surface-initiated ATRP (METAC (2M)/Cu(I)/Cu(II)/2,2'-bipyridyl: 2000/1/0.1/2.2) for 20 h were used to produce the anion-exchange membranes. Two measurements were taken at each flow rate and data represent the average of these two measurements. The error bars represent ± 1 std. deviation from the average value.

Flow rate			Dynamic binding capacity
mL/min	cm/h	CVs/min	mg SS-DNA/mL
1	39	15	24 ± 0.8
3	117	46	30 ± 1.0
5	195	77	32 ± 0.7

5.4 Conclusions

A simple and effective two-step surface modification protocol has been described to prepare strong anion-exchange membranes with high and fully reversible protein binding capacities for chromatographic bioseparations. The results show the following important trends: the chain density of poly(METAC) grown from the pore surface of the membrane can be varied by changing the concentration ratio of ATRP-initiator to non-ATRP analogue during membrane activation. The mass of poly(METAC) grafted from the membrane surface, and, thus, the average molecular weight of polymer chains increases with increasing polymerization time. Overall, the proposed graft polymerization protocol offers independent and nearly linear control of grafting density and average molecular weight of poly(METAC) chains grown from cellulose macroporous membranes.

The dynamic binding capacity of IgG increases nearly linearly with increasing poly(METAC) chain density. This result suggests that the spacing between polymer chains is sufficient for IgG to access binding sites all along the polymer chains. Furthermore, the dynamic binding capacity of IgG did not change by increasing linear flow velocity, which suggests that the mass transfer of IgG molecules to the binding sites is primarily via convection, not diffusion. The same conclusions were derived from the dynamic binding capacity measurements of Salmon Sperm DNA. One additional finding for DNA is that the insertion of linear DNA chains occurs in a parallel orientation to the grafted polymer chains. At higher volumetric flow rate, the DNA elongates due to shear forces, which lead to higher dynamic binding capacity.

Overall, the results clearly demonstrate that the accessibility of binding sites and the diffusional mass transfer are not limiting factors for the high dynamic binding capacities of large size biomolecules. Using controlled polymerization and high polymer chain density, strong anion-exchange membrane adsorbers with unusually high and flow rate-independent binding capacities can be designed.

5.5 References

Balachandra, A. M., Baker, G. L., Bruening, M. L., Preparation of composite membranes by atom transfer radical polymerization initiated from a porous support, J. Membr. Sci. 227 (2003) 1-14.

Baruah, G. L., Nayak, A., Belfort, G., Scale-up from laboratory microfiltration to a ceramic pilot plant: Design and performance, J. Membr. Sci. 274 (2006) 56–63.

Bhut, B. V., Christensen, K. A., Husson, S. M., Membrane chromatography: Protein purification from *E. coli* lysate using newly designed and commercial anion-exchange stationary phases, J. Chromatogr. A (2010) doi:10.1016/j.chroma.2010.05.049.

Bhut, B. V., Husson, S. M., Dramatic performance improvement of weak anion-exchange membranes for chromatographic bioseparations, J. Membr. Sci. 337 (2009) 215-223.

Bhut, B. V., Wickramasinghe, S. R., Husson, S. M., Preparation of high-capacity, weak anion-exchange membranes for protein separations using surface-initiated atom transfer radical polymerization, J. Membr. Sci. 325 (2008) 176-183.

Bowes, B. D., Koku, H., Czymmek, K. J., Lenhoff, A. M., Protein adsorption and transport in dextran-modified ion-exchange media. I: Adsorption, J. Chromatogr. A 1216 (2009) 7774–7784.

Charcosset, C., Purification of proteins by membrane chromatography, J. Chem. Technol. Biotechnol. 71 (1998) 95-110.

Camperi, S. A., Navarro del Cañizo, A. A., Wolman, F. J., Smolko, E. E., Cascone, O., Grasselli, M., Protein adsorption onto tentacle cation-exchange hollow-fiber membranes, Biotechnol. Prog. 15 (1999) 500-505.

Dileo, A. J., McCue, J., Moya, W., Quinones-Garcia, Socie, N. P., Thom, V., Yuan, S., Porous adsorptive or chromatographic media, U.S. Patent, US 2007/0256970 A1, 2007.

Eon-Duval, A., Burke, G., Purification of pharmaceutical-grade plasmid DNA by anion-exchange chromatography in an RNase-free process, J. Chromatogr. B 804 (2004) 327–335.

Franke, A., Forrer, N., Butté, A., Cvijetič, B., Morbidellia, M., Jöhnck, M., Schulte, M., Role of the ligand density in cation exchange materials for the purification of proteins, J. Chromatogr. A 1217 (2010) 2216–2225.

Friebe, A., Ulbricht, M., Controlled pore functionalization of poly(ethylene terephthalate) track-etched membranes via surface-initiated atom transfer radical polymerization, Langmuir 23 (2007) 10316-10322.

Gebauer, K. H., Thömmes, J., Kula, M. R., Breakthrough performance of high-capacity membrane adsorbers in protein chromatography, Chem. Eng. Sci. 52 (1996) 405-419.

Ghosh, R., Protein separation using membrane chromatography: opportunities and challenges, J. Chromatogr. A 952 (2002) 13–27.

Ghose, S., Hubbard, B., Cramer, S. M., Binding capacity differences for antibodies and Fc-Fusion proteins on protein A chromatographic materials, Biotech. Bioeng. 96 (2007) 768−779.

Gottschalk, U., Downstream processing of monoclonal antibodies: From high dilution to high purity, Biopharm. Int. 18 (2005) 42-58.

Gottschalk, U., Fischer-Fruehholz, S., Reif, O., Membrane adsorbers—A cutting edge process technology at the threshold. Bioprocess Int. 5 (2004) 56–65.

Hahn, R., Schulz, P. M., Schaupp, C., Jungbauer, A., Bovine whey fractionation based on cation-exchange chromatography, J. Chromatogr. A 795 (1998) 277–287.

He, D., Ulbricht, M., Preparation and characterization of porous anion-exchange membrane adsorbers with high protein-binding capacity, J. Membr. Sci. 315 (2008) 155–163.

Hemmings, W. A., Jones, R. E., Isoelectric focusing analysis of transmission of fractions of bovine IgG across the gut of the suckling rat, Immunology 27 (1974) 343-350.

Hou, C. J., Konstantin, P., Yang, Y., Negatively charged membrane, US 7132049 B, 2006.

Jain, P., Sun, L., Dai, J., Baker, G. L., Bruening, M. L., High-capacity purification of his-tagged proteins by affinity membranes containing functionalized polymer brushes, Biomacromolecules 8 (2007) 3102–3107.

Knudsen, H. L., Fahrner, R. L., Xu, Y., Norling, L. A., Blank, G. S., Membrane ion-exchange chromatography for process-scale antibody purification, J. Chromatorg. A 907 (2001) 145–154.

Kozlov, M., Media for membrane ion-exchange chromatograph, U.S. Patent, US 2009/0130738 A1, 2009.

Langer, E.S., Downstream production challenges in 2007: Study indicates problems may not be resolved before 2011, Biopharm. Int. 5(6), (2007) 22-28.

Langford Jr. J. F., Xu, X., Yao, Y., Maloney, S. F., Lenhoff, A. M., Chromatography of proteins on charge-variant ion exchangers and implications for optimizing protein uptake rates, J. Chromatorg. A 1163 (2007) 190–202.

Latulippe, D. R., Ager, K., Zydney, A. L., Flux-dependent transmission of supercoiled plasmid DNA through ultrafiltration membranes, J. Membr. Sci. 294 (2007) 169–177.

Latulippe, D. R., Zydney, A. L., Elongational flow model for transmission of supercoiled plasmid DNA during membrane ultrafiltration, J. Membr. Sci. 329 (2009) 201–208.

McMurray, J. E., Organic chemistry, 2nd ed., Thomson Brooks/Cole, Belmont, CA, 1988.

Müller, W., New phase supports for liquid-liquid partition chromatography of biopolymers in aqueous poly(ethyleneglycol)-dextran systems. Synthesis and application for the fractionation of DNA restriction fragments, Eur. J. Biochem. 155 (1986) 213-22.

Pavlou, A. K., Reichert, J. M., Recombinant protein therapeutics—success rates, market trends and values to 2010, Nat. Biotechnol. 22 (2004) 1513–1519.

Van Reis, R., Zydney, A. L, Bioprocess membrane technology, J. Membr. Sci. 297 (2007) 16-50.

Roper, K. D., Lightfoot, E. N., Separation of biomolecules using adsorptive membranes, J. Chromatogr. A, 702 (1995) 3-26.

Samadi, A., Synthesis and analysis of nano-thin polymer films for separation applications, PhD dissertation, Clemson University (2009) P. 104-108.

Shukla, A. A., Etzel, M. R., Gadam, S., Process scale bioseparations for the biopharmaceutical industry, CRC Press, Boca Raton, FL, 2007.

Singh, N., Wang, J., Ulbricht, M., Wickramasinghe, S. R., Husson, S. M., Surfaceinitiated atom transfer radical polymerization: a new method for the preparation of polymeric membrane adsorbers, J. Membr. Sci. 309 (2008) 64–72.

Staby, A., Jensen, I. H., Comparison of chromatographic ion-exchange resins II. More strong anion-exchange resins, J. Chromatogr. A 908 (2001) 149–161.

Staby, A., Jensen, I. H., Mollerup, I., Comparison of chromatographic ion-exchange resins I. Strong anion-exchange resins, J. Chromatogr. A 897 (2000) 99–111.

Subramanian, G., Bioseparation and bioprocessing, 2nd ed., Wiley-VCH, Weinheim, 2007.

Syrén, P., Rozkov, A., Schmidt, S. R., Strömberg, P., Milligram scale parallel purification of plasmid DNA using anion-exchange membrane capsules and a multi-channel peristaltic pump, J. Chromatogr. B 856 (2007) 68–74.

Tao, Y., Carta, G., Rapid monoclonal antibody adsorption on dextran-grafted agarose media for ion-exchange chromatography, J. Chromatorg. A 1211 (2008) 70–79.

Tarmann, C., Jungbauer, A., Adsorption of plasmid DNA on anion exchange chromatography media, J. Sep. Sci. 31 (2008) 2605 – 2618.

Thommes, J., Kula, M. R., Membrane chromatography-An integrative concept in the downstream processing of proteins, Biotechnol. Prog., 11 (1995) 357-367.

Teeters, M. A., Conrardy, S. E., Thomas, B. L., Root, T. W., Lightfoot, E. N., Adsorptive membrane chromatography for purification of plasmid DNA, J. Chromatogr. A 989 (2003) 165–173.

Tsuneda, S., Saito, K., Furusaki, S., Sugo, T., High-throughput processing of proteins using a porous and tentacle anion-exchange membrane, J. Chromatogr. A 689 (1995) 211-218.

Tsuneda, S., Shinano, H., Saito, K., Furusaki, S., Sugo, T., Binding of lysozyme onto a cation-exchange microporous membrane containing tentacle-type grafted polymer branches, Biotechnol. Prog. 10 (1994) 76–81.

Wang, J., Faber, R., Ulbricht, M., Influence of pore structure and architecture of photo-grafted functional layers on separation performance of cellulose-based macroporous membrane adsorbers, J. Chromatogr. A 1216 (2009) 6490–6501.

Wurm, F. M., Production of recombinant protein therapeutics in cultivated mammalian cells, Nat. Biotech. 22 (2004) 1393–1398

Wu, X., Hou, C. J., Dharia, J., Konstantin, P., Yang, Y., Positively charged membrane, US 7396465 B2, 2008.

Zeng, X., Ruckenstein, E., Membrane chromatography: preparation and applications to protein separation, Biotechnol. Prog. 15 (1999) 1003-1019.

Zhang, S., Sun, Y., Study on protein adsorption kinetics to a dye–ligand adsorbent by the pore diffusion model, J. Chromatorg. A 964 (2002) 35–46.

Zhou J. X., Tressel, T., Basic concepts in Q membrane chromatography for large-scale antibody production, Biotechnol. Prog. 22 (2006) 341-349.

Zhou J. X., Tressel, T., Yang, X., Seewoester, T., Implementation of advanced technologies in commercial monoclonal antibody production, Biotechnol. J. 3 (2008) 1185.

CHAPTER 6

CONCLUSIONS AND RECOMMENDATIONS

6.1 Conclusions

The overall goal of my PhD research was to design advanced weak and strong anion-exchange membranes with high protein binding capacities and characterize their performance for downstream chromatographic separation of therapeutic proteins. The concept of my PhD research was to use a commercial membrane as the base chromatography matrix and incorporate adsorptive functionalities onto the pore surface of these membranes via polymer grafting. I have developed simple, versatile and unique surface-initiated graft polymerization protocols to coat internal surfaces of a base membrane substrate with polymer nanolayer films for the preparation of anion-exchange membranes.

In the first project, a two-step surface-modification methodology was designed and implemented to prepare weak anion-exchange membranes for chromatographic bioseparations. Surface-initiated atom transfer radical polymerization (ATRP) was used to graft weak anion polyelectrolytes from a regenerated cellulose macroporous membrane substrate. I characterized the physicochemical and performance properties of these newly designed membranes. AFM and SEM characterization confirmed that the membrane pore morphology was intact after the surface modification of base cellulose membranes. Because the performance properties of an adsorptive membrane depend primarily on the chemistry and architecture of the adsorptive polymer layer, I developed a representative

model to study the three-dimensional evolution of the polymer nanolayers from the membrane surface using a silicon substrate. Use of this substrate enabled measurements of nanolayer thickness via ellipsometry. Polymer growth kinetic data collected using this model were used to guide the further studies of polymer film growth from the membrane surface, with the objective to balance the protein binding capacity with permeability of surface-modified membranes. From the permeability and protein static adsorption capacity measurements, I demonstrated that the polymerization time can be used to achieve high capacity while maintaining adequate permeability by controlling the amount of polymer grafted from the membrane surface.

In the second project, I increased the dynamic protein adsorption capacities significantly compared to the initial work done in the first project and characterized the protein chromatography performance properties of the newly designed weak anion-exchange membranes. I demonstrated that the protein binding capacities of membranes modified by surface-initiated ATRP can be increased by increasing initiator precursor concentration during the membrane-activation step or/and by increasing polymerization time. This project yielded weak anion-exchange membranes with very high volumetric protein binding capacities (static binding capacity~140 mg BSA/mL and dynamic capacity ~130 mg/mL) at high linear flow velocities (>350 cm/h) and relatively low transmembrane pressure drop (<3 bar). I studied the effect of volumetric flow rate on the dynamic binding capacity and demonstrated that the dynamic binding capacity of the newly designed membranes is independent of the linear flow velocity.

Subsequently, I conducted a systematic study to evaluate the role of adsorptive polymer nanolayer architecture on the separation properties of surface-modified, strong anion-exchange membranes for large size biomolecules. In this stage of my work, surface-initiated ATRP was used to graft polyelectrolytes from the membrane substrate to prepare strong anion-exchange membrane adsorbers. The grafting density of polymer chains, and, thus, the spacing between them, was varied using a novel membrane surface activation method. In a comprehensive set of experiments, I demonstrated that the accessibility of IgG and DNA molecules to the binding sites along the polymer chains is not impeded by the highest graft densities achieved in that work. Therefore, I concluded that the spacing between polymer chains is large enough for IgG and DNA to access binding sites all along the polymer chains grafted from the membrane pore surface. In a separate set of experiments, I varied volumetric flow rate to study the effects of polymer chain density on the mass transfer resistance of IgG and DNA biomolecules to the binding sites inside the polymer network. The results of these experiments suggest that the mass transport of large size biomolecules is predominantly convective and the diffusional limitations are minimal. This project yielded strong Q-type anion-exchange membranes with very high volumetric protein binding capacities (dynamic binding capacity ~140 mg IgG/mL and ~27 mg DNA/mL) at high linear flow velocities (>190 cm/h) and relatively low transmembrane pressure drop (<3.5 bar). Overall, findings from these three projects strengthen the argument that membrane chromatography has great potential to reduce process times and costs for therapeutic biomolecule purifications.

Recognizing that the separation performance evaluation and comparison of newly designed membranes with benchmark commercial products for the separation of recombinant proteins from complex bio-mixtures is essential to demonstrate the high-resolution separation of membrane chromatography, I evaluated and compared the protein separation performance of our newly designed weak anion-exchange membrane adsorber with a commercial and widely used membrane adsorber and resin column chromatography. Anion-exchange chromatography was performed to separate anthrax protective antigen protein from periplasmic *Escherichia coli* lysate using all three stationary phases. The results from this part of the study showed that the newly designed membrane adsorber has three times higher dynamic binding capacities than the commercial membrane adsorber at the same volumetric throughput and higher capacities than the widely used resin column at 15 times higher volumetric throughput. Overall, results of my separation performance comparison case study clearly demonstrate that membrane chromatography with a properly designed adsorptive membrane is a high-capacity, high-throughput, high-resolution separation technique and that resolution in membrane chromatography is as high as or higher than resin column chromatography under preparative conditions and at much higher volumetric throughput.

Traditionally, the dynamic protein binding capacities of membrane adsorbers have been lower than conventional resin columns, and the relatively lower capacities have tempered the broader implementation of membrane chromatography in the biopharmaceutical industry. The separation resolution of membrane adsorbers also has remained questionable. My PhD results provides sufficient evidence to dispel both of

these misperceptions and show that (1) membrane chromatography can be a higher capacity process than resin chromatography in the purification of protein therapeutics and (2) membrane chromatography can be a higher resolution process than resin chromatography.

6.2 Recommendations

For future work, I would strongly suggest designing a novel strategy to increase polymer chain graft density further than what I have achieved in my work. One idea in that direction would be to anchor an initiator with star-like structure that consumes a single functional group of the base membrane and offers multiple initiation sites for polymer chain growth. I anticipate that implementation of this strategy would increase adsorption capacities of the membranes to a new level. A systematic study of the impact of grafting density on the accessibility and mass transfer limitation of biomolecules to the binding sites would be required to design membranes with optimum grafting density.

In my studies, I found that the DNA dynamic binding capacity of newly designed strong anion-exchange membranes is remarkably high. However, the binding capacity is not completely reversible and that leads to the loss of DNA during separation. Given the disposable nature of adsorptive membrane beds used for polishing purification, irreversible binding is not problematic. However, for membranes to be considered for DNA purification, I would suggest developing polymer chains with variable charge density and studying the effects of charge dilution on the reversible dynamic binding capacities of strong anion-exchange membranes. The charge dilution can be achieved by

using a mixture of monomers and manipulating the ratio of these monomers during surface-initiated graft copolymerization.

I demonstrated that the surface-initiated ATRP has great potential to design membrane adsorber with remarkably high protein binding capacity. However, the longer polymerization times used in my studies may be outlined as critical drawback for industrial implementation of this process. Therefore, a future study to increase the rate of polymerization significantly while maintaining a sufficient control over molar mass of polymer chain would be an interesting area to explore.

In my PhD work, I used regenerated cellulose membranes with 1 μm average pore diameter. I belive there is a reasonable opportunity to optimize the pore size of base membranes substrate. As example, the use of smaller pore size (<1 μm) would provide more cellulose material per unit volume and therefore, the higher amount of reactive sites that can be used to graft high density polymer chains. On the other hand the use of membranes with smaller pore size will reduce the permeability of the membrane bed.

Finally, regarding the separation performance evaluation, I would recommend a comprehensive set of experiments to demonstrate the purification of FDA grade plasmid DNA using novel anion-exchange membrane adsorbers. Considering the market potential of plasmid DNA for vaccine and gene therapy application, a study that reports the purification of plasmid DNA using membrane anion-exchange chromatography in bind-and-elute mode will certainly increase the viability of membrane chromatography at large scale plasmid DNA production. However, the performance comparision of membrane chromatography and resin chromatography using dimensional analysis (e.g., the Thomas

206

model for breakthrough to compare dimensionless throughput and capacity parameters) would be more appropriate and clearly the way forward.